How much inundation occurs in the Amazon River basin?

Ayan Fleischmann[1], Fabrice Papa[2], Alice Fassoni-Andrade[3], John M Melack[4], Sly Wongchuig[5], Rodrigo Cauduro Dias De Paiva[1], Stephen K Hamilton[6], Etienne Fluet-Chouinard[7], Rafael Barbedo[1], Filipe Aires[8], Ahmad Al Bitar[9], Marie-Paule Bonnet[10], Michael Coe[11], Jefferson Ferreira-Ferreira[12], Laura Hess[4], Katherine Jensen[13], Kyle Mcdonald[13], Alex Ovando[14], Edward Park[15], Marie Parrens[16], Sébastien Pinel[17], Catherine Prigent[18], Angélica F Resende[19], Menaka Revel[20], Ake Rosenqvist[21], Jessica Rosenqvist[21], Conrado Rudorff[14], Thiago S F Silva[22], Dai Yamazaki[20], and Walter Collischonn[1]

[1]Institute of Hydraulic Research, Universidade Federal do Rio Grande do Sul (UFRGS), Porto Alegre, RS, Brazil

[2]Laboratoire d'Etudes en Géophysique et Océanographie Spatiales (LEGOS), Université Toulouse, IRD, CNRS, CNES, USP, Toulouse, France ; Institut de Recherche pour le Développement (IRD), Universidade de Brasília (UnB), Institute of Geosciences, Campus Universitário Darcy Ribeiro, 70910-900, Brasilia, Brazil

[3]Laboratoire d'Etudes en Géophysique et Océanographie Spatiales (LEGOS)

[4]University of California

[5]Univ. Grenoble Alpes

[6]Kellogg Biological Station

[7]Stanford University

[8]Laboratoire d'Etudes du Rayonnement et de la Matière en Astrophysique et Atmosphères, Observatoire de Paris, UMR 8112, Paris, France.

[9]Centre d'Etudes Spatiales de la Biosphère (CESBIO), Toulouse University (CNES, CNRS, INRAe, IRD, UPS), Toulouse, France

[10]Espace-DEV, Univ Montpellier, Institute of Research for Development, Univ Guyane, Univ Reunion, Montpellier, France

[11]Woodwell Climate Research Center, Falmouth, MA

[12]Instituto de Desenvolvimento Sustentável Mamirauá

[13]City College of New York

[14]Centro Nacional de Monitoramento de Desastres Naturais (CEMADEN), São José dos Campos, São Paulo, Brazil

[15]National Institute of Education, Earth Observatory of Singapore and Asian School of the Environment, Nanyang Technological University, Singapore

[16]Centre d'Etudes Spatiales de la Bioshpère (CESBIO), CNES, Université de Toulouse (UPS), France ; Dynafor, Université de Toulouse, INRAE, INPT, INP-PURPAN, Castanet-Tolosan, France

[17]CEFREM, University of Perpignan Via Domitia, Perpignan, France

[18]CNRS, Sorbonne Université, Observatoire de Paris, Université PSL, Lerma, Paris, France

[19]Universidade de São Paulo, Departamento de Ciências Florestais (ESALQ), Piracicaba, SP, Brazil

[20]Institute of Industrial Science, The University of Tokyo, Tokyo, Japan.

[21]solo Earth Observation (soloEO), Tokyo 104-0054, Japan

[22]Biological and Environmental Sciences, Faculty of Natural Sciences, University of Stirling, Stirling, UK Fk9 4LA.

November 22, 2022

Abstract

The Amazon River basin harbors some of the world's largest wetland complexes, which are of major importance for biodiversity, the water cycle and climate, and human activities. Accurate estimates of inundation extent and its variations across spatial and temporal scales are therefore fundamental to understand and manage the basin's resources. More than fifty inundation estimates have been generated for this region, yet major differences exist among the datasets, and a comprehensive assessment of them is lacking. Here we present an intercomparison of 29 inundation datasets for the Amazon basin derived from remote sensing-based products, hydrological models and multi-source products. Spatial resolutions range from 12.5 m to 25 km, and temporal resolution from static to monthly intervals, covering up to a few decades. Overall, 26% of the lowland Amazon basin is estimated as subject to inundation by at least one product. The long-term maximum inundated area across the entire basin (lowland areas with elevation < 500 m) is estimated at 599,700 $\pm$ 81,800 km^2 if considering only higher quality SAR-based products and 490,300 $\pm$ 204,800 km^2 if considering 18 basin-scale datasets. However, even the highest resolution SAR-based product underestimates the local maximum values, as estimated by subregional products, suggesting a basin-wide underestimation of ˜10%. The minimum inundation extent shows greater disagreements among products than the maximum extent: 139,300 $\pm$ 127,800 km^2 for SAR-based products and 112,392 $\pm$ 79,300 km^2 for the overall average. Discrepancies arise from differences among sensors, time periods, dates of acquisition, spatial resolution, and data processing algorithms. The median total area subject to inundation in medium to large river floodplains (drainage area > 1,000 km^2) is 323,700 km^2. The highest spatial agreement is observed for floodplains dominated by open water such as along the lower mainstem rivers, whereas intermediate agreement is found along major vegetated floodplains fringing larger rivers (e.g., Amazon mainstem floodplain). Especially large disagreements exist among estimates for interfluvial wetlands (Llanos de Moxos, Pacaya-Samiria, Negro, Roraima), where inundation tends to be shallower and more variable in time. Our data inter-comparison helps identify the current major knowledge gaps regarding inundation mapping in the Amazon and their implications for multiple applications. In the context of forthcoming hydrology-oriented satellite missions, we make recommendations for future developments of inundation estimates in the Amazon and present a WebGIS application (https://amazon-inundation.herokuapp.com/) we developed to provide user-friendly visualization and data acquisition of current Amazon inundation datasets.

Hosted file

`essoar.10508718.1.docx` available at https://authorea.com/users/533146/articles/598622-how-much-inundation-occurs-in-the-amazon-river-basin

How much inundation occurs in the Amazon River basin?

Ayan Santos Fleischmann[1], Fabrice Papa[2,3], Alice Fassoni-Andrade[2,3], John M. Melack[4], Sly Wongchuig[5], Rodrigo Cauduro Dias de Paiva[1], Stephen K. Hamilton[12], Etienne Fluet-Chouinard[6], Rafael Barbedo[1], Filipe Aires[7], Ahmad Al Bitar[8], Marie-Paule Bonnet[9], Michael Coe[10], Jefferson Ferreira-Ferreira[11], Laura Hess[4], Katherine Jensen[14,15], Kyle McDonald[14,15], Alex Ovando[16], Edward Park[17], Marie Parrens[18,19], Sébastien Pinel[20], Catherine Prigent[21], Angélica F. Resende[22], Menaka Revel[23], Ake Rosenqvist[24], Jessica Rosenqvist[24], Conrado Rudorff[16], Thiago S. F. Silva[25], Dai Yamazaki[23], Walter Collischonn[1]

1 Institute of Hydraulic Research, Universidade Federal do Rio Grande do Sul (UFRGS), Porto Alegre, RS, Brazil
2 Laboratoire d'Etudes en Géophysique et Océanographie Spatiales (LEGOS), Université Toulouse, IRD, CNRS, CNES, USP, Toulouse, France
3 Institut de Recherche pour le Développement (IRD), Universidade de Brasília (UnB), Institute of Geosciences, Campus Universitário Darcy Ribeiro, 70910-900, Brasilia, Brazil
4 Earth Research Institute, University of California, Santa Barbara
5 Univ. Grenoble Alpes, IRD, CNRS, Grenoble INP, Institut des Géosciences de l'Environnement (IGE, UMR 5001), 38000, Grenoble, France
6 Department of Earth System Science, Stanford University, Stanford, California, CA
7 Laboratoire d'Etudes du Rayonnement et de la Matière en Astrophysique et Atmosphères, Observatoire de Paris, UMR 8112, Paris, France.
8 Centre d'Etudes Spatiales de la Biosphère (CESBIO), Toulouse University (CNES, CNRS, INRAe, IRD, UPS), Toulouse, France
9 Espace-DEV, Univ Montpellier, Institute of Research for Development, Univ Guyane, Univ Reunion, Montpellier, France
10 Woodwell Climate Research Center, Falmouth, MA
11 Instituto de Desenvolvimento Sustentável Mamirauá, Tefé, AM, Brazil
12 Kellogg Biological Station, Michigan State University, Hickory Corners, MI 49060, USA and Cary Institute of Ecosystem Studies, Millbrook, NY 12545 USA
14 Department of Earth and Atmospheric Sciences, City College of New York, City University of New York, New York, NY 10031, USA
15 Department of Earth and Environmental Science, The Graduate Center, City University of New York, New York, NY 10031, USA
16 Centro Nacional de Monitoramento de Desastres Naturais (CEMADEN), São José dos Campos, São Paulo, Brazil
17 National Institute of Education, Earth Observatory of Singapore and Asian School of the Environment, Nanyang Technological University, Singapore
18 Centre d'Etudes Spatiales de la Bioshpère (CESBIO), CNES, Université de Toulouse (UPS), France
19 Dynafor, Université de Toulouse, INRAE, INPT, INP-PURPAN, Castanet-Tolosan, France

[20] CEFREM, University of Perpignan Via Domitia, Perpignan, France

[21] CNRS, Sorbonne Université, Observatoire de Paris, Université PSL, Lerma, Paris, France

[22] Universidade de São Paulo, Departamento de Ciências Florestais (ESALQ), Piracicaba, SP, Brazil

[23] Institute of Industrial Science, The University of Tokyo, Tokyo, Japan.

[24] solo Earth Observation (soloEO), Tokyo 104-0054, Japan

[25] Biological and Environmental Sciences, Faculty of Natural Sciences, University of Stirling, Stirling, UK Fk9 4LA.

Corresponding author: Ayan Santos Fleischmann (`ayan.fleischmann@gmail.com`)

Abstract

The Amazon River basin harbors some of the world's largest wetland complexes, which are of major importance for biodiversity, the water cycle and climate, and human activities. Accurate estimates of inundation extent and its variations across spatial and temporal scales are therefore fundamental to understand and manage the basin's resources. More than fifty inundation estimates have been generated for this region, yet major differences exist among the datasets, and a comprehensive assessment of them is lacking. Here we present an intercomparison of 29 inundation datasets for the Amazon basin derived from remote sensing-based products, hydrological models and multi-source products. Spatial resolutions range from 12.5 m to 25 km, and temporal resolution from static to monthly intervals, covering up to a few decades. Overall, 26% of the lowland Amazon basin is estimated as subject to inundation by at least one product. The long-term maximum inundated area across the entire basin (lowland areas with elevation < 500 m) is estimated at 599,700 $\pm$ 81,800 km² if considering only higher quality SAR-based products and 490,300 $\pm$ 204,800 km² if considering 18 basin-scale datasets. However, even the highest resolution SAR-based product underestimates the local maximum values, as estimated by subregional products, suggesting a basin-wide underestimation of ~10%. The minimum inundation extent shows greater disagreements among products than the maximum extent: 139,300 $\pm$ 127,800 km² for SAR-based products and 112,392 $\pm$ 79,300 km² for the overall average. Discrepancies arise from differences among sensors, time periods, dates of acquisition, spatial resolution, and data processing algorithms. The median total area subject to inundation in medium to large river floodplains (drainage area > 1,000 km²) is 323,700 km². The highest spatial agreement is observed for floodplains dominated by open water such as along the lower mainstem rivers, whereas intermediate agreement is found along major vegetated floodplains fringing larger rivers (e.g., Amazon mainstem floodplain). Especially large disagreements exist among estimates for interfluvial wetlands (Llanos de Moxos, Pacaya-Samiria, Negro, Roraima), where inundation tends to be shallower and more variable in time. Our data inter-comparison helps identify the current major knowledge gaps regarding inundation mapping in the Amazon and their implications for multiple applications. In the context of forthcoming hydrology-oriented satellite missions, we make recommendations

2

for future developments of inundation estimates in the Amazon and present a WebGIS application (https://amazon-inundation.herokuapp.com/) we developed to provide user-friendly visualization and data acquisition of current Amazon inundation datasets.

Key words: flooding, surface water, floodplains, interfluvial wetlands

1. Introduction

Aquatic ecosystems cover extensive areas of the Amazon basin, and are associated with temporally and spatially dynamic habitats such as floodable forests, savannas, grasslands, large and small rivers, and lakes (Hess et al., 2015; Junk et al., 2011; Melack and Coe, 2021; Reis et al., 2019a). These systems, hereafter called wetlands, support plants and animals that are adapted to the flood pulse (Junk et al., 1989), play key roles in regional and global biogeochemical cycles, especially the carbon cycle (Richey et al 1990; Dunne et al., 1998; Abril et al., 2014; Melack et al., 2004; Pangala et al., 2017; Martínez-Espinosa et al., 2020), and regulate the riverine transport of dissolved and particulate material, including sediment and organic matter (Armijos et al., 2020; Fassoni-Andrade and Paiva, 2019; Melack and Forsberg, 2001; Ward et al., 2017). Additionally, human settlements along Amazonian wetlands (Blatrix et al., 2018; Denevan, 1996) benefit from ecosystem services, including food provision from native plants and animals as well as crop and livestock production (Coomes et al., 2016; Jardim et al., 2020).

Much of the wetland of the Amazon Basin is considered floodplain because it is subject to seasonal or periodic inundation by river overflow (i.e., the flood pulse; Junk et al., 1989). The region also hosts large interfluvial wetlands, which unlike floodplains, are flooded mainly by local rainfall and runoff and characterized with shallow water (Belger et al., 2011; Bourrel et al., 2009; Junk et al., 2011). Water sources, inundation patterns, and geomorphology interact to determine the structure and function of these biodiverse ecosystems (Junk et al., 2011; Latrubesse, 2012; Park and Latrubesse, 2017).

The extent of inundated land (also called flooded land or surface water extent), and its temporal variation, are core variables to understand wetland processes and are of interest for multiple scientific disciplines, including ecology (Silva et al., 2013; Hawes et al., 2012; Luize et al. 2015), land-atmosphere interactions (Prigent et al., 2011; Santos et al., 2019; Taylor et al., 2018), carbon cycling and greenhouse gas emissions (Guilhen et al., 2020; Melack et al., 2004; Richey et al., 2002), and natural hazard management (Restrepo et al., 2020; Trigg et al., 2016). The Amazon Basin has been a focus for remote sensing developments and applications in hydrology (Fassoni-Andrade et al., 2021), especially for inundation estimation, given the basin's large scale and global environmental relevance, relatively pristine landscape, and technical challenges posed by persistent cloud cover (Asner, 2001) and dense vegetation. This resulted in the development of more than fifty inundation maps and datasets for this region in recent decades. Tables 1 (datasets used in this study) and S1 (datasets not used

due to redundancy or unavailability) summarize most of the datasets developed for mapping inundation in the Amazon basin.

Wetland maps were first produced for the Amazon basin by Matthews and Fung (1987) from aeronautical charts. Optical remote sensing systems in the visible or thermal spectral range, such as Landsat, are of limited value for most Amazonian wetlands, since inundation under persistent cloud cover, and vegetation canopies can be difficult to detect. Because of this, microwave sensor systems have been employed. Large-scale wetland inundation mapping was pioneered in the region through analysis of Scanning Multi-channel Microwave Radiometer (SMMR) and Special Sensor Microwave/Imager (SSM/I) passive microwave observations, which provided all-weather capability and sensitivity to inundation even in the presence of partial vegetative cover (Hamilton et al., 2002; Prigent et al., 2001; Sippel et al., 1998). Meanwhile, research demonstrated the all-weather capability and superior spatial resolution of synthetic aperture radar (SAR) systems. L-band SAR that can penetrate forest canopies and reveal underlying water through the "double bounce" effect was shown to be promising for mapping inundation in the Amazon (Hess et al., 2003). More specifically, the high-resolution, dual-season classification of the Japan Earth Resources Satellite-1 (JERS-1) L-band SAR data for the entire lowland Amazon basin by Hess et al. (2015), validated with airborne videography images, has been used as a benchmark for the inundation extent of Amazonian wetlands. Since these initial studies, and with the availability of other imagery (e.g., Advanced Land Observing Satellite (ALOS) 1 and 2 missions), the remote sensing community seeking to map and characterize inundation employed various combinations of active and passive microwave data to benefit from the higher spatial resolution of the former and the higher temporal resolution of the latter (Aires et al., 2013; Jensen and Mcdonald, 2019; Papa et al., 2010; Parrens et al., 2019, 2017; Prigent et al., 2007, 2020; Schroeder et al., 2015).

Besides basin-scale mappings of annual maximum and minimum inundation (Chapman et al., 2015; Hess et al., 2015; Rosenqvist et al., 2020), dynamic datasets with high spatial and temporal resolution are mainly based on satellite passive microwave observations of coarse spatial resolution (Global Inundation Extent Multi-Satellite (hereafter GIEMS), Surface Water Microwave Product Series (hereafter SWAMPS), Surface Water Fraction (hereafter SWAF), Wetland Area and Dynamics for Methane Modeling (hereafter WAD2M) products - Table 1), which can be downscaled using ancillary data (Aires et al., 2017, 2013; Parrens et al., 2019). Basin-scale, dynamic inundation estimates based on the ALOS satellite are limited given its low temporal resolution (repeat cycle of 46 days). Thus, some studies have analyzed time series of ALOS-Phased Array L-band Synthetic Aperture Radar (PALSAR) (Arnesen et al., 2013; Ferreira-Ferreira et al., 2015) and ALOS-2 PALSAR-2 backscatter retrievals (Jensen et al., 2018) for subsets of Amazon wetlands. However, with a few exceptions using local scale datasets (Arnesen et al., 2013; Ferreira-Ferreira et al., 2015; Hess et al., 2003; Jensen et al., 2018; Resende et al., 2019), in situ validation of the basin-scale estimates has seldom been performed, given the remoteness of much

4

of the Amazon basin and the often dense forest cover, which hampers airborne monitoring of below-canopy surface waters.

Complementarily, process-based hydrological models estimating variables such as river discharge and flood extent have been developed and assessed from basin to local scales in the major rivers of the basin (Beighley et al., 2009; Coe et al., 2008; Getirana et al., 2017, 2012; Hoch et al., 2017; Luo et al., 2017; Miguez-Macho and Fan, 2012; Paiva et al., 2013; Yamazaki et al., 2011), thanks to the advent of new computational and modeling capabilities. Local scale hydraulic models with coarse (Trigg et al., 2009; Wilson et al., 2007; Fleischmann et al., 2020) and detailed input data (Ji et al., 2019; Pinel et al., 2019; Rudorff et al., 2014; Fassoni-Andrade, 2020) have further developed model capabilities for mapping inundation dynamics, especially for the floodplains fringing the Amazon mainstem.

Among these numerous inundation datasets for the Amazon basin (Tables 1 and S1), divergences can be substantial due to the differences in sensor systems, timing, and data processing algorithms (Aires et al., 2018; Fleischmann et al., 2020; Parrens et al., 2019; Pham-Duc et al., 2017; Rosenqvist et al., 2020), and a comprehensive assessment of inundation estimates for the Amazon is lacking. The need to compare different hydrological datasets for the Amazon has been recently highlighted in the context of river discharge (Towner et al., 2019), precipitation (Wongchuig et al., 2017; Zubieta et al., 2019) and evapotranspiration (Paca et al., 2019; Wu et al., 2020). Meanwhile, rapid environmental changes in the basin underscore the urgency for a better understanding of Amazon water resources (Fassoni-Andrade et al., 2021), for which management and planning can be hindered by the discrepancies among datasets. These questions regarding current data limitations in the largest basin in the world are also timely in anticipation of forthcoming hydrological satellite missions such as Surface Water and Ocean Topography (SWOT) and NASA-ISRO SAR (NISAR).

Such better understanding starts with the central question of "how much area is subject to inundation and seasonal flooding in the Amazon lowlands?" Although this question does not have a simple answer, quantifying our current knowledge and its uncertainty through evaluation of the existing inundation datasets is a necessary first step. To assess the state of understanding of inundation patterns in the Amazon wetlands, we address the following questions: 1) How much Amazon land area is subject to seasonal or permanent flooding, and how accurate are the estimates? 2) Which areas are in particular disagreement and thus deserve further attention? 3) How do basin-scale estimates with coarser resolution and less calibrated classification methods differ from the local- or large-scale ones with independent validation? 4) How do the various inundation estimation approaches (optical imagery, SAR, passive microwave, hydrologic models) differ in terms of inundation mapping and for different wetland types (e.g., floodplains and interfluvial areas)? In order to answer these questions, we gathered 29 inundation datasets for the Amazon basin, spanning a wide range of spatial (12.5 m to 25 km) and temporal (static, dual-season, monthly, daily) scales,

and from basin to local coverage (Table 1), into a framework that provides a comprehensive assessment of current knowledge of Amazon inundation.

Table 1. List of 29 studies that mapped inundated areas over scales ranging from the entire Amazon basin to local scales. These data sources were selected based on data availability and relevance for this intercomparison study. In the case of hydrological models, time resolutions are the values assessed or provided by the models, which can be provided at finer time resolution if necessary, since many of them actually compute flood maps at daily or sub-daily time steps and report time-integrated results. The column "Data type" refers to: OS: Optical Sensor; SAR: Synthetic Aperture Radar; HM: Hydrological Model; HR: multiple datasets at High Resolution; CR: multiple datasets at Coarse Resolution. The column "Type of inundation captured" has three classes: "All", meaning both open water and vegetated wetlands, "Open water", and "Wetland only (no open water)".

Product or main satellite name	Data type	Spatial resolution	Temporal resolution	Time
GIEMS-2	CR	25 km	Monthly	1992-
SWAF-HR	HR	1 km	Weekly to monthly	2010-
SWAMPS	CR	25 km	Monthly	1992-
WAD2M	CR	25 km	Monthly	2000-
Bonnet model	HM	180 m	Monthly	2006-
LISFLOOD-FP	HM	90 m	Monthly	1994-
MGB	HM	500 m	Monthly	1980-
TELEMAC-2D	HM	30 m	Monthly	2006-
THMB	HM	5-min	Monthly	1961-
CaMa-Flood	HM	500 m	Monthly	1980-
GIEMS-D3	HR	90 m	Monthly	1993-
CIFOR	HR	232 m	Static (max inundation)	1950-
ESA-CCI	HR	300 m	Annual	1992-
GIEMS-D15	HR	500 m	Monthly climatology	1993-
GLWD	HR	1 km	Static	1992-
G3WBM / Landsat	OS	30 m	Static (open water areas)	1990-
GLAD / Landsat	OS	30 m	Annual and monthly climatology	1999-
GSWO / Landsat	OS	30 m	Monthly (cloud cover may occur)	1984-
MODIS	OS	500 m	8 days	2001-
MODIS	OS	230 m	Monthly climatology	2000-
JERS-1	SAR	90 m	Max. and min. annual inundation	1995-
ALOS-2 PALSAR-2	SAR	50 m	Irregular (26 images)	2014-
ALOS-2 PALSAR-2	SAR	50 m	Max. and min. annual inundation	2014-
ALOS-PALSAR	SAR	90 m	Irregular (12 images)	2006-
ALOS-PALSAR	SAR	90 m	Monthly	2006-
ALOS-PALSAR	SAR	12.5 m	Flood frequency	2007-
ALOS-PALSAR	SAR	100 m	Irregular (6 images)	2006-
ALOS-PALSAR	SAR	30 m	Irregular (16 images)	2007-
ALOS-PALSAR	SAR	25 m	Static (max inundation)	2006-

2. Methodology

2.1 Study area

The Amazon basin spans around 6 million km² in nine South American countries (Figure 1). We delimited the catchment area upstream from Gurupá city, within the tidal river ~390 km from the ocean; hence not including the Tocantins-Araguaia basin and parts of the Amazon estuary and Marajó Island. We selected the 5.11×10^6 km² of Amazon lowlands defined as areas with an altitude lower than 500 m based on the Shuttle Radar Topography Mission Digital Elevation Model (SRTM DEM) for the area of dataset comparisons in our study. This decision is consistent with several studies limited to lowlands because of the limitations of certain methods in estimating flooding in mountainous terrain (Hess et al., 2015).

In addition to basin-scale products, estimates of inundated areas from 11 wetland complexes in the Amazon basin are used to understand how estimates may vary in accuracy across different wetland types (Figure 1): Curuai floodplain lake (Arnesen et al., 2013; Rudorff et al., 2014), Janauacá floodplain lake (Bonnet et al., 2017; Pinel et al., 2019), Uatumã river floodplain (Resende et al., 2019), Mamirauá Reserve (Ferreira-Ferreira et al., 2015), Pacaya-Samiria wetlands (Jensen et al., 2018), Llanos de Moxos wetlands (Ovando et al., 2016), lower Amazon floodplain (Park and Latrubesse, 2019), Amazon mainstem floodplain (from Iquitos to Gurupá), Purus floodplain, Roraima savannas, and Negro savannas. A brief summary of these wetlands is provided in supplementary Table S2, and their main features are summarized in the following. Curuai is representative of the shallow lakes in the lower Amazon floodplain. It is separated from the river by narrow levees (Rudorff et al., 2014) and has a high suspended sediment concentration. Janauacá is typical of the middle Amazon River floodplain, and is composed of a ria lake (i.e., a blocked valley lake with relatively sediment-free waters; Latrubesse (2012)) and "várzea" environments (white-water floodplains) in its northern part (Pinel et al., 2019). Uatumã River is an Amazon tributary with black-water floodplain ("igapó"), and includes Balbina hydroelectric reservoir, operating since 1987, which affects the river's hydrological regime (Schöngart et al., 2021). The Uatumã floodplain reach assessed here is the 300-km reach between Balbina dam and the confluence with the Amazon River. The Mamirauá Sustainable Development Reserve is located in the confluence between Solimões and Japurá rivers, and is characterized by a mosaic of "chavascal", herbaceous, and low and high várzea vegetation (Ferreira-Ferreira et al., 2015). The Purus River is a major tributary, and its floodplain was chosen because of its large floodplain to river width ratio. Pacaya-Samiria wetlands are composed of flooded forests, palm swamps and peatlands in the upper Solimões River (Draper et al., 2014; Lähteenoja et al., 2012). The Llanos de Moxos floodable savannas occupy the interfluvial areas between the Beni, Mamoré and Madre de Dios rivers in the upper Madeira basin (Hamilton et al., 2004). The Negro savannas, locally known as "campina wetlands" and "campinarana wetlands", depending on the vegetation density, are thought to have

7

formed from regional neotectonic depressions and were called the "Septentrional Pantanal" given their large area (Rossetti et al., 2017a, 2017b; Santos et al., 1993). The Roraima floodable savannas extend from Roraima State in Brazil to the Rupununi savannas in Guyana, and comprise mainly smaller river floodplains interspersed with poorly drained interfluvial savannas subject to flooding by local rainfall (Hamilton et al., 2002); here we only considered the Roraima wetlands in the upper Branco River basin, which is within the Amazon basin.
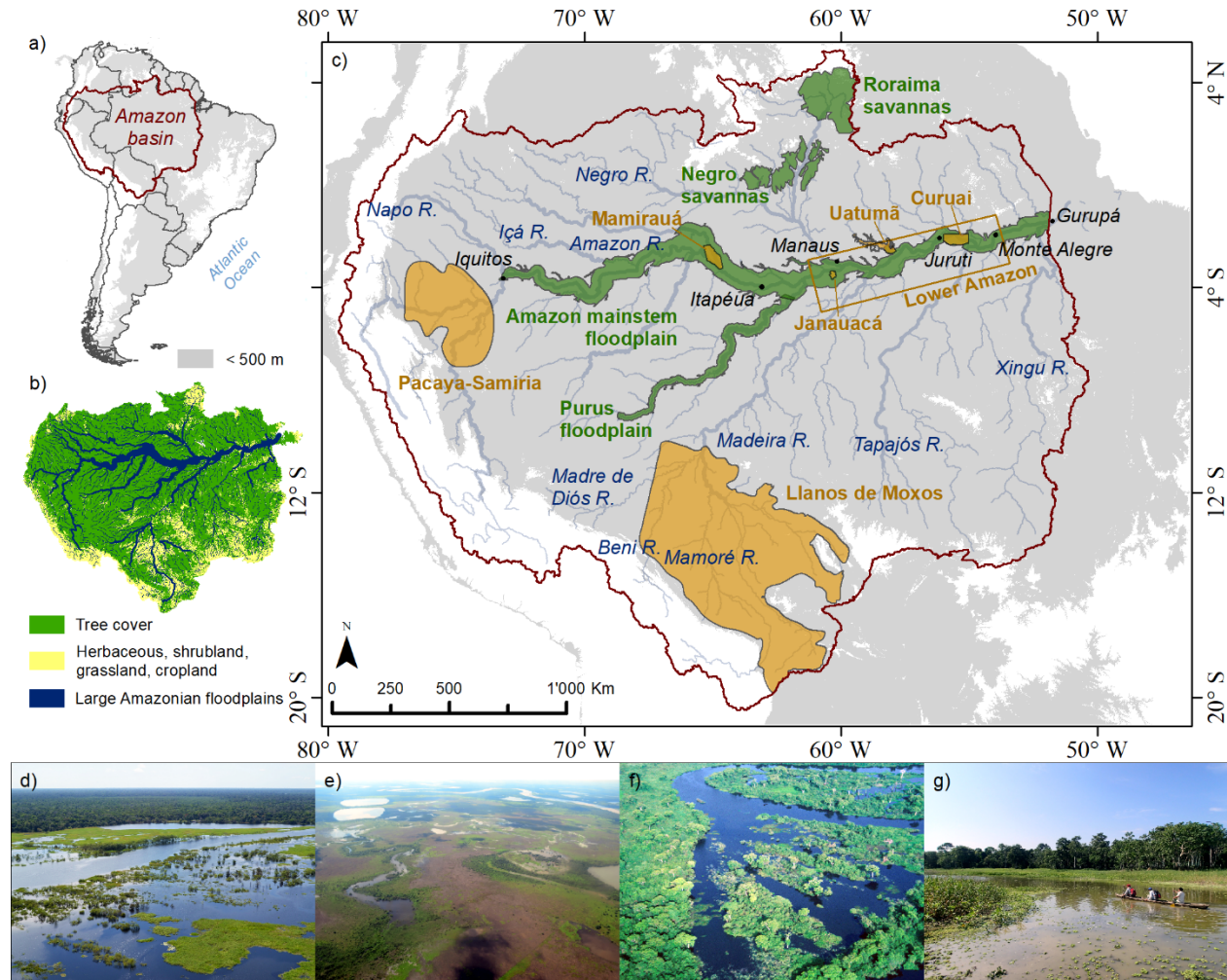
Figure 1. The Amazon basin and its major wetland systems: (a) Amazon basin delineation (red lines) over the countries of South America (black lines). (b) Land cover based on a 2010 map from the European Space Agency Climate Change Initiative (ESA-CCI) (Bontemps et al., 2013), showing the distribution of forest and savanna across the basin, as well as large floodplains (see methodology Section 2.3). (c) Basin distribution of major wetland systems showing

locations of interest for this study. Elevations lower than 500 m are shown in grey (based on SRTM DEM). The orange polygons show the areas for which a local dataset was available for this study (Figure 4), and the green ones show wetland areas of interest that do not have products specifically designed for these subregions. Photos depicting different wetland complexes for (d) Mamirauá (courtesy of João Paulo Borges Pedro), (e) Llanos de Moxos (courtesy of Alex Ovando), (f) Cabaliana floodplain lake close to Manacapuru (courtesy of Stephen Hamilton), and (g) Pacaya-Samiria (courtesy of Katherine Jensen) regions, respectively.

2.2 Datasets

Twenty-nine inundation datasets covering areas ranging from the whole-basin scale to local wetlands, based on multiple data sources and spatiotemporal resolutions, were assembled for our comparison (Table 1). In recent years, the proliferation of inundation datasets is evident by the number of products published in the last five years: 18 out of the 29 inundation datasets had their original publication since 2016, and 27 of them since 2011. These were chosen due to data availability and representativeness; other data products that were either unavailable or methodologically redundant to others in our comparison were not used but are catalogued in Table S1.

Regarding spatial and temporal resolution, the basin-scale datasets are divided into dynamic hydrological models (CaMa-Flood, MGB, THMB), dynamic coarse-scale (GIEMS-2, SWAMPS, WAD2M), dynamic fine-scale (GIEMS-D3 and SWAF-HR), annual fine-scale (GSWO and GLAD), dual-season fine-scale (Rosenqvist, Hess, Chapman), and static fine-scale (ESA-CCI, G3WBM, CIFOR, GIEMS-D15 and GLWD) observations. Thus, there are eight dynamic products and 11 static or dual-season basin-scale products. Figures 2 and 3 provide long-term flood frequency maps for the dynamic products and maximum flood extent for the static/dual-season ones.
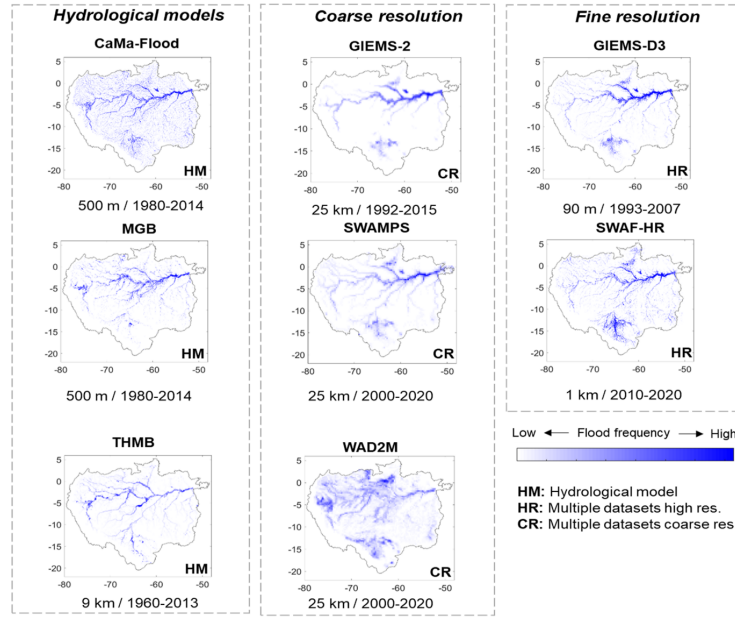
Figure 2. Basin-scale, dynamic inundation products used in this study, for three classes (hydrological models; fusion of multiple datasets at high resolution; fusion of multiple datasets at coarse resolution). Long-term flood frequency maps are provided for each dataset, calculated as the percentages of observations labelled as flooded throughout the entire time-series.
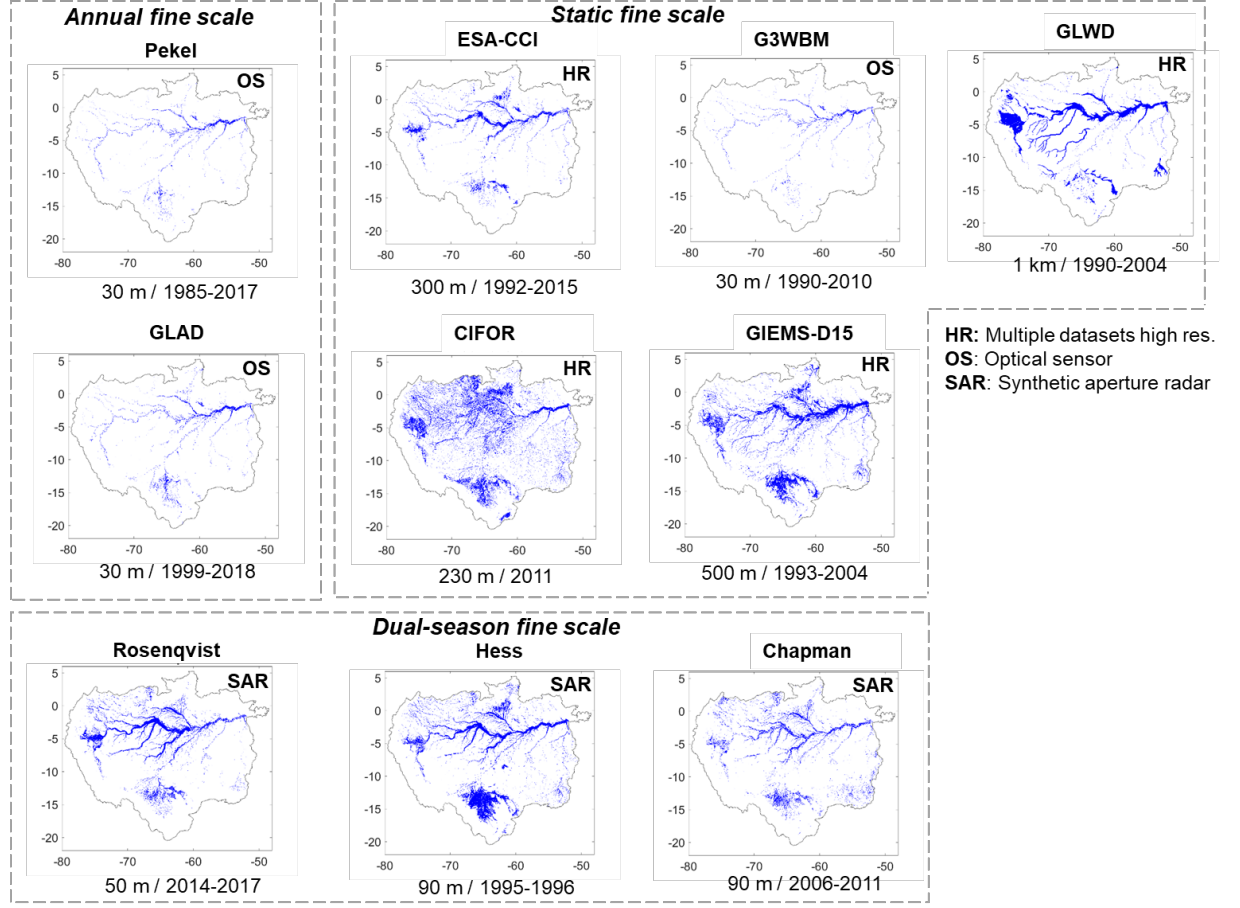
Figure 3. Basin-scale, static or dual-season inundation products used in this study, including three classes (fusion of multiple datasets at high resolution; based on optical sensors; and based on SAR data). Flood frequency maps are not provided because the products are mainly static or annual-based.

Passive microwave (PM) data are the basis of SWAF-HR, GIEMS family (GIEMS-D15, GIEMS-D3, GIEMS-2), and SWAMPS, while ancillary data (i.e., optical imagery and microwave scatterometry) are used to complement the PM signal. SWAF-HR data result from the disaggregation of water surface fraction at coarse spatial resolution product (SWAF), based on L-band passive microwave observations from the Soil Moisture and Ocean Salinity (SMOS) satellite (Parrens et al. 2017). The disaggregation of SWAF relies on water occurrence maps from GSWO and the Digital Elevation Model (DEM) Multi-Error-Removed-Improved-Terrain (MERIT) (Parrens et al., 2019). A global implementation of SWAF (G-SWAF) based on multi-angular and multi-polarization information has also been implemented (Al Bitar et al. 2020). GIEMS merges multiple satellite passive and active microwave observations,

11

along with optically-derived NDVI (Normalized Difference Vegetation Index), to detect the surface water and estimate the vegetation attenuation, for a monthly quantification of the surface water extent at ~25 km scale (Prigent et al., 2001, 2007, 2020; Papa et al., 2010). It is further disaggregated at 90-m resolution (GIEMS-D3) using topographical downscaling methodology (Aires et al. 2017).

Three basin-scale products are based mainly on SAR data from JERS-1 (Hess et al., 2003, 2015), and its successor missions ALOS-PALSAR (Chapman et al., 2015) and ALOS-2 PALSAR-2 (Rosenqvist et al., 2020). These three products cover different decades of observation but are methodologically similar.

Three of the optical-based products are based on Landsat data: GSWO (Pekel et al., 2016), G3WBM (Yamazaki et al., 2015) and GLAD (Pickens et al., 2020). Although GSWO and GLAD can provide monthly estimates for the Landsat archive (1984-today), given the inability of optical data to estimate flooding under cloud cover or vegetated waters, only annual maximum and minimum values are used. For GLAD and GSWO, we consider a threshold of occurrence of surface water of 95% to estimate the minimum inundation (i.e., for the permanently inundated areas; Aires et al., 2018); otherwise, only a few isolated open water areas would be considered for the minimum extent.

The European Space Agency Climate Change Initiative (ESA-CCI) product is based on surface reflectance from MERIS, the Advanced Very High-Resolution Radiometer (AVHRR) and PROBA-V data and Global Water Bodies from the Envisat Advanced Synthetic Aperture Radar (ASAR) (Bontemps et al., 2013). Since the wetland pixels in this product varied negligibly throughout the years of observations, we choose to use only the 2010 product as the ESA-CCI estimate for maximum wetland inundation.

Another set of products is based on the fusion of multiple global datasets: GLWD, GIEMS-D15 and WAD2M. GLWD is one of the first globally consistent databases of wetlands, which was based on a collection of wetland estimates from diverse institutions worldwide (Lehner and Döll, 2004). GIEMS-D15 combines GLWD, the Hydrosheds drainage network, and Global Land Cover 2000. WAD2M is based on SWAMPS and CIFOR within its merging framework. WAD2M is the only product to exclude open water areas (removal based on GSWO) due to its goal of estimating wetland methane emissions. The SWAF-HR (Parrens et al., 2019) and GIEMS-D3 (Aires et al., 2017) products use additional data and methodologies to downscale the original passive microwave-based SWAF (Parrens et al., 2017) and GIEMS (Papa et al., 2010; Prigent et al., 2007) products from 25 km to 1 km and 90 m, respectively. While GIEMS-D3 has a different inundation magnitude than the original GIEMS product due to data fusion with ancillary data, SWAF-HR conserves the same inundation magnitude across scales.

Among hydrological models, we selected representative ones from each of the following broad modeling types: 1) process-based hydrologic models that use

flood routing to represent inundation processes (i.e., from a simple kinematic wave model coupled to an inundation method to more complex flow routing methods); or 2) hydraulic (or hydrodynamic) models that consider the shallow water equations (or its simplifications) at any dimension (1D, 2D or 3D). For our analysis, we adopted two basin-scale models – one hydrologic (THMB; Coe et al. (2008)) and one hydrologic-hydrodynamic (MGB, Siqueira et al. (2018)), and a global-scale hydrodynamic model (CaMa-Flood, Yamazaki et al. (2011)), in the Earth2Observe version available at <http://www.earth2observe.eu/>). The inundated area estimation is largely affected by the DEMs. The DEMs adopted in the model runs were: Bare-Earth (O'Loughlin et al., 2016) for MGB, MERIT (Yamazaki et al., 2017) for CaMa-Flood, and SRTM (Farr et al., 2007) for THMB. The rainfall/runoff input data are MSWEP v.1.1 daily precipitation (Beck et al., 2017) for MGB, HTESSEL daily runoff (Balsamo et al., 2009) for CaMa-Flood, and CRU TS v.3.2.1 monthly precipitation (Harris et al. 2014) for THMB. Although other hydrologic models have been applied to the Amazon basin (Tables 1 and 2), the models chosen here were selected as representative of global to local models, for having been well validated and applied over the Amazon basin, and for representing state-of-the-art Amazonian hydrologic modeling. All basin-scale models represent one-dimensional (1D) flows only (i.e., floodplains are represented as storage units without active flow), and thus do not represent 2D surface flows that occur in wetlands (Alsdorf et al., 2007; Fleischmann et al., 2020). A detailed comparison of model capabilities and structural uncertainties is beyond our current scope. Hydrologic models have different temporal resolution depending on their numerical stability and forcing data. For instance, MGB and CaMa-Flood models run at an adaptive time step (sub-minute timestep in the case of MGB), but are assessed at daily resolution given their daily precipitation forcing. We aggregated the models' estimates to monthly averages to make them comparable to the remote sensing dynamic products.

The products available at local or regional scales are presented in Figure 4. ALOS-2 PALSAR-2 data were used for the Pacaya-Samiria region (Jensen et al., 2018), and the ScanSAR mode of ALOS/PALSAR for the following local products: Curuai floodplain lake (Arnesen et al., 2013), Mamirauá Reserve (Ferreira-Ferreira et al., 2015), Uatumã river floodplain (Resende et al., 2019), and Janauacá floodplain lake (Pinel et al., 2019). MODIS optical data were used for the Llanos de Moxos savannas in the upper Madeira River basin (Ovando et al., 2016) and the lower Amazon floodplain (Park and Latrubesse, 2019). Two local scale 2D hydraulic models (LISFLOOD-FP for Curuai lake, Rudorff et al. (2014), and TELEMAC-2D for Janauacá lake, Pinel et al. (2019)), and one local-scale hydrologic model (for Janauacá lake; Bonnet et al. (2017)) were considered; together, these are representative of the state-of-the-art of hydrological modeling in Amazonian wetlands.

The products were stored in various formats (i.e., raster and polygon shapefiles) and projections (mainly projected UTM and geographic coordinate system with WGS84 datum), and were converted to the WGS84 geographic coordinate sys-

tem to compute areas. SWAMPS was provided at the Equal-Area Scalable Earth (EASE) Grid, which was used to estimate its flooded areas. Hydrologic model outputs were provided as either binary inundation maps or flood depth raster files, which were then converted into binary maps by assuming depth > 0 m as inundated pixels.
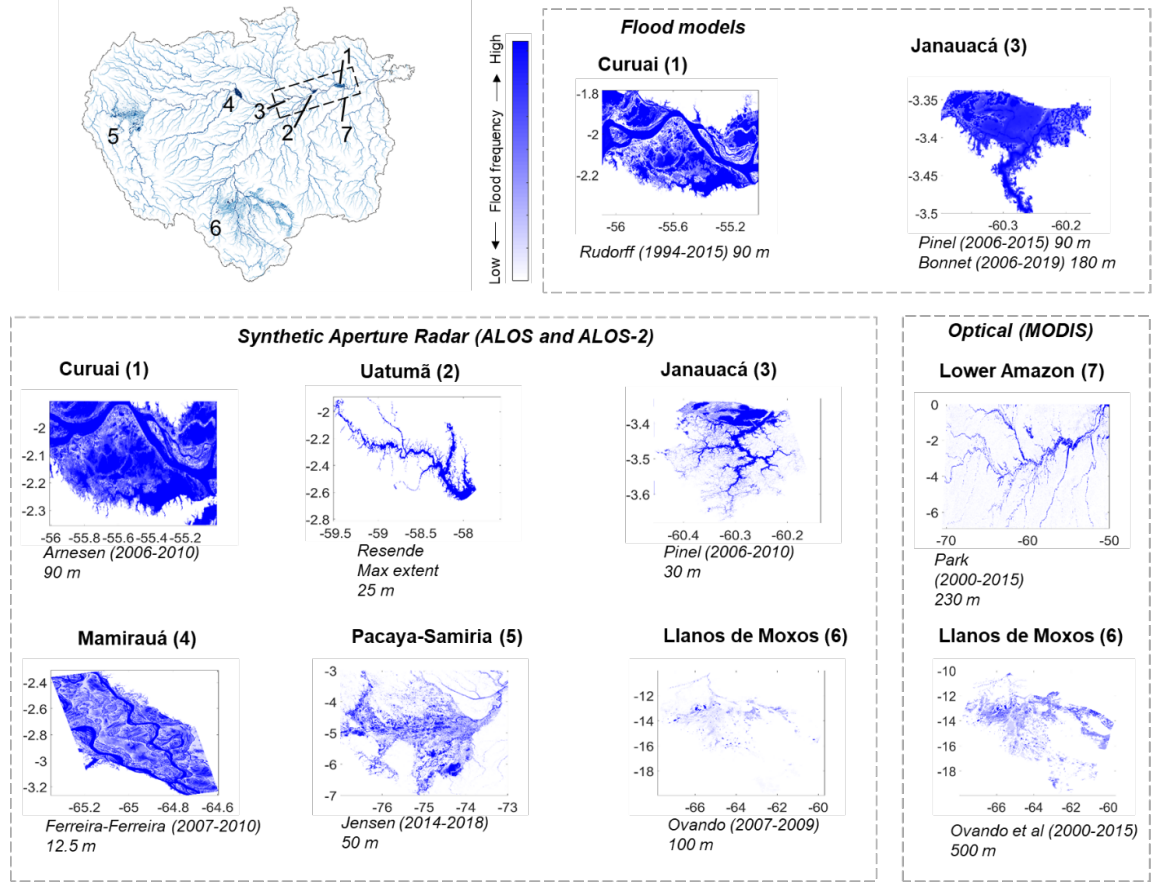

Figure 4. Long-term flood frequency maps from local-scale inundation products used for comparison in this study. The Uatumã product (2) is static and is displayed as the maximum extent. Flood frequency maps are produced by computing the long-term average of all inundation maps available for each dataset.

2.3 Comparison framework

The comparison framework involved the following analyses, considering the entire basin and 11 wetland subregions (seven areas with available local inundation estimates and four additional areas; Figure 1):

- Annual maximum and minimum inundation estimates for each of the 18 basin-scale products (Section 3.1);

14

- Basin-scale, long-term maximum and minimum inundation estimates for each of the 18 basin-scale products (Section 3.1);

- Long-term maximum and minimum inundation estimates for each of the 18 basin-scale and 11 local-scale products for individual wetland complexes (Section 3.2);

- Comparison between basin-scale and local products with temporal (nRMSD and Pearson correlation) and spatial (Fit metric) assessment (Section 3.2);

- Assessment of basin-wide agreement among the 18 basin-scale products at 1 km, for both long-term maximum and minimum inundation maps (Section 3.3);

- Estimation of long-term maximum inundation for two classes of wetlands for the entire basin: (i) medium to large river floodplains and (ii) interfluvial wetlands and small floodplains (Section 3.4).

The long-term maximum and minimum inundation extents were computed for each product as the area of all pixels that were inundated at least once in the whole monthly time series, for the maximum, and as those pixels that were always inundated, for the minimum. We stress that analyzing long-term changes in inundation patterns is beyond the scope of this study, and thus we assumed stationarity in our comparisons of long-term maximum and minimum inundation extents from different time-periods.

The agreement of all basin-scale, high-resolution products (i.e., all products except for THMB, GIEMS-2, SWAMPS and WAD2M, which have a coarse resolution between 9 and 25 km) was assessed for long-term maximum and minimum inundation at 1 km resolution, which is the resolution of SWAF-HR, the coarsest resolution among the high-resolution products. For each 1 km pixel, the total number of products agreeing that it was inundated (either for maximum or minimum extent) was computed, following Trigg et al. (2016). Given the size of the Amazon basin, a 1 km resolution was considered adequate for the analysis. The analysis was done by aggregating all products to 1 km, and considering that a 1 km pixel is flooded if more than 50% of its area is flooded (following Hamilton et al., 2002). A sensitivity test was performed using a 25% threshold and led to similar conclusions basin-wide (Figure S1).

The basin-scale and four additional local datasets (mainly based on hydrological models) were compared to seven local products, which were assumed as local references, and cover the following sites: Curuai (Arnesen et al., 2013), Uatumã (Resende et al., 2019), Janauacá (Pinel et al., 2019), Mamirauá (Ferreira-Ferreira et al., 2015), Pacaya-Samiria (Jensen et al., 2018), Llanos de Moxos MODIS (Ovando et al., 2016) and lower Amazon (Park and Latrubesse, 2019). Varying degrees of validation exercises were performed for these reference datasets, with some being extensively validated with airborne videography (Hess et al., 2003) or local surveys (Arnesen et al., 2013; Ferreira-Ferreira

et al., 2015; Jensen et al., 2018; Resende et al., 2019), while others were assessed through comparisons with other datasets (Pinel et al., 2019), or visually inspected, as in the large domains of the Llanos de Moxos (Ovando et al., 2016) and lower Amazon (Park and Latrubesse, 2019) subregional datasets. The four additional local products are: Curuai LISFLOOD-FP model (Rudorff et al., 2014), Janauacá hydrological model (Bonnet et al., 2017), Janauacá TELEMAC-2D model (Pinel et al., 2019), and Llanos de Moxos ALOS-PALSAR (Ovando et al., 2016).

To assess the representation of the local inundation dynamics, the basin-scale and four additional local products were compared to the local references at monthly time scale, considering the total inundated area per wetland area (i.e., the whole Curuai Lake domain, the whole Uatumã floodplain, and so forth). The polygons of each wetland area, used to extract the information from the basin-scale datasets, were delineated as a buffer around the maximum inundated area, according to each locally derived product. For the four areas without local products (Amazon mainstem and Purus floodplains, and Roraima and Negro wetlands), the polygons were created considering the maximum lateral extent in accordance with the MERIT DEM (Yamazaki et al., 2017) and ESA-CCI land cover for savannas. The time series were compared with the Pearson linear correlation (R) and the normalized root mean square deviation (nRMSD), computed as the RMSD between a given inundation map and the reference map (i.e., the local wetlands) divided by the reference long-term average inundation. The term 'deviation' was preferred over 'error' to stress the uncertainties inherent to all products, for both basin and local scales, although the local ones are considered as a reference for having a more dedicated product development for that particular area, and being validated with ground surveys in some cases.

The product ability to estimate the local spatial patterns at maximum inundation was assessed with the Fit metric (Bates and De Roo, 2000), which has been successfully applied to compare inundation datasets to local references (Bernhofen et al., 2018), and is computed as:

$$Fit = 100\% * \frac{A \cap B}{A \cup B} \quad (1)$$

Where A and B are the reference (e.g., the local map that corresponds to maximum inundation) and the basin-scale maximum inundation maps.

To differentiate medium to large river floodplains from interfluvial wetlands and small floodplains, an estimation of the total flooded area of the former was computed, considering river reaches with upstream drainage area larger than 1,000 km², and a buffer mask around the river reaches (mask presented in Figure 1). The buffer was defined based on the Hydrosheds drainage network (Lehner and Grill, 2013), segmented into 15 km-long reaches as in Siqueira et al. (2018). The buffer was proportional to the local reach drainage area and further manually adjusted to include the maximum floodplain lateral extent, as

estimated from a visual inspection of the MERIT DEM (Yamazaki et al., 2017) and the three basin-scale SAR-based products (Hess, Chapman and Rosenqvist datasets). Buffer values varied from 4 km in upper reaches to 150 km on the Amazon mainstem close to the Mamirauá Reserve. Estimating floodplain total inundated area is relevant to differentiate the Amazonian floodplains from non-floodplain wetlands (here referred to as interfluvial wetlands).

Finally, in order to assess the current capabilities of basin-wide mapping of inundation dynamics at high spatial and temporal resolution, a further assessment of the four high-resolution dynamic products (GIEMS-D3, CaMa-Flood, SWAF-HR and MGB) at their native resolutions was performed by computing their long-term flood frequency for the entire basin.

3. Results and Discussion

3.1 How much inundation is estimated to occur in the Amazon basin?

Overall assessment

We analyzed the annual maximum and minimum inundation estimates for the entire basin scale (Figure 5), as well as the long-term maxima and minima (Figure 6 and Table 2). The annual values vary widely. Annual values for the 18 basin-scale products are displayed together, though some products provide only long-term average estimates (e.g., GLWD, Chapman, G3WBM). SAR estimates, especially those based on L-band sensors and those having undergone validation, are usually assumed the most accurate given their high spatial resolution and capability of mapping flooded areas under trees and cloud cover.

By computing average and standard deviation of the long-term maximum inundation by type of data (Table 2), we obtain the following values: 138,200 $\pm$ 45,300 km² (average $\pm$ S.D.) for optical, 533,500 $\pm$ 217,800 km² for multiple products at high resolution, and 579,100 $\pm$ 108,900 km² for those at coarse resolution, 542,800 $\pm$ 80,600 km² for hydrological models, and 599,700 $\pm$ 81,800 km² for SAR. The average figure for optical-based datasets is thus around 23% of the SAR-based estimate. If we assume that the ensemble of products could be a proxy of inundation uncertainty in the Amazon basin, and neglecting the optical and land cover-based data (G3WBM, GLAD, GSWO and ESA-CCI) and CIFOR products, given their lower capability to map wetlands as discussed below, 13 products are left, yielding an estimation for the long-term maximum inundation of 559,300 $\pm$ 81,100 km². This value is around 40,000 km² lower than the mean estimated inundation area from the three SAR products. The estimates considering all 18 products average 490,300 $\pm$ 204,800 km². Regarding the long-term minimum inundation area, the relative variance among available estimates is higher than for the long-term maximum extent —125,900 $\pm$ 77,600 km² for the 12 basin-scale products that provide an estimate for the low-water period, and 139,300 $\pm$ 127,800 km² for the three SAR-based datasets.

None of the products can map small, narrow floodplains or riparian zones, for which only simple calculations are currently available (Junk et al., 1993), and

whose total area can only be estimated through statistical extrapolation of observable rivers. For instance, a wetland mask developed by Hess et al. (2015) in order to assist their SAR classification technique yielded a basin-wide estimation of wetland area including the smallest floodplains of 840,000 km². This estimate is much larger than the largest long-term maximum inundated area obtained with SAR data (659,100 km² with Rosenqvist's product). In Section 3.2, it will be shown that almost all products tend to underestimate the maximum inundation, when compared to specific local/subregional products. The two SAR-based products with highest accuracy underestimate inundation by 9% (Rosenqvist) and 13% (Hess) in these comparisons. If this holds true for the whole basin, the basin-scale maximum inundation would be around 10% higher.

A focus on SAR datasets

Basin-wide, SAR-based estimates range from maximum annual inundation of 424,600 km² (Rosenqvist) to 633,500 km² (Hess), and minima from 53,900 km² (Rosenqvist) to 284,200 km² (Hess), as shown in Figure 5. By considering long-term maximum inundation (i.e., all pixels that were inundated at least once in the entire available series), instead of annual maxima, the SAR-based estimates range from 506,400 km² (Chapman) to 659,100 km² (Rosenqvist) for the entire basin (Table 2). The minima vary from 42,400 km² (Rosenqvist) to 284,200 km² (Hess). This highlights the large differences that exist, especially for the minima, usually referred to as the "low-water period." Chapman's product, based on the 2006-2011 ALOS-PALSAR archive, has a smaller total maximum inundation area than the other two SAR datasets, as well as a smaller estimate for minimum inundation in relation to Hess' estimate, which in turn was developed for one year only (1995). Differences among the three products may originate from differences in acquisition dates, interannual inundation variability, algorithms, spatial resolutions, or inconsistencies regarding the data processing. For example, Chapman estimates long-term maxima and minima while Hess and Rosenqvist provide annual values. The calibration uncertainty was also higher for the JERS-1 data used in Hess' mapping than in the subsequent satellites (ALOS-PALSAR and ALOS-2 PALSAR-2) (Hess et al., 2003). For long-term minimum inundation, the interannual variability seems to be a minor factor since the Hess dataset, which estimated a larger figure than the other ones, was developed for a year with minimum water levels higher than those during Chapman's acquisition dates, but lower than those during Rosenqvist's ones (see Fig. 8 in Rosenqvist et al., 2020). Thus, the larger minimum inundation extent by Hess et al. (2015) seems to be more related to algorithm differences (Figure S2). For the maximum water levels, Hess's period was associated with an average year condition, below the water levels in Chapman and Rosenqvist, and this may explain the relatively higher long-term maximum inundation by Rosenqvist, while Chapman's smaller values are likely due to algorithm differences. For the western basin, Hess's estimate is based on JERS-1 data mostly from June 1996 (Hess et al., 2015), which could have missed some of the inundation in this region as in the Pacaya-Samiria region, and may partly explain the larger value by Rosenqvist (see next section). Spatial resolution is also an important factor: Rosenqvist's

resolution is 50 m, and is capable of representing smaller floodplains than the other two (Figure S3), as will be discussed in the next section.

Assessment of other datasets

The coarse-scale products and hydrologic models generally estimate smaller annual inundation areas in comparison to the SAR datasets, with the exception of SWAF-HR, WAD2M and CaMa-Flood that yield similar annual maximum inundation. This results from the low sensitivity of the passive microwave signal, which underlies most coarse-scale datasets, to detect small fractional flooded areas within the grid cells, flooding under particularly dense vegetation, and flooding of short duration (i.e., less than one month of consecutive inundation) (Hamilton et al., 2002). The higher sensitivity of the SWAF-HR may be associated with the use of L-Band passive microwave. Given the long-term data availability from dynamic, coarse-scale datasets, their long-term estimates are closer to the SAR ones, varying from 450,800 km² (THMB) to 630,900 km² (SWAF-HR), when compared to the annual scale analysis. Therefore, no clear relationship between long-term minimum or maximum inundation and the spatial resolution of the products is observed (Figure 6), which could be expected if analyzing the annual values (Figure 5).

As expected, the optical-based products (GSWO, G3WBM, GLAD) cannot map flooded vegetation and thus lead to much lower inundation area estimates at the basin scale (Aires et al., 2018; Parrens et al. 2017). Similarly, the ESA-CCI product, based on land cover classification of optical imagery with the addition of SAR inputs for delineation of wetland areas, yields low basin-wide inundation areas, although relatively higher than the purely optical-based estimates. In turn, the multi-satellite-based CIFOR provides an unrealistically large estimate of maximum inundation area (872,700 km²), which may be due to overestimation of soil moisture by the topographic index used. This method is sensitive to rainfall overestimation, which may have occurred in 2011, the year for which CIFOR was developed (Gumbricht et al., 2017). While the product does represent well the spatial extent of peatlands across the Pacaya-Samiria region (Gumbricht et al., 2017), its estimation of widespread inundation across the basin has limitations to represent the large Amazonian river floodplains, especially the forested ones, which are classified as "swamps (including bogs)" by this dataset together with large patches of interfluvial areas (Figure S4).
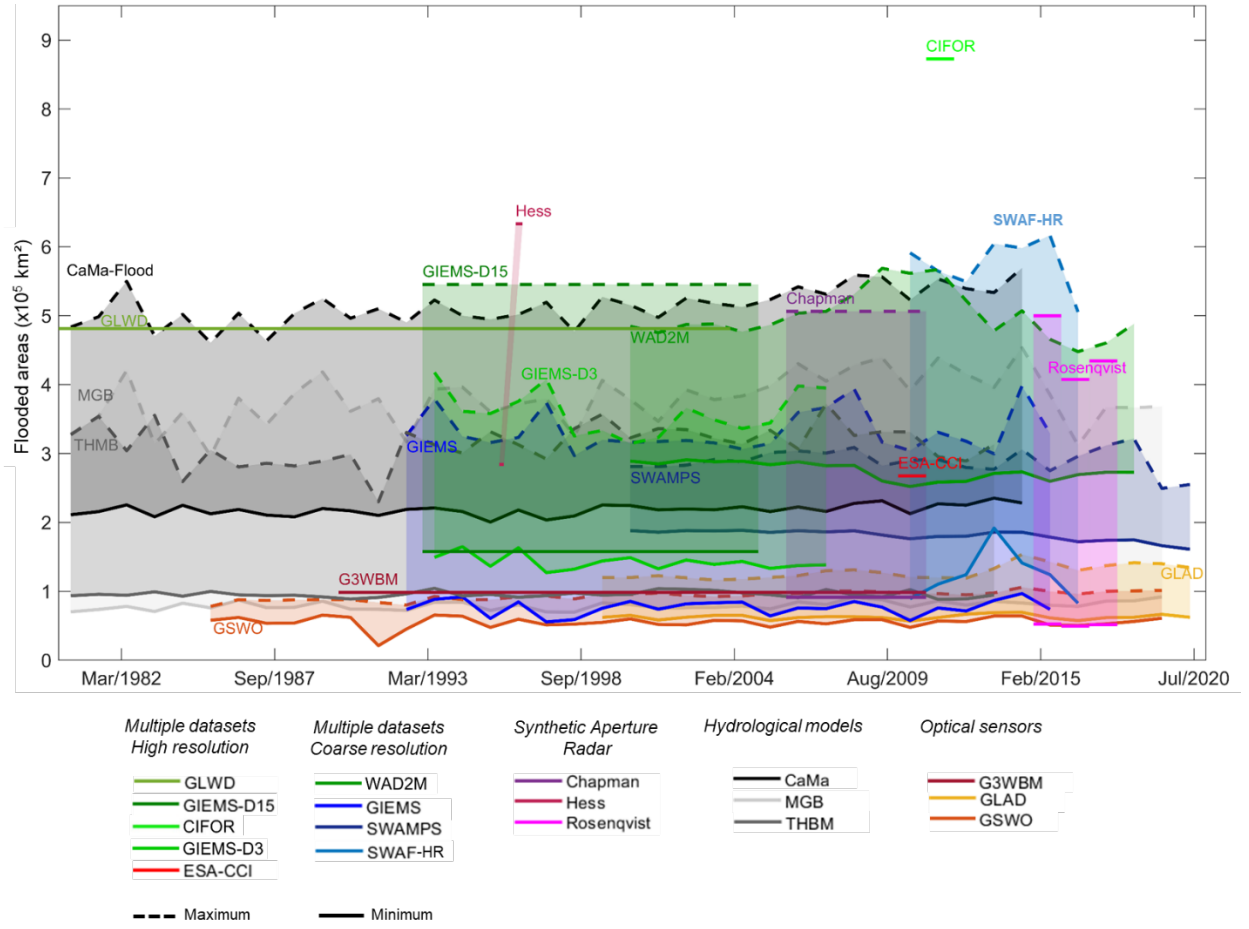
19

Figure 5. (a) Annual minimum and maximum flooded areas for the Amazon basin (< 500 m) for 18 basin-scale products over their respective observation time periods.
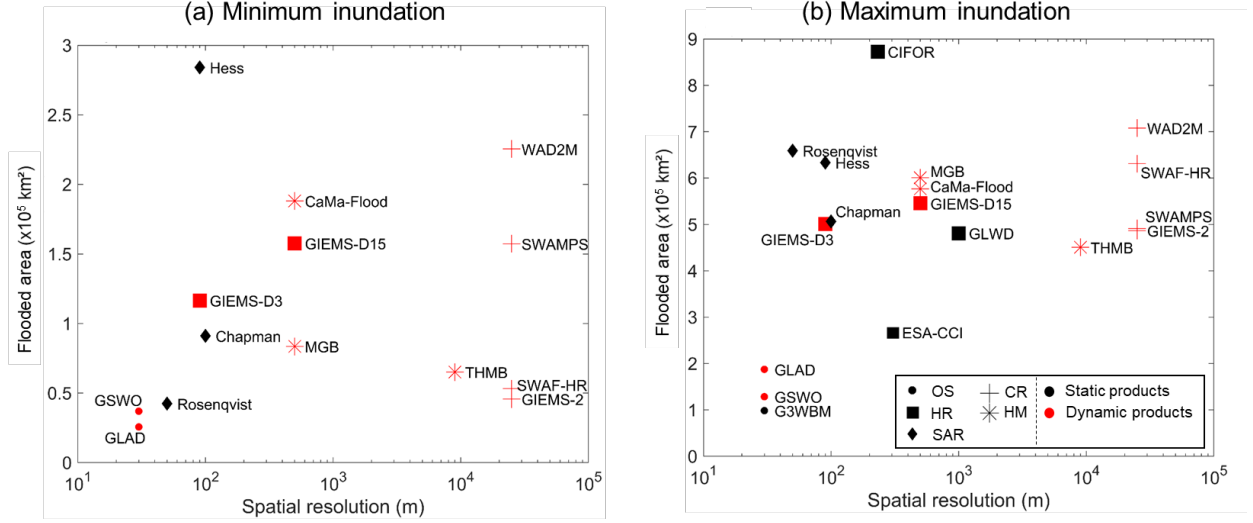
Figure 6. Summary of long-term (a) minimum and (b) maximum inundation for the 18 basin-scale products, which are categorized into five types (optical data; combination of datasets at high resolution; combination of datasets at low resolution; synthetic aperture radar; and hydrological models). The dynamic product estimates are not directly comparable to the static ones; thus, each is colored differently: red (dynamic) and black (static). Legend for product tyes: OS: Optical Sensor; SAR: Synthetic Aperture Radar; HM: Hydrological Model; HR: multiple datasets at High Resolution; CR: multiple datasets at Coarse Resolution.

Table 2. Basin-wide, long-term minimum and maximum inundation estimates for the 18 basin-scale products.

Product	Minimum (km²)	Maximum (km²)
G3WBM	–	98,500
GSWO	37,000	128,500
GLAD	25,700	187,600
ESA-CCI	–	267,400
THMB	65,200	450,800
GLWD	–	481,200
GIEMS-2	45,800	486,600
SWAMPS	157,400	491,100
GIEMS-D3	116,600	500,700
Chapman	91,200	506,400
GIEMS-D15	157,700	545,400
CaMa-Flood	188,100	576,700
MGB	83,600	600,900
SWAF-HR	53,200	630,900
Hess	284,200	633,500

21

Rosenqvist	42,400	659,100
WAD2M	225,500	707,900
CIFOR	-	872,700

3.2 How much inundation is estimated to occur at individual wetland scales?

Overall assessment

Inundation estimates for the 18 basin datasets were compared with the estimates for 11 individual wetland complexes, which are assessed through long-term maximum inundated areas (Table 3), long-term minimum areas (Supplementary Table S3), and performance metrics between basin-scale datasets and local reference sites (Supplementary Table S4). The subregional products are considered local references, given the ground validation performed for most of them, as well as the use of a region-specific classification, and the often higher spatial resolution (12.5 m for some based on ALOS-PALSAR imagery).

Which are the largest Amazon wetland complexes, in terms of long-term maximum inundation extent? The Amazon River floodplains (from Iquitos to Gurupá) and the Llanos de Moxos regions present the largest values: 106,800 $\pm$ 25,800 km² and 113,500 $\pm$ 53,400 km², respectively when considering the three SAR-based products, and 94,100 $\pm$ 32,500 km² and 85,300 $\pm$ 52,400 km² when considering all 18 basin-scale datasets. Besides these two areas, the third largest Amazon wetland region is Pacaya-Samiria, with 29,700 $\pm$ 20,600 km² (all products) and 40,000 $\pm$ 4,200 km² (SAR).

The comparison of the long-term maximum and minimum observed inundation over the available time periods indicates differences between basin-scale products, subsampled for the subregions, and the local references. Overall, the local products had a larger maximum inundation extent. The underestimation by the basin-scale datasets varied from 49% for the Pacaya-Samiria region to 5% for the lower Amazon. Only three products overestimated the locally estimated maximum extent of inundation: GIEMS-D3, GIEMS-D15 and GLWD. The three basin-scale SAR products (Hess, Chapman and Rosenqvist) underestimated the maximum extent in the regions represented by all local products, except Rosenqvist for Janauacá Lake, and Hess for the Llanos de Moxos region. This is likely related to the higher resolution of many of the individual products (e.g., 12.5 m original and 25 m final resolution for the Uatumã ALOS-PALSAR classification by Resende et al., 2019), image acquisition period, as well as fine-tuning that may occur with dedicated products for a particular region.

To investigate the depiction of inundation seasonal patterns by the various products, we assessed the correlation between the absolute inundated areas from the dynamic products and the local wetland time series in each local area (Table S3). Overall, all products agreed well (average Pearson correlation larger than 0.63

for the four local wetlands with available time series), showing a similar depiction of the inundation seasonality. However, their ability to monitor high-resolution flood frequency is limited, as will be further discussed in the "Perspectives and Recommendations" section. A visual comparison of the time series (Figure S6) shows agreement on seasonal timing of flooding and drainage, but disagreement in the extent of inundation. In particular, two datasets have a small overall annual amplitude (SWAMPS and WAD2M).

Overall, four products had the best overall representation of inundation spatial patterns (Fit metric; see Equation 1 in Methods section 2.3), as analyzed at 1 km pixel resolution, in comparison to the reference data: Hess, GLWD and the two hydrodynamic models (MGB and CaMa-Flood), which were associated with an average Fit metric between 0.64 and 0.67 (Table S3). While hydrologic models such as MGB, CaMa-Flood and THMB have a satisfactory agreement basin wide, they are unable to represent wetlands not primarily inundated by rivers (Fleischmann et al., 2020; Zhou et al., 2021). For example, the Llanos de Moxos inundation is underestimated by both CaMa-Flood and MGB with low Fit metric values (0.19-0.28; Table S3). This is expected for interfluvial wetlands such as Llanos de Moxos and Roraima, where much of the flooding is caused by poor drainage of local rainfall and tends to be shallower, as opposed to overflow of large rivers onto adjacent floodplains. The four alternative local products assessed here - three hydrological models (one for Curuai and two for Janauacá) and one classification of ALOS-PALSAR data for the Llanos de Moxos area - were generally better or similar to some of the best-performing basin-scale products, as could be expected given their fine tuning for the specific areas, which often includes local topography surveys.

Some of the products fusing multiple data sources overestimated the local wetland inundation area the most, especially GIEMS-D15, GIEMS-D3 and GLWD. Furthermore, the CIFOR product was originally designed for peatland mapping in the tropics, and generally overestimates inundation, suggesting a widespread distribution of wetlands along interfluvial terraces across the whole basin. For the local floodplain areas, however, CIFOR generally underestimated inundation and had a poor representation of spatial patterns of inundation (low Fit metric). WAD2M underestimated the maximum inundation the most, which is understandable given its removal of open water areas and because its main inputs (CIFOR and SWAMPS) also underestimate local inundated areas. This does not mean, however, that WAD2M underestimates basin-wide inundation, since it tends to scatter floodable areas around the basin, as does the CIFOR product.

Individual wetland inundation patterns with SAR data

Regarding the maximum inundation extent, the Janauacá case provides a representative example to understand the differences among multiple L-band SAR products: these estimated total inundated area as 209 km², 184 km² and 446 km² for Hess, Chapman and Rosenqvist, respectively, in contrast to 404 km² with the local ALOS-PALSAR-based data (12.5 m resolution; Pinel et al., 2019). Part of

these differences occur because of interannual variability, but other factors such as spatial resolution and algorithm differences seem relevant. The Rosenqvist product led to a more consistent estimation of the spatial inundation extent in terms of maximum inundation (Table 3) and inundation spatial patterns (Fit metric; Table S3), which can be a consequence of its higher spatial resolution (50 m) in contrast to the other two (90 m; Figure S3). Overall, Rosenqvist provided the largest inundation extent among SAR products across all areas along the Amazon mainstem floodplain, except for the Curuai floodplain and the savanna wetlands, as well as the smallest differences with reference data (-9% ± 13%; average ± S.D.). Hess estimated the largest inundation values in the savanna wetlands (Llanos de Moxos, Roraima and Negro). However, Hess's values are larger than the subregional estimate for Llanos de Moxos (+39%), while the other two SAR estimates are lower (-26% and -41% for Chapman and Rosenqvist, respectively).

One important question remains about the low-water period, as discussed in the previous section for the basin-scale analysis. Hess's product suggests much more inundation for this period for the Amazon mainstem floodplains (54,500 km²), mainly for the upstream forested reaches, and for the whole basin in general (284,200 km²), than recent estimates with ALOS (28,500 and 91,200 km²) and ALOS-2 data (19,500 and 42,400 km²). An assessment with the local products along the Amazon floodplain suggests that Hess overestimates the minimum extent for Curuai, Mamirauá and lower Amazon, and is accurate for the Janauacá floodplain lake. Rosenqvist generally underestimates the minimum inundation. For instance, for the Mamirauá dataset, the minimum extent (i.e., permanently flooded areas) sums up to 715 km², which is increased to 1545 km² if considering all pixels flooded for more than 295 days per year. For this area, the SAR estimates are 1756 km² (Hess), 866 km² (Chapman) and 422 km² (Rosenqvist). Overall, this suggests that the actual value of minimum inundation across the central Amazon floodplains is somewhere between Hess and Rosenqvist's estimates.

Challenges over floodable savannas

Large discrepancies are observed for the Roraima and Negro floodable savannas. Roraima wetlands are small river floodplains interspersed with open savannas subject to flooding, which can be identified by optical data. In addition, the typical timing of high and low water in the Roraima region coincides approximately with the JERS-1 dual-season mosaics that were designed to reflect the seasonality of the central Amazon River floodplain (Hamilton et al. 2002). For these reasons, the Hess product seems to satisfactorily represent most of the Roraima wetlands, but misses some small-scale riparian forests, given its 90 m spatial resolution and snapshot coverage that likely missed flooding events on smaller, flashier rivers (Figure S5). Thus, the maximum inundation is likely higher than the Hess estimate (8,900 km²), which in turn is larger than the other SAR products (1,900 - 4,100 km²). The only dataset to estimate a higher value is the coarse SWAF-HR product (18,100 km²), which is similar to the value pre-

viously estimated by Hamilton et al. (2002) (16,500 km²), also with coarse data (SMMR passive microwave), though a part of the discrepancy may be due to interannual variability. More studies are necessary for this area to understand its actual inundation extent and dynamics. Similarly, the inundation estimates in the Negro interfluvial savannas are subject to large uncertainty, with the long-term maximum inundation varying between 95 (GLWD) and 20,700 km² (CIFOR), considering all basin-scale datasets. SAR-based product estimates were between 5,900 and 15,800 km². In turn, for the Pacaya-Samiria interfluvial area, which includes a large complex of forested wetlands, peatlands and palm swamps, the discrepancies are smaller than for the savanna interfluvial regions, although still considerable. The SAR basin-scale estimates range was between 24,000 (Chapman) and 56,200 km² (Rosenqvist), with the local reference yielding 57,900 km². The good agreement between Rosenqvist and the local reference product was already reported by Rosenqvist et al. (2020).

Table 3. Long-term maximum inundation areas for the 11 local wetland areas, for the local products (up to three local products per area) and the 18 basin-scale products. The comma-separated values refer to the following local scale products, respectively: Curuai - ALOS (Arnesen et al., 2013) and LISFLOOD-FP model (Rudorff et al., 2014); Uatumã - ALOS (Resende et al., 2019); Janauacá - ALOS (Pinel et al,. 2019), hydrologic model (Bonnet et al., 2017) and TELEMAC-2D model (Pinel et al., 2019); Mamirauá - ALOS (Ferreira-Ferreira et al., 2015); Pacaya-Samiria - ALOS-2 PALSAR-2 (Jensen et al., 2020); Llanos de Moxos - MODIS (Ovando et al., 2016) and ALOS (Ovando et al., 2016); and Lower Amazon - MODIS (Park et al., 2019). Average, standard deviation (S.D.) and coefficient of variation (CV) are presented for each area in the last row.

		Product	Curuai	Uatumã	Janauacá	Mamirauá	Pacaya-Sami
		Local	4162, 3720	1471	404, 336, 176	4476	57913
Optical sensors	1	G3WBM	2732	628	135	795	2694
	2	ESA-CCI	3236	855	260	3045	28727
	3	GLAD	3479	832	204	1141	4196
	4	GSWO	3163	675	150	962	3637
Multiple datasets	5	GLWD	4275	2267	535	4259	79124
	6	CIFOR	3796	994	177	1714	52590
	7	GIEMS-D15	4635	2681	416	2444	44536
	8	GIEMS-D3	4643	2732	505	3569	11562
	9	WAD2M	681	243	166	888	42635
SAR	10	Chapman	2796	934	184	2694	24001
	11	Hess	3996	1045	209	3985	39741
	12	Rosenqvist	3055	1238	446	4362	56160
Passive micro-wave	13	GIEMS-2	3080	984	623	3344	23344
	14	SWAMPS	3359	722	280	1131	9929
	15	SWAF-HR	4439	2199	388	3205	16900
Hydro-logical models	16	CaMa-Flood	4246	1613	534	3208	34096

17	MGB	4098	1549	474	3750	33344
18	THMB	2883	554	164	2840	27748
	Average	3477	1264	325	2630	29720
	S.D.	949	748	163	1226	20591
	CV	27%	59%	50%	47%	69%

3.3 How much do the products agree on the spatial distribution of inundation?

Agreement maps of the 14 high resolution products (< 1 km) were developed for both long-term maximum and minimum inundation areas, based on the number of inundation products coinciding over a 1 km pixel (Figures 7 and 8 and their categorization for specific regions in Figure 9). Overall, 26% of the Amazon lowlands area has been estimated as subject to inundation by at least one product (bottom left panel, Figure 7). Based on the agreement between two datasets, this value decreases to 948,300 km², which is larger than the value estimated when four products agree (553,200 km²). This latter estimate is more similar to the average maximum inundation as estimated by the ensemble of datasets (559,300 km²) and the three SAR-based ones (599,700 km²). Furthermore, there is a lower agreement for the minimum inundation than for the maximum inundation among individual regions (Figure 9).

For specific regions, a high degree of agreement for floodplains dominated by open water areas is evident for the lower Amazon reaches, followed by the forested floodplains fringing large rivers, especially along the Amazon mainstem, Purus and Negro rivers. The generally higher accuracies over central Amazon floodplains may also be related to the attention that product developers have devoted to it, in contrast to other regions. Furthermore, the maximum floodplain extent can be somewhat delineated with terrain elevation data (i.e., DEMs) with algorithms such as HAND (Rennó et al., 2008), which helps to explain the relatively small disagreement for floodplains fringing the largest rivers, particularly effective with vegetation bias-removed DEMs (O'Loughlin et al., 2016; Yamazaki et al., 2017). The best agreement (for both maximum and minimum inundation extent) occurred over the Curuai floodplain along the lower Amazon mainstem, with 37% of its area being estimated as flooded by all 14 products for the maximum inundation (Figure 9a). An agreement among all 14 products occurred, in part (i.e., more than 10% of the wetland area), for the central Amazon floodplains (Curuai, Uatumã, Janauacá and lower Amazon) because of their relatively large fractions of open water areas.

In the interfluvial wetlands (Negro and Roraima savannas, Pacaya-Samiria and Llanos de Moxos), the inundation patterns are less dependent on riverine overflow and more dependent on local rainfall, making them less predictable (Hess et al., 2003). The disagreement for both maximum and minimum inundation area is the largest across all regions, e.g., 65–78% of their flooded areas were mapped by only one model for the minimum inundation (Figure 9b). The Llanos de

26

Moxos is conspicuous as a region of particular disagreement, perhaps because flooding is mainly shallow and in vegetated areas (mainly savannas/grasslands), and is highly variable from year to year. In general, the smaller the flooded patches the higher the challenge to map them, not only because of resolution but also due to small scale topography and more surface heterogeneity. Similar disagreement occurred in other interfluvial wetlands as the Negro and Roraima savannas, and would be expected elsewhere in savanna floodplains of South America (e.g., Pantanal, Llanos de Orinoco and Bananal Island; Hamilton et al., 2002). The poor agreement over interfluvial areas, however, may also partly reflect the longer history of study of Amazon mainstem floodplains, for which there are river gage records that reflect floodplain water levels and inundation, while more remote areas such as the Negro savannas and Pacaya-Samiria regions are more challenging to represent with a few gages, and have received less attention. The challenges in estimating inundation over interfluvial areas also affect the SAR-based products, which disagreed over these regions (see Section 3.5 and discussion in Rosenqvist et al., 2020).
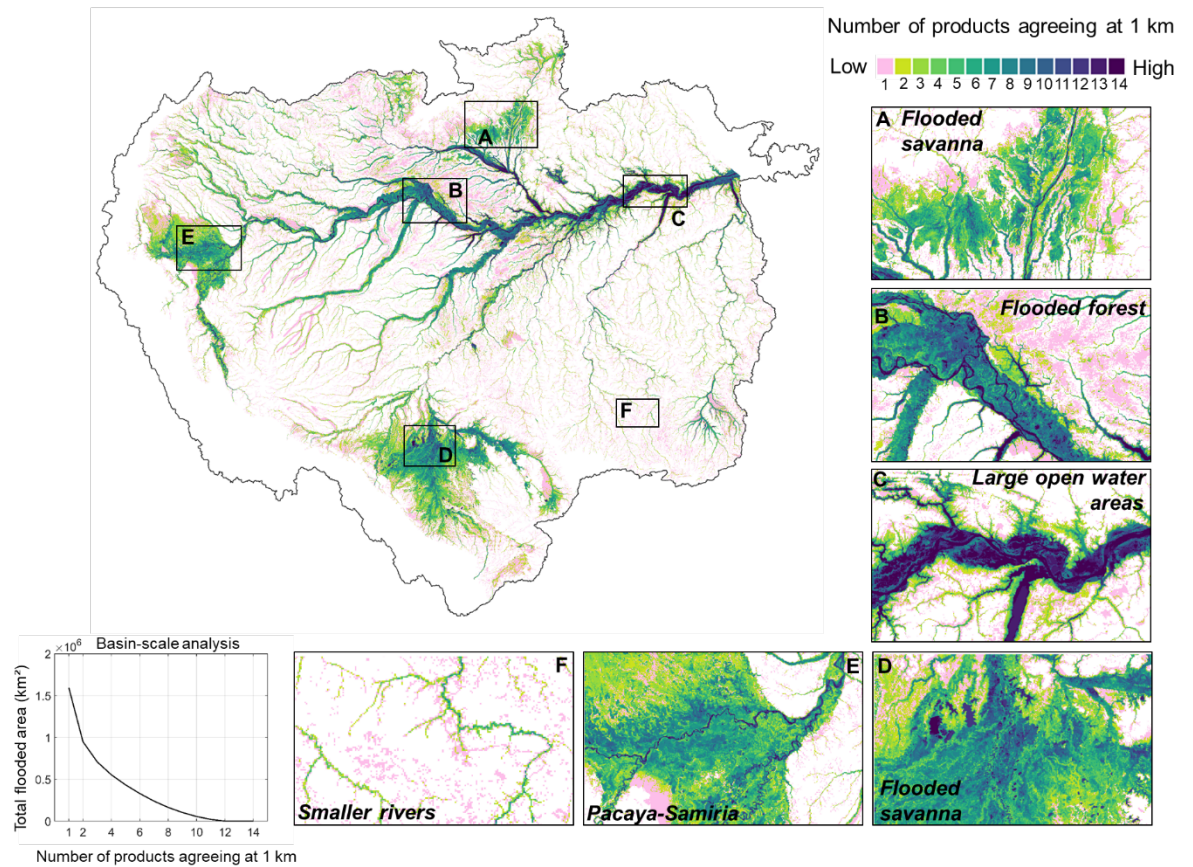
Figure 7. Agreement for maximum flood extent among 14 basin-scale prod-

ucts at high resolution ($\leq$1 km): G3WBM, ESA-CCI, GLAD, GSWO, GLWD, Gumbricht, GIEMS-D15, GIEMS-D3, Chapman, Hess, Rosenqvist, SWAF-HR, CaMa-Flood, MGB. For a given pixel of a product with resolution higher than 1 km, more than 50% of flooding at the maximum inundation extent is classified as flooded.
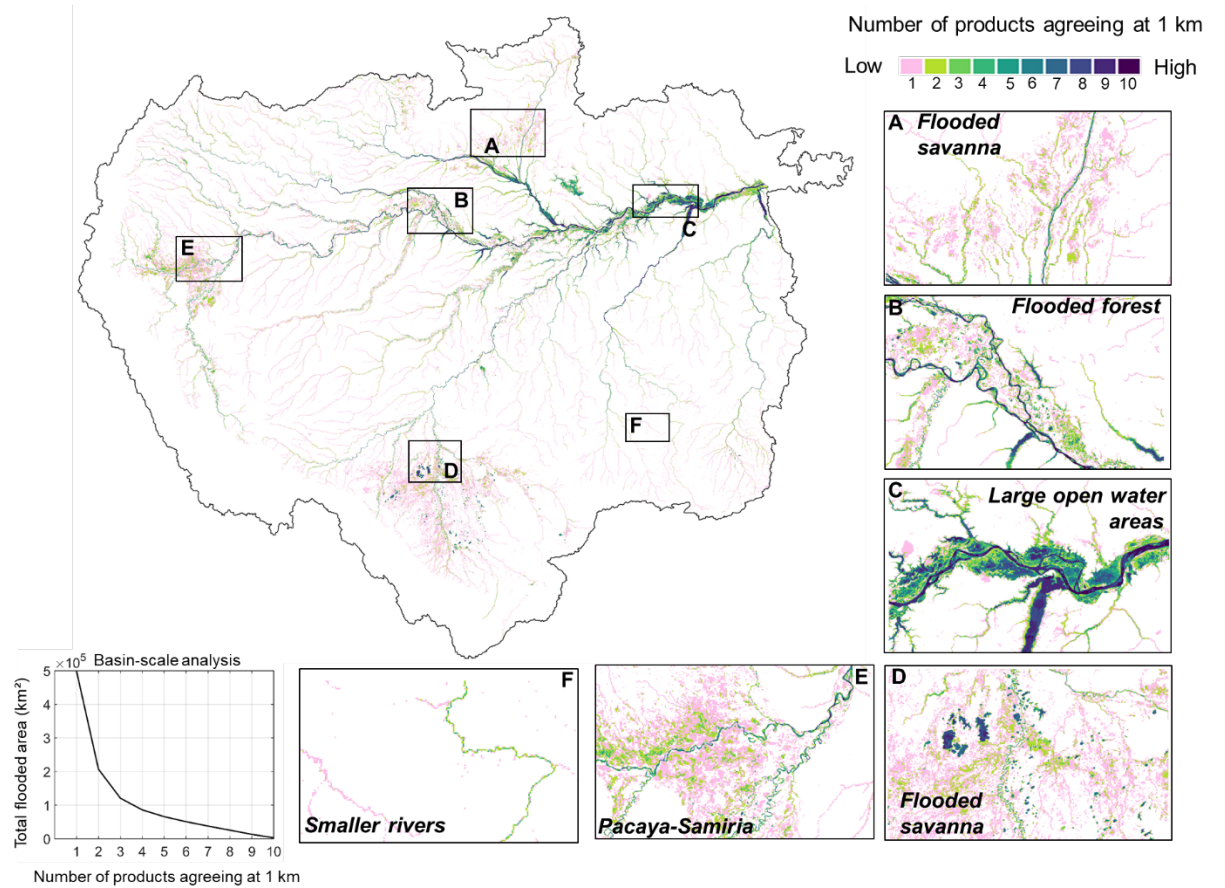
Figure 8. Agreement of minimum flood extent at 1 km resolution. 10 basin-scale products at high resolution ($<=$ 1 km) are compared in this analysis at 1 km: GIEMS-D15, Chapman, Hess, Rosenqvist, SWAF-HR, CaMa-Flood, MGB, GIEMS-D3, GSWO, GLAD. For a given pixel of a product with resolution higher than 1 km, more than 50% of flooding for the minimum inundation extent is classified as flooded.
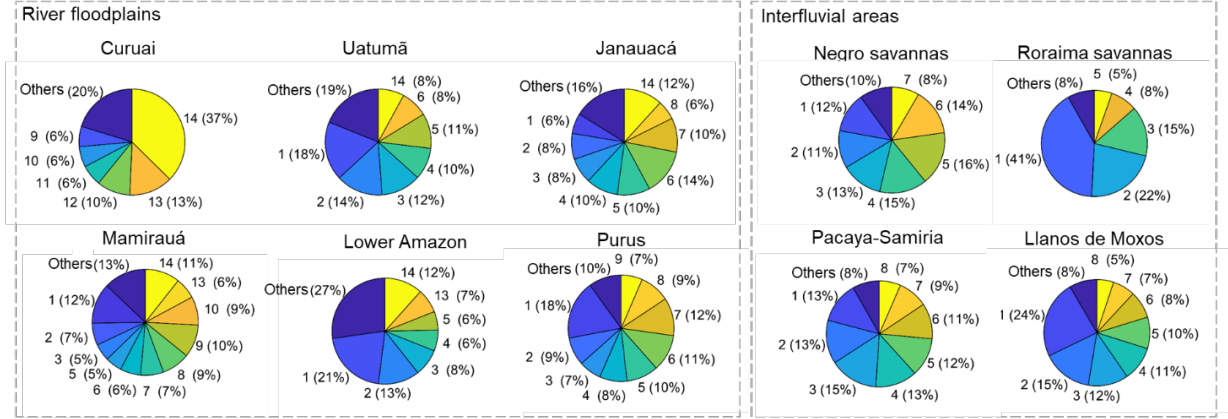
Figure 9. Degree of agreement for (a) maximum and (b) minimum inundation area for 10 local wetland regions, based on the 1 km agreement map (Figures 7 and 8). The percentage values indicate the fraction of each area where a given number of products agreed that it was flooded, e.g., 14 models agreed on 37% of the Curuai area to be flooded in the maximum inundation extent. The class with number 1 indicates the fraction of the area that only one product estimated as being flooded. The class "others" refers to all classes that had less than 5% of pixels.

3.4 Quantifying the inundation extent of different wetland types

Amazon wetlands include a myriad of ecosystems varying in geomorphology, hydrology, and vegetation cover. The classification system proposed by Junk et al. (2011) differentiated Amazonian wetlands according to amplitude and range of water level change. Wetland types ranged from the forested swamps with stable water levels to river floodplains with oscillating water levels, and to interfluvial areas with small seasonal water level amplitude due to the main

29

contribution of local rainfall and runoff (Fleischmann et al., 2020; Junk et al., 2011; Ovando et al., 2018).

A simpler yet hydrologically meaningful classification is the categorization into river floodplains and interfluvial wetlands adopted here, since the former typically have a greater hydrological connection to the main river and thus are subject to a different control of inundation area by river levels (Reis et al., 2019a). We performed a quantitative analysis of the inundation area in these two main hydrological classes. All pixels considered flooded by at least two products, based on the 1 km agreement map for maximum inundation extent (Figure 7), are presented in Figure 10. Overall, the medium to large river floodplains (upstream drainage area > 1000 km²) have a larger inundation extent than the category with small floodplains and interfluvial areas. An average total area subject to inundation of 317,800 ± 84,400 km² (average ± S.D.; median equal to 323,700 km²) was obtained, not including the optical and land cover products (G3WBM, GLAD, GSWO and ESA-CCI). A greater area for large floodplains was estimated by all products except for CIFOR, SWAMPS and WAD2M. Two datasets estimated a similar value between the two classes (Chapman and GIEMS-2), which may be related to an overestimation of basin-scale isolated flooded patches.

Large floodplains fringing the main rivers, especially along the Amazon River, has been largely addressed by previous studies (Table 1 and Table S1). However, large river floodplains are also present in less studied reaches, e.g., in the upper Napo and Içá rivers in northwest Amazon basin, and upper Xingu in the southeastern portion (see location in Figure 1). These upper reaches are subject to more sporadic, flashy river hydrological regimes (Hamilton et al., 2007), which make their inundation area difficult to map with current products of relatively low temporal resolution. In our analysis, the non-floodplain areas include mainly the large interfluvial areas (black rectangles in Figure 10), small river floodplains that are challenging to detect with currently available products, and some reservoirs, such as Balbina reservoir on the Uatumã River.

Besides the central Amazon floodplains, which have been widely studied, other wetland complexes require more attention, as the Negro and Roraima savannas; the latter was only assessed by a single study to our knowledge (Hamilton et al., 2002). The inundation mapping of the Pacaya-Samiria region in upper Amazon has received scientific attention recently (Jensen et al., 2018; Rodriguez-Alvarez et al., 2019), partially because of the region's role as a carbon sink via formation of peat (Draper et al., 2014; Lähteenoja et al., 2012). Regarding open water areas, Melack (2016) reported values ranging from 64,800 km² (Melack and Hess, 2010) to 72,000 km² (SRTM) and 92,000 km² (Hansen et al., 2013) for the Amazon basin (< 500 m). The three Landsat-based products assessed here, which are mainly capable of detecting open water areas, estimate 98,500 km² (G3WBM), 128,500 km (GSWO) and 187,600 km² (GLAD).
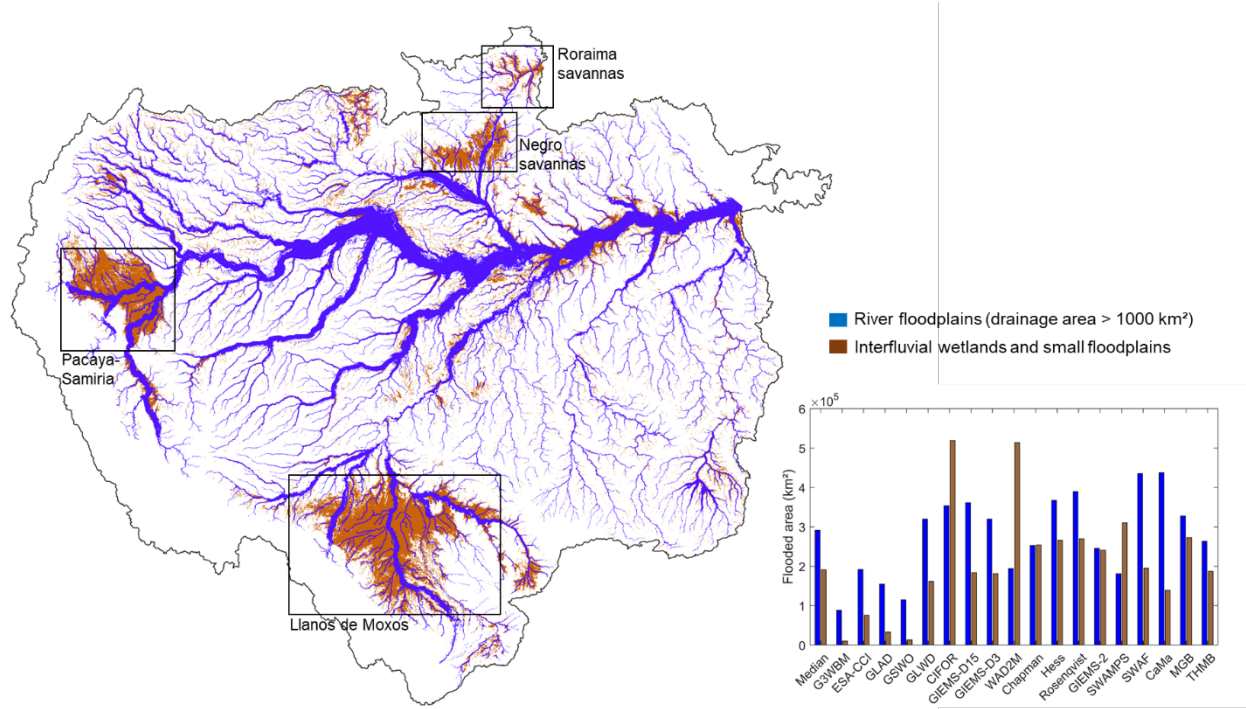
Figure 10. Quantification of maximum inundated areas over river floodplains with drainage area larger than 1,000 km², and interfluvial wetlands and small floodplains (area < 1,000 km²) within the Amazon basin. The maximum inundation map depicts all 1 km pixels with at least two products agreeing (i.e., a reclassification of Fig. 5), in order to avoid overestimation caused by pixels with one only product classifying them as subject to inundation. The four large areas of interfluvial wetlands are highlighted (Pacaya-Samiria, Llanos de Moxos, Negro and Roraima savannas).

3.5 Limitations in comparing the inundation area products

Some of the differences in large-scale inundation mapping highlighted by our comparison occur because distinct products map temporal inundation in different ways, varying for instance in sensor type, post processing, spatial resolution, among others. Figure 11 shows the agreement maps for maximum inundation for four classes of products, considering the 14 basin-scale high-resolution datasets. Those based on multiple datasets (GLWD, CIFOR, GIEMS-D3, GIEMS-D15, SWAF-HR) have the best agreement for the Llanos de Moxos area, and to a smaller degree, for Pacaya-Samiria, Negro and Roraima wetlands. The L-band SAR datasets have less overall agreement (Figure 11c), while the optical data are mainly limited to open water areas in the Amazon mainstem floodplain (Figure 11b). The 1D hydrological models cannot represent interfluvial wetlands where flooding is not controlled by river level and discharge (Figure 11d).
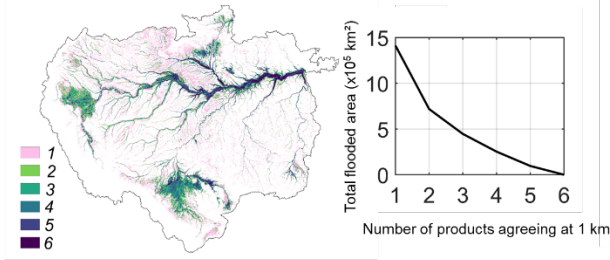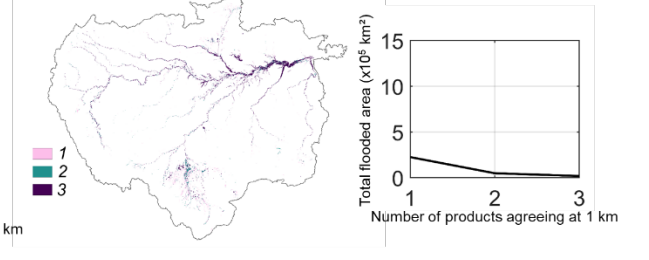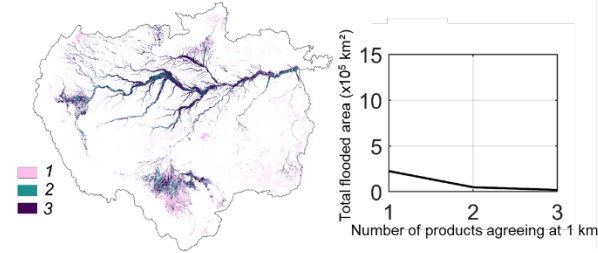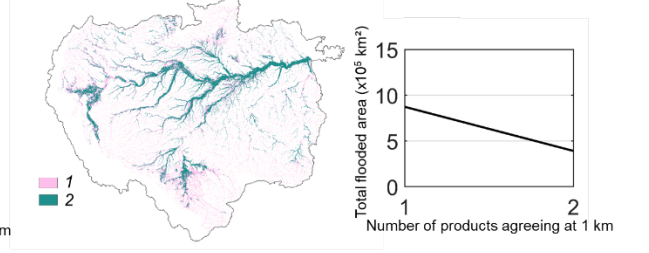
Figure 11. Amazon basin (< 500 m elevation) agreement maps at 1 km resolution, for maximum inundation and for each type of product, considering only the high-resolution products (>1 km spatial resolution): (a) six datasets based on multiple sensor systems (GLWD, CIFOR, GIEMS-D3, GIEMS-D15, SWAF-HR, ESA-CCI), (b) three datasets based on optical sensors (G3WBM, GLAD, GSWO), (c) three datasets based on synthetic aperture radar (Hess, Chapman, Rosenqvist), and (d) two hydrological models (MGB and CaMa-Flood). The right column graphs present the total inundation area in the Amazon basin for a given number of products agreeing, e.g., the basin area where the two hydrological models (Fig. d) agree to be flooded is 390,900 km².

The different methodologies used to produce each dataset complicate their direct comparison (Rosenqvist et al., 2020), and some methodological differences produce systematic differences and bias among the data sources included in our comparison. Here we used long-term dynamic inundation datasets (e.g., GIEMS or hydrologic models), short-term dual-season products (e.g., Rosenqvist, based on four years), and products derived for a particular year (e.g., Hess product). Some datasets use alternative approaches to derive long-term maximum inundation area, such as GIEMS-D15, which generated estimates by fusing 3-year moving-window maximum values of GIEMS with the GLWD dataset. Therefore, a comparison of all these datasets must be performed with consideration of their methodology. For instance, the comparison of dual-season products against monthly datasets can yield erroneous conclusions, although it has been a common practice to directly compare such datasets. Some datasets also consider a "high-water assumption" (Ferreira-Ferreira et al., 2015; Hess et al., 2003), whereby the high-water maps are forced to contain all flooded pixels from the

low-water map.

In addition to methodological differences, each dataset was developed for different periods (Table 1), and thus interannual and seasonal variability accounts for some of the differences among them. To address this, we performed an annual analysis (Figure 5), which suggests that the long-term inundation estimate is fairly stable for each product despite some interannual differences. In fact, the temporal variability of each product is generally smaller than the differences in comparison with the other estimates. However, the Amazon hydrological cycle has been shifting over decades (Barichivich et al., 2018; Gloor et al., 2013), and a recent increase in recorded floods over central Amazon suggests a new hydro-climatic state (Espinoza et al., 2019). Some wetlands have also been subject to forest loss, and so the detectability of inundation by remote sensing may have increased over time, e.g., major deforestation has occurred along the lower Amazon floodplain (Renó et al., 2011). Similarly, widespread burning might be converting black-water floodplain forests into savanna vegetation (Flores and Holmgren, 2021). In addition, in some regions, such as the southern Amazon, an increase in the dry-season length has been observed, which is a major climatic constraint for forest sustainability (Fu et al. 2013; Staver et al., 2011). However, analyzing long-term change in inundation patterns is beyond the scope of this study, and thus we assumed stationarity in our comparison framework.

Another important challenge is to find a common definition of wetlands among products. Here we focused on inundation extent, however some products (e.g., CIFOR) represent peatland locations instead of inundated areas, although their peat formation can broadly be found within inundated areas. Also, Amazonian floodplains that regularly dry completely often do not accumulate peat. Some products based on SAR or passive microwave may also be sensitive to saturated soil without standing water above it, and thus the observed inundation can have some ambiguity. Hydrologic models provide simulated surface water extent, and we mapped inundation accounting for pixels with water depth greater than zero. While hydrologic models have uncertainties related to model structure (e.g., are the represented processes adequate to simulate inundation?), input data (e.g., DEM and climate forcing) and parameterization (e.g., soil water capacity and river channel width and depth; assumptions of level water surfaces between rivers and their floodplains), remote sensing-based datasets have uncertainties related to spatial and temporal scales (e.g., coarse-scale products not capable of detecting small patches), and detection uncertainty (e.g., dense vegetation canopies can obscure passive microwave emission from underlying surfaces). Thus, a comparative framework provides an opportunity to highlight and stress the uncertainties and limitations of each dataset.

Hydrologic models currently available at the Amazon basin scale are one-dimensional, and thus are capable of simulating flooding mainly along river floodplains, as corroborated by various validation exercises in the Amazon that have relied on the Hess, GIEMS and SWAF-HR datasets (Fleischmann et al., 2020; Luo et al., 2017; Paiva et al., 2013; Zhou et al., 2021). These models

are also largely dependent upon accurate DEMs, which are still challenging to obtain over tropical forested floodplains. Furthermore, given that a 500 m elevation mask (Amazon lowlands) has been used for some SAR products (Hess et al., 2015), and the difficulty of some radar and passive microwave products to detect inundation at high elevations due to slope and snow effects, for instance (Parrens et al., 2017), we have adopted this lowlands mask to improve the comparability among datasets. However, some products, especially the hydrological models (MGB, CaMa-Flood and THMB), are capable of estimating inundation in higher elevation parts of the basin, although in this case uncertainties may also be large given errors in precipitation (low density of in situ gauges and high rainfall spatial heterogeneity) and thus runoff fields over mountainous areas, as well as the tendency for river flows to vary over short time scales (Espinoza Villar et al., 2009; Zubieta et al., 2015). Furthermore, the availability of in situ river discharges for model calibration and validation is also low in the Andean and highland portions of the western Amazon (Feng et al., 2020; Wongchuig et al., 2019; Zubieta et al., 2017).

Our analyses were performed at 1 km resolution and at regional scales, which avoids geolocation problems that are common if performing analyses at higher resolutions (e.g., 30 or 90 m). Small disagreements among our estimates and the values presented in the original publication may arise from the use of the WGS84 datum with a geographical coordinate system for all datasets (except for SWAMPS which was provided in the EASE-Grid format). Also, the coarse-resolution products, especially GIEMS-2 and SWAMPS with 25 km spatial resolution, can be difficult to compare with local wetland products (e.g., Curuai and Janauacá), since only a few 25-km pixels may be located within the wetland boundaries.

The quantification of inundation over larger river floodplains (Figure 10) is also subject to uncertainties. The maximum floodplain lateral extent was estimated based on an automatic buffer procedure around the Hydrosheds drainage network, further manually edited by considering the three SAR-based, basin-scale products and the MERIT DEM-based topography. Although it captures the basin-wide geomorphological differences along major floodplains, some uncertainties remain regarding the true lateral extent for areas where rain-fed savanna floodplains are present (e.g., Llanos de Moxos, Roraima), and areas of widespread flooding extending far from the main rivers (e.g., Pacaya-Samiria). For these areas in particular, we assumed buffer values similar to adjacent upstream and downstream floodplains (e.g., the Amazon River downstream of Pacaya-Samiria), which is reasonable but should undergo future scrutiny, mainly with local ground-based surveys.

4. Perspectives and recommendations

Considerable advances have been achieved in recent decades in the mapping of inundation extent across the Amazon basin. Here, we have presented an analysis of 29 inundation datasets for the basin, covering multiple scales, spatial and temporal resolutions, and data sources. We showed that large discrepancies

persist, and this is especially true at local scales. This final section presents some perspectives and recommendations for future development of inundation mapping in the world's largest river basin.

Which are the most reliable data sources for inundation mapping in the Amazon River basin available today?

At basin scale, the Rosenqvist ALOS-2 PALSAR-2 product is available at 50 m, and shows a good overall agreement with the 90 m Hess product over the large river floodplains, while the latter seems more accurate for interfluvial savanna floodplains (e.g., Negro and Roraima ones). The high agreement is observed mainly for the maximum inundation estimates, while for the minimum inundation area, important disagreements persist and more studies should be performed to understand them. Overall, Hess's product has been the Amazon inundation benchmark for many years, and still provides satisfactory estimates. Detection of inundation by L-band SAR has a sound theoretical and empirical basis that has been validated for the Amazon (Rosenqvist et al., 2002; Hess et al., 2003). Optical products with resolution higher than 30 m are available, but detection of inundation is restricted to non-vegetated wetlands and clear-sky periods, as in the lower Amazon floodplains. ALOS-PALSAR at 12.5 m resolution and Sentinel SAR at 10 m resolution (with C-band and limited vegetation penetration) can be applied to specific regions. Time series of these products can estimate seasonal variations in inundation, but are limited by the length of the acquisitions. Weekly to monthly, spatially coarser data (25 km) are available from passive microwave-based datasets such as GIEMS, SWAF and SWAMPS. Downscaling techniques have improved their spatial resolution to 90 m (GIEMS-D3) and 1 km (SWAF-HR). Hydrological models (e.g., CaMa-Flood and MGB) are capable of accurately estimating inundation over river floodplains, and at temporal resolution depending on the input rainfall data (e.g., hourly to daily). However, they are still limited over interfluvial wetlands with less connection with rivers, unless they are upgraded for simulating 2D inundation processes and complex floodplain flow paths (Fleischmann et al., 2020; Yamazaki et al., 2014).

What are the current capabilities of flood frequency mapping?

At the basin scale, high-resolution, long-term average flood frequency can be estimated by four of the products analyzed here (GIEMS-D3, SWAF-HR, MGB and CaMa-Flood), with spatial resolution ranging from 90 m to 1 km. Although multiple SAR data are currently available (e.g., Sentinel-1, ALOS-PALSAR and ALOS-2 PALSAR-2), they have a limited temporal resolution, and we still do not have a flood frequency product of higher spatial resolution (i.e., better than 90 m) for the whole basin based on SAR. The discrepancies among the available products are notable (Figure 12). The average of the basin-scale flood frequency based on the four products shows a higher agreement for areas with high flood frequency along the lower Amazon (Figure 12a). These are associated with a high proportion of open water areas, and have lower uncertainty across the basin (Figure 12b). Generally, there is a smaller variation along floodplains bordering

the major rivers (except for their fringes) than in interfluvial areas, especially in the Negro and Roraima wetlands (Figure 12b). Detailed inundation mapping for the Mamirauá Sustainable Development Reserve in the Amazon mainstem flood-plain (Figure 12c) reinforces the challenges for mapping local spatio-temporal inundation dynamics. The northern part of the Mamirauá reserve has a shorter flood frequency in all products, while three products (SWAF-HR, GIEMS-D3, CaMa-Flood) estimate that large portions are never flooded. For the southern part, there is some convergence for areas that are frequently flooded.
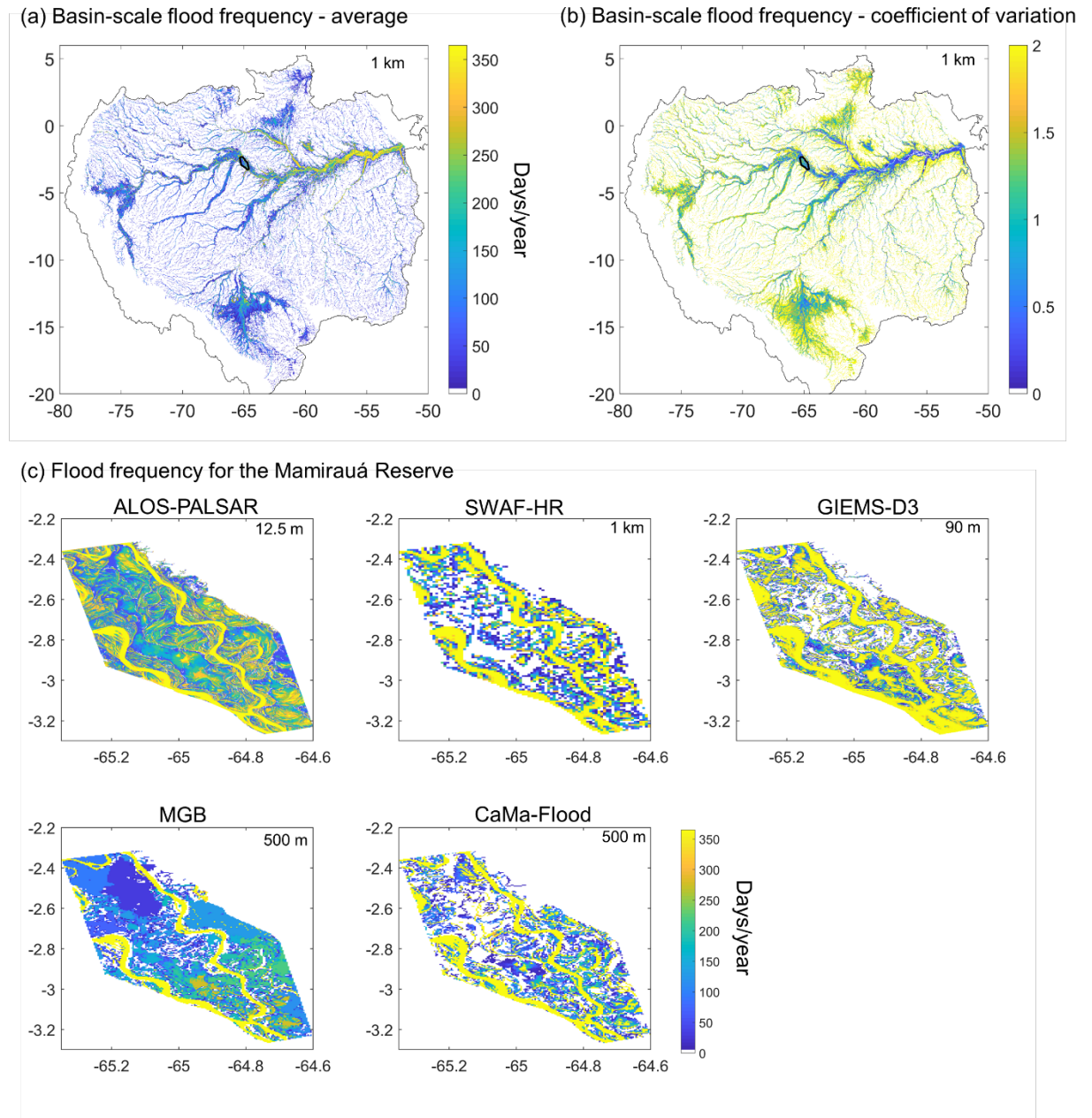
Figure 12. Analysis of flood frequency for (a) basin-wide average and (b) coefficient of variation of the long-term flood frequency estimated from four high-resolution dynamic products (GIEMS-D3, SWAF-HR, CaMa-Flood and MGB). (c) The four basin-scale products are compared to a local reference product (Ferreira-Ferreira et al., 2015) for the Mamirauá Sustainable Development Re-

serve along the central Amazon River mainstem (location shown by black outline in figure a).

Implications for biogeochemistry, ecology and flood management

The divergent estimates of Amazon inundation extent have major implications for the quantification of the role of wetlands in global biogeochemical cycles, ecosystem processes and natural disaster management.

First, different products have been used to quantify the role of Amazon wetlands in the carbon cycle (Guilhen et al., 2020; Melack et al., 2004; Richey et al., 2002; Saunois et al., 2020). An intercomparison assessment of global models forced with different inundation datasets for the Amazon could provide insights into their sensitivity to the estimated inundation. This would be particularly important for modeled estimates of methane flux, given the region's significant contribution to global methane emissions from natural wetlands (Covey et al., 2021). Furthermore, for a proper estimation of methane and carbon dioxide fluxes, dynamic inundation estimates are necessary; this study shows that most coarse-scale dynamic datasets capture relatively well the seasonality (i.e., the timing of high and low water periods) of annual flooding at a large scale (but not at the local scales), but the magnitude of inundation area over time is still associated with significant errors (Fig. S6).

The understanding of the ecology of Amazon freshwaters has benefited from advances in remote sensing-based mapping of inundation. Hydrological variables of interest in relation to wildlife (Alvarenga et al., 2018; Bodmer et al., 2018) and vegetation distribution (Hess et al., 2015, 2003) include hydroperiod, floodplain water depth (Arantes et al., 2013; Fassoni-Andrade et al., 2020), and (lateral) surface water connectivity (Castello, 2008; Duponchelle et al., 2021; Reis et al., 2019a, 2019b), and should be better estimated by future datasets. In addition, many wetland ecosystem studies are performed at the tree stand level (e.g., floristic inventories) and require high spatial resolution inundation estimates to perform meaningful spatial analyses accounting for spatial heterogeneity of wetland vegetation. Furthermore, besides a simple interfluvial/floodplain categorization of wetlands as performed here (Section 3.4), which is reasonable from a hydrologic perspective, improving our understanding of the ecology of Amazon freshwater systems requires accurate mapping of habitats and their diverse vegetation types (e.g., grasslands, particular monodominant tree species, herbaceous plants). For instance, floodplain forest cover has been positively correlated to fishery yields (Arantes et al., 2018) and fish abundance (Lobón-Cerviá et al., 2015). While this wetland habitat mapping has already been done by some initiatives at the basin (Hess et al., 2015, 2003) and subregional scale (Ferreira-Ferreira et al., 2015; Silva et al., 2013), there is still a need for higher resolution and dynamic datasets.

Regarding flood monitoring in the context of natural hazard management, the flood warning systems of regional water authorities in the basin provide information based on river discharge and water level

at monitoring stations (e.g., Brazilian's Geological Survey SACE system; <http://sace.cprm.gov.br/amazonas/#>). In addition, there are other available monitoring and forecasting services that have been developed for the global scale, such as the Global Flood Detection System (https://www.gdacs.org/flooddetection/) based on remote sensing, and the Global Flood Monitoring System (http://flood.umd.edu/) and the Global Flood Awareness System (https://www.globalfloods.eu/), based on hydrological modeling. The currently available, basin-scale inundation datasets are unable to map flood hazard at the detailed resolution required for flood management applications, especially concerning urban areas (Almeida et al., 2018). High-resolution flood mapping has been achieved using hydraulic modeling based on local surveys of river bathymetry and floodplain LiDAR DTM, but only for a few specific sites such as the lower Madeira River (Fleischmann et al., 2021).

Future opportunities and recommendations

Future satellite missions will provide opportunities for improved inundation mapping in the Amazon, especially the polarimetric and interferometric L-band SAR data from the upcoming NASA/ISRO mission (NISAR), the P-Band BIOMASS mission from ESA, and the Ka-band Radar Interferometer (KaRIn) swath observations from the forthcoming SWOT mission (Biancamaria et al., 2016). New inundation detection technology under development with Global Navigation Satellite System-Reflectometry (GNSS-R), such as the Cyclone GNSS (CYGNSS) constellation of GNSS-R satellites, holds promise to improve the current inundation mapping capabilities for Amazon wetlands (Jensen et al., 2018; Ruf et al., 2018; Rodriguez-Alvarez et al., 2019). Further studies with the ALOS-2 PALSAR-2 data also are promising, in order to achieve new dynamic inundation detection, as well as ongoing assessments of the accuracy of the now available high temporal resolution inundation products (e.g., SWAF-HR with 3-day availability). Consistent and updated validation products of Amazon inundation are required, which could be derived from airborne, satellite, or UAV-based LiDAR surveys along multiple wetlands, in particular for overlooked wetlands such as the Negro and Roraima floodable savannas. This is especially important for the minimum inundation extent, which showed large uncertainties among the multiple datasets.

The combination and integration of multiple inundation products seem a promising and effective approach (Gumbricht et al., 2017; Hu et al., 2017). We recommend that future developments include optimal data fusion approaches, e.g., by integrating inundation extent into models accounting for water cycle components with multiple constraints (Meyer Oliveira et al, 2020; Pellet et al., 2021), and by considering new types of datasets (e.g., GNSS-R; Jensen et al., 2018). Bias correction of different datasets could be achieved by considering the errors of each product, as estimated here for various wetland complexes across the basin. For instance, recent studies have performed inundation bias correction using the Hess product (Aires et al., 2013; Sorribas et al., 2016). However,

merging of different datasets must be performed with caution, in a consistent way, avoiding double counting of surfaces, as well as missing others: its success critically depends upon a good understanding of the limitations and assets of each individual dataset. The optimal combination of hydrological-hydraulic models with satellite flood maps using techniques such as data assimilation is also a promising alternative at the basin scale (Wongchuig et al., 2020).

There is a need for the development of more large-scale 2D hydrological model applications, especially for large wetland complexes such as the Llanos de Moxos and Pacaya-Samiria, to better represent inundation dynamics (Fleischmann et al., 2020). 2D models have been applied mainly to some local-scale areas in the Amazon mainstem floodplain (Pinel et al., 2019; Rudorff et al., 2014; Trigg et al., 2009; Wilson et al., 2007). Furthermore, inundation anomalies are still poorly understood owing to the lack of ground-based inundation observations during extreme floods and droughts. Therefore, validation of estimates for extreme years has usually been performed with river water level data (in situ or from satellite altimetry) (Silva et al., 2018; Wongchuig et al., 2019). Future works should address which products and methodologies are the most suitable for mapping extreme events. Furthermore, besides inundation extent, flood storage (Frappart et al., 2005; Papa et al., 2008; Schumann et al., 2016; Papa and Frappart, 2021) and water velocity (Pinel et al., 2019) are necessary hydraulic variables to properly address multiple environmental studies (e.g., flood monitoring, flood attenuation by floodplains, fish floodplain habitats), but to date have not been well studied in the Amazon.

Finally, there is a need for better-informed usage of the currently available inundation datasets by multiple local and regional stakeholders (e.g., local water authorities, national water agencies), as well as research communities not close to remote sensing groups. This will only be achieved through a two-way interaction with these actors and development of easy-to-access visualization platforms (i.e., investment in hydroinformatics), as well as training of regional/local user communities. To this end, we have developed a WebGIS platform (https://amazon-inundation.herokuapp.com/) to display and provide data acquisition links for the inundation datasets assessed here. The interaction with local users would bring important feedback on the large-scale datasets as well, for instance through citizen science initiatives that are ongoing in the Amazon (https://www.amazoniacienciaciudadana.org/).

Acknowledgments

References

Abril, G., Martinez, J.-M., Artigas, L.F., Moreira-Turcq, P., Benedetti, M.F., Vidal, L., Meziane, T., Kim, J.-H., Bernardes, M.C., Savoye, N., Deborde, J., Souza, E.L., Albéric, P., Landim de Souza, M.F., Roland, F., 2014. Amazon River carbon dioxide outgassing fuelled by wetlands. Nature 505, 395–398. https://doi.org/10.1038/nature12797

Aires, F., Miolane, L., Prigent, C., Pham, B., Fluet-Chouinard, E., Lehner, B., Papa, F., 2017. A Global Dynamic Long-Term Inundation Extent Dataset at High Spatial Resolution Derived through Downscaling of Satellite Observations. J. Hydrometeorol. 18, 1305–1325. https://doi.org/10.1175/JHM-D-16-0155.1

Aires, F., Papa, F., Prigent, C., 2013. A Long-Term, High-Resolution Wetland Dataset over the Amazon Basin, Downscaled from a Multi-wavelength Retrieval Using SAR Data. J. Hydrometeorol. 14, 594–607. https://doi.org/10.1175/JHM-D-12-093.1

Aires, F., Prigent, C., Fluet-Chouinard, E., Yamazaki, D., Papa, F., Lehner, B., 2018. Comparison of visible and multi-satellite global inundation datasets at high-spatial resolution. Remote Sens. Environ. 216, 427–441. https://doi.org/10.1016/j.rse.2018.06.015

Al Bitar, A., Parrens, M., Fatras, C., & Luque, S. P., 2020. Global Weekly Inland Surface Water Dynamics from L-Band Microwave. In IGARSS 2020-2020 IEEE International Geoscience and Remote Sensing Symposium, 5089-5092.

Alsdorf, D., Bates, P., Melack, J., Wilson, M., Dunne, T., 2007. Spatial and temporal complexity of the Amazon flood measured from space. Geophys. Res. Lett. 34. https://doi.org/10.1029/2007GL029447

Alvarenga, G.C., Ramalho, E.E., Baccaro, F.B., da Rocha, D.G., Ferreira-Ferreira, J., Dineli Bobrowiec, P.E., 2018. Spatial patterns of medium and large size mammal assemblages in várzea and terra firme forests, Central Amazonia, Brazil. PLoS One 13, 1–19. https://doi.org/10.1371/journal.pone.0198120

Andrade, M.M.N. de, Bandeira, I.C.N., Fonseca, D.D.F., Bezerra, P.E.S., Andrade, Á. de S., Oliveira, R.S. de, 2017. Flood Risk Mapping in the Amazon, in: Flood Risk Management. InTech, p. 13. https://doi.org/10.5772/intechopen.68912

Arantes, C.C., Castello, L., Cetra, M., Schilling, A., 2013. Environmental influences on the distribution of arapaima in Amazon floodplains. Environ. Biol. Fishes 96, 1257–1267. https://doi.org/10.1007/s10641-011-9917-9

Arantes, C.C., Winemiller, K.O., Petrere, M., Castello, L., Hess, L.L., Freitas, C.E.C., 2018. Relationships between forest cover and fish diversity in the Amazon River floodplain. J. Appl. Ecol. 55, 386–395. https://doi.org/10.1111/1365-2664.12967

Armijos, E., Crave, A., Espinoza, J.C., Filizola, N., Espinoza-Villar, R., Ayes, Fonseca, P., Fraizy, P., Gutierrez, O., Vauchel, P., Camenen, B., Martinez, J.M., Dos Santos, A., Santini, W., Cochonneau, G., Guyot, J.L., 2020. Rainfall control on Amazon sediment flux: synthesis from 20 years of monitoring. Environ. Res. Commun. 2, 051008. https://doi.org/10.1088/2515-7620/ab9003

Arnesen, A.S., Silva, T.S.F., Hess, L.L., Novo, E.M.L.M., Rudorff, C.M., Chapman, B.D., McDonald, K.C., 2013. Monitoring flood extent in the lower Amazon River floodplain using ALOS/PALSAR ScanSAR images. Remote Sens. Environ. 130, 51–61. https://doi.org/10.1016/j.rse.2012.10.035

Asner, G.P., 2001. Cloud cover in Landsat observations of the Brazilian Amazon. Int. J. Remote Sens. 22, 3855–3862. https://doi.org/10.1080/01431160010006926

Balsamo, G., Beljaars, A., Scipal, K., Viterbo, P., van den Hurk, B., Hirschi, M., and Betts, A. K.: A Revised Hydrology for the ECMWF Model: Verification from Field Site to Terrestrial Water Storage and Impact in the Integrated Forecast System, J. Hydrometeorol., 10, 623–643, https://doi.org/10.1175/2008jhm1068.1, 2009.

Barichivich, J., Gloor, E., Peylin, P., Brienen, R.J.W., Schöngart, J., Espinoza, J.C., Pattnayak, K.C., 2018. Recent intensification of Amazon flooding extremes driven by strengthened Walker circulation. Sci. Adv. 4. https://doi.org/10.1126/sciadv.aat8785

Batalha, M.A., Cianciaruso, M. V., Silva, I.A., Delitti, W.B.C., 2005. Hyperseasonal cerrado, a new brazilian vegetation form. Brazilian J. Biol. 65, 735–738. https://doi.org/10.1590/S1519-69842005000400021

Bates, P.D., De Roo, A.P.J., 2000. A simple raster-based model for flood inundation simulation. J. Hydrol. https://doi.org/10.1016/S0022-1694(00)00278-X

Beck, H.E., Van Dijk, A.I.J.M., Levizzani, V., Schellekens, J., Miralles, D.G., Martens, B., De Roo, A., 2017. MSWEP: 3-hourly 0.25° global gridded precipitation (1979-2015) by merging gauge, satellite, and reanalysis data. Hydrol. Earth Syst. Sci. https://doi.org/10.5194/hess-21-589-2017

Beighley, R.E., Eggert, K.G., Dunne, T., He, Y., Gummadi, V., Verdin, K.L., 2009. Simulating hydrologic and hydraulic processes throughout the Amazon River Basin. Hydrol. Process. 23, 1221–1235. https://doi.org/10.1002/hyp.7252

Belger, L., Forsberg, B.R., Melack, J.M., 2011. Carbon dioxide and methane

emissions from interfluvial wetlands in the upper Negro River basin , Brazil 171–183. https://doi.org/10.1007/s10533-010-9536-0

Bernhofen, M. V, Whyman, C., Trigg, M.A., Sleigh, P.A., Smith, A.M., Sampson, C.C., Yamazaki, D., Ward, P.J., Rudari, R., Pappenberger, F., Dottori, F., Salamon, P., Winsemius, H.C., 2018. A first collective validation of global fluvial flood models for major floods in Nigeria and Mozambique. Environ. Res. Lett. 13, 104007. https://doi.org/10.1088/1748-9326/aae014

Biancamaria, S., Lettenmaier, D.P., Pavelsky, T.M., 2016. The SWOT Mission and Its Capabilities for Land Hydrology. Surv. Geophys. https://doi.org/10.1007/s10712-015-9346-y

Blatrix, R., Roux, B., Béarez, P., Prestes-Carneiro, G., Amaya, M., Aramayo, J.L., Rodrigues, L., Lombardo, U., Iriarte, J., De Souza, J.G., Robinson, M., Bernard, C., Pouilly, M., Durécu, M., Huchzermeyer, C.F., Kalebe, M., Ovando, A., McKey, D., 2018. The unique functioning of a pre-Columbian Amazonian floodplain fishery. Sci. Rep. 8. https://doi.org/10.1038/s41598-018-24454-4

Bodmer, R., Mayor, P., Antunez, M., Chota, K., Fang, T., Puertas, P., Pittet, M., Kirkland, M., Walkey, M., Rios, C., Perez-Peña, P., Henderson, P., Bodmer, W., Bicerra, A., Zegarra, J., Docherty, E., 2018. Major shifts in Amazon wildlife populations from recent intensification of floods and drought. Conserv. Biol. 32, 333–344. https://doi.org/10.1111/cobi.12993

Bonnet, M.P., Barroux, G., Martinez, J.M., Seyler, F., Moreira-Turcq, P., Cochonneau, G., Melack, J.M., Boaventura, G., Maurice-Bourgoin, L., León, J.G., Roux, E., Calmant, S., Kosuth, P., Guyot, J.L., Seyler, P., 2008. Floodplain hydrology in an Amazon floodplain lake (Lago Grande de Curuaí). J. Hydrol. 349, 18–30. https://doi.org/10.1016/j.jhydrol.2007.10.055

Bonnet, M.P., Pinel, S., Garnier, J., Bois, J., Resende Boaventura, G., Seyler, P., Motta Marques, D., 2017. Amazonian floodplain water balance based on modelling and analyses of hydrologic and electrical conductivity data. Hydrol. Process. 31, 1702–1718. https://doi.org/10.1002/hyp.11138

Bontemps, S., Defourny, P., Radoux, J., Van Bogaert, E. Lamarche, C., Achard, F., Mayaux, P., Boettcher, M., Brockmann, C., Kirches, G., 2013. Consistent global land cover maps for climate modelling communities: current achievements of the ESA's land cover CCI, in: Proceedings of the ESA Living Planet Symposium. Edinburgh.

Bourgoin, L.M., Bonnet, M.P., Martinez, J.M., Kosuth, P., Cochonneau, G., Moreira-Turcq, P., Guyot, J.L., Vauchel, P., Filizola, N., Seyler, P., 2007. Temporal dynamics of water and sediment exchanges between the Curuaí floodplain and the Amazon River, Brazil. J. Hydrol. 335, 140–156. https://doi.org/10.1016/j.jhydrol.2006.11.023

Canisius, F., Brisco, B., Murnaghan, K., Van Der Kooij, M., Keizer, E., 2019. SAR backscatter and InSAR coherence for monitoring wetland extent, flood

pulse and vegetation: A study of the Amazon lowland. Remote Sens. 11, 1–18. https://doi.org/10.3390/RS11060720

Castello, L., 2008. Lateral migration of Arapaima gigas in floodplains of the Amazon. Ecol. Freshw. Fish 17, 38–46. https://doi.org/10.1111/j.1600-0633.2007.00255.x

Chapman, B., Mcdonald, K., Shimada, M., Rosenqvist, A., Schroeder, R., Hess, L., 2015. Mapping Regional Inundation with Spaceborne L-Band SAR 5440–5470. https://doi.org/10.3390/rs70505440

Coe, M.T., Costa, M.H., Howard, E.A., 2008. Simulating the surface waters of the Amazon River basin: impacts of new river geomorphic and flow parameterizations. Hydrol. Process. 22, 2542–2553. https://doi.org/10.1002/hyp.6850

Coomes, O.T., Lapointe, M., Templeton, M., List, G., 2016. Amazon river flow regime and flood recessional agriculture: Flood stage reversals and risk of annual crop loss. J. Hydrol. 539, 214–222. https://doi.org/10.1016/j.jhydrol.2016.05.027

Coomes, O.T., Takasaki, Y., Abizaid, C., Barham, B.L., 2010. Floodplain fisheries as natural insurance for the rural poor in tropical forest environments: Evidence from Amazonia. Fish. Manag. Ecol. 17, 513–521. https://doi.org/10.1111/j.1365-2400.2010.00750.x

Covey, K., Soper, F., Pangala, S., Bernardino, A., Pagliaro, Z., Basso, L., Cassol, H., Fearnside, P., Navarrete, D., Novoa, S., Sawakuchi, H., Lovejoy, T., Marengo, J., Peres, C.A., Baillie, J., Bernasconi, P., Camargo, J., Freitas, C., Hoffman, B., Nardoto, G.B., Nobre, I., Mayorga, J., Mesquita, R., Pavan, S., Pinto, F., Rocha, F., de Assis Mello, R., Thuault, A., Bahl, A.A., Elmore, A., 2021. Carbon and Beyond: The Biogeochemistry of Climate in a Rapidly Changing Amazon. Front. For. Glob. Chang. 4. https://doi.org/10.3389/ffgc.2021.618401

Dalmagro, H.J., de A. Lobo, F., Vourlitis, G.L., Dalmolin, Â.C., Antunes, M.Z., Ortíz, C.E.R., de S. Nogueira, J., 2016. Photosynthetic response of a wetland- and an upland-adapted tree species to seasonal variations in hydrology in the Brazilian Cerrado and Pantanal. Acta Physiol. Plant. 38, 107. https://doi.org/10.1007/s11738-016-2125-7

de Almeida, G.A.M., Bates, P., Ozdemir, H., 2018. Modelling urban floods at submetre resolution: challenges or opportunities for flood risk management? J. Flood Risk Manag. 11, S855–S865. https://doi.org/10.1111/jfr3.12276

Denevan, W.M., 1996. A Bluff Model of Riverine Settlement in Prehistoric Amazonia. Ann. Assoc. Am. Geogr. 86, 654–681. https://doi.org/10.1111/j.1467-8306.1996.tb01771.x

Draper, F.C., Roucoux, K.H., Lawson, I.T., Mitchard, E.T.A., Honorio Coronado, E.N., Lähteenoja, O., Montenegro, L.T., Sandoval, E.V., Zaráte, R., Baker, T.R., 2014. The distribution and amount of carbon in the largest peatland complex in Amazonia. Environ. Res. Lett. 9. https://doi.org/10.1088/1748-9326/9/12/124017

Dunne, T., Mertes, L.A.K., Meade, R.H., Richey, J.E., Forsberg, B.R., 1998. Exchanges of sediment between the flood plain and channel of the Amazon River in Brazil. Bull. Geol. Soc. Am. 110, 450–467. https://doi.org/10.1130/0016-7606(1998)110<0450:EOSBTF>2.3.CO;2

Duponchelle, F., Isaac, V.J., Doria, C., Van Damme, P.A., Herrera-R, G.A., Anderson, E.P., Cruz, R.E.A., Hauser, M., Hermann, T.W., Agudelo, E., Bonilla-Castillo, C., Barthem, R., Freitas, C.E.C., García-Dávila, C., García-Vasquez, A., Renno, J., Castello, L., 2021. Conservation of migratory fishes in the Amazon basin. Aquat. Conserv. Mar. Freshw. Ecosyst. aqc.3550. https://doi.org/10.1002/aqc.3550

Espinoza Villar, J.C., Ronchail, J., Guyot, J.L., Cochonneau, G., Naziano, F., Lavado, W., De Oliveira, E., Pombosa, R., Vauchel, P., 2009. Spatio-temporal rainfall variability in the Amazon basin countries (Brazil, Peru, Bolivia, Colombia, and Ecuador). Int. J. Climatol. 29, 1574–1594. https://doi.org/10.1002/joc.1791

Espinoza, J.C., Ronchail, J., Marengo, J.A., Segura, H., 2019. Contrasting North–South changes in Amazon wet-day and dry-day frequency and related atmospheric features (1981–2017). Clim. Dyn. 52, 5413–5430. https://doi.org/10.1007/s00382-018-4462-2

Farr, T.G., Rosen, P.A., Caro, E., Crippen, R., Duren, R., Hensley, S., Kobrick, M., Paller, M., Rodriguez, E., Roth, L., Seal, D., Shaffer, S., Shimada, J., Umland, J., Werner, M., Oskin, M., Burbank, D., Alsdorf, D.E., 2007. The shuttle radar topography mission. Rev. Geophys. 45, 1–25. https://doi.org/10.1029/2005RG000183

Fassoni-Andrade, 2020. PhD thesis. Mapeamento e caracterização do sistema rio-planície da Amazônia central via sensoriamento remoto e modelagem hidráulica. Federal University of Rio Grande do Sul. Available at <https://lume.ufrgs.br/handle/10183/211269>.

Fassoni-Andrade, A.C., Fleischmann, A.S., Papa, F., Paiva, R.C.D. de, Wongchuig, S., Melack, J.M., Moreira, A.A., Paris, A., Ruhoff, A., Barbosa, C., Maciel, D.A., Novo, E., Durand, F., Frappart, F., Aires, F., Abrahão, G.M., Ferreira-Ferreira, J., Espinoza, J.C., Laipelt, L., Costa, M.H., Espinoza-Villar, R., Calmant, S., Pellet, V., 2021. Amazon Hydrology From Space: Scientific Advances and Future Challenges. Rev. Geophys. 59, 1–97. https://doi.org/10.1029/2020RG000728

Fassoni-Andrade, A.C., Paiva, R.C.D. de, 2019. Mapping spatial-temporal sediment dynamics of river-floodplains in the Amazon. Remote Sens. Environ. https://doi.org/10.1016/j.rse.2018.10.038

Fassoni-Andrade, A.C., Paiva, R.C.D. de, Rudorff, C. de M., Barbosa, C.C.F., Novo, E.M.L. de M., 2020. High-resolution mapping of floodplain topography from space: A case study in the Amazon. Remote Sens. Environ. 251, 112065. https://doi.org/10.1016/j.rse.2020.112065

Feng, D., Raoufi, R., Beighley, E., Melack, J.M., Goulding, M., Barthem, R.B., Venticinque, E., Cañas, C., Forsberg, B., Sorribas, M.V., 2020. Future climate impacts on the hydrology of headwater streams in the Amazon River Basin: Implications for migratory goliath catfishes. Hydrol. Process. hyp.13952. https://doi.org/10.1002/hyp.13952

Ferreira-Ferreira, J., Silva, T.S.F., Streher, A.S., Affonso, A.G., de Almeida Furtado, L.F., Forsberg, B.R., Valsecchi, J., Queiroz, H.L., de Moraes Novo, E.M.L., 2015. Combining ALOS/PALSAR derived vegetation structure and inundation patterns to characterize major vegetation types in the Mamirauá Sustainable Development Reserve, Central Amazon floodplain, Brazil. Wetl. Ecol. Manag. 23, 41–59. https://doi.org/10.1007/s11273-014-9359-1

Fleischmann, A.S., Fialho Brêda, J.P., Rudorff, C., Dias de Paiva, R.C., Collischonn, W., Papa, F., Ravanello, M.M., 2021. River Flood Modeling and Remote Sensing Across Scales: Lessons from Brazil, in: Schumann, G.J.P. (Ed.), Earth Observation for Flood Applications. Elsevier, pp. 61–103. https://doi.org/10.1016/B978-0-12-819412-6.00004-3

Fleischmann, A.S., Paiva, R.C.D., Collischonn, W., Siqueira, V.A., Paris, A., Moreira, D.M., Papa, F., Bitar, A.A., Parrens, M., Aires, F., Garambois, P.A., 2020. Trade-Offs Between 1-D and 2-D Regional River Hydrodynamic Models. Water Resour. Res. 56. https://doi.org/10.1029/2019WR026812

Flores, B.M., Holmgren, M., 2021. White-Sand Savannas Expand at the Core of the Amazon After Forest Wildfires. Ecosystems. https://doi.org/10.1007/s10021-021-00607-x

Fluet-Chouinard, E., Lehner, B., Rebelo, L.M., Papa, F., Hamilton, S.K., 2015. Development of a global inundation map at high spatial resolution from topographic downscaling of coarse-scale remote sensing data. Remote Sens. Environ. 158, 348–361. https://doi.org/10.1016/j.rse.2014.10.015

Frappart, F., Seyler, F., Martinez, J., León, J.G., Cazenave, A., 2005. Floodplain water storage in the Negro River basin estimated from microwave remote sensing of inundation area and water levels. Remote Sens. Environ. 99, 387–399. https://doi.org/10.1016/j.rse.2005.08.016

Fu, R., Yin, L., Li, W., Arias, P.A., Dickinson, R.E., Huang, L., Chakraborty, S., Fernandes, K., Liebmann, B., Fisher, R., Myneni, R.B., 2013. Increased dry-season length over southern Amazonia in recent decades and its implication for future climate projection. Proc. Natl. Acad. Sci. U. S. A. 110, 18110–18115. https://doi.org/10.1073/pnas.1302584110

Getirana, A., Boone, A., Yamazaki, D., Decharme, B., Papa, F., Mognard, N., 2012. The Hydrological Modeling and Analysis Platform (HyMAP): Evaluation in the Amazon Basin. J. Hydrometeorol. 13, 1641–1665. https://doi.org/10.1175/JHM-D-12-021.1

Getirana, A., Peters-Lidard, C., Rodell, M., Bates, P.D., 2017. Trade-off be-

tween cost and accuracy in large-scale surface water dynamic modeling. Water Resour. Res. 53, 4942–4955. https://doi.org/10.1002/2017WR020519

Gloor, M., Brienen, R.J.W., Galbraith, D., Feldpausch, T.R., Schöngart, J., Guyot, J.L., Espinoza, J.C., Lloyd, J., Phillips, O.L., 2013. Intensification of the Amazon hydrological cycle over the last two decades. Geophys. Res. Lett. 40, 1729–1733. https://doi.org/10.1002/grl.50377

Guilhen, J., Al Bitar, A., Sauvage, S., Parrens, M., Martinez, J., Abril, G., Moreira-Turcq, P., Sánchez-Pérez, J.-M., 2020. Denitrification and associated nitrous oxide and carbon dioxide emissions from the Amazonian wetlands. Biogeosciences 17, 4297–4311. https://doi.org/10.5194/bg-17-4297-2020

Guimberteau, M., Drapeau, G., Ronchail, J., Sultan, B., Polcher, J., Martinez, J.M., Prigent, C., Guyot, J.L., Cochonneau, G., Espinoza, J.C., Filizola, N., Fraizy, P., Lavado, W., De Oliveira, E., Pombosa, R., Noriega, L., Vauchel, P., 2012. Discharge simulation in the sub-basins of the Amazon using ORCHIDEE forced by new datasets. Hydrol. Earth Syst. Sci. https://doi.org/10.5194/hess-16-911-2012

Gumbricht, T., Roman-Cuesta, R.M., Verchot, L., Herold, M., Wittmann, F., Householder, E., Herold, N., Murdiyarso, D., 2017. An expert system model for mapping tropical wetlands and peatlands reveals South America as the largest contributor. Glob. Chang. Biol. 23, 3581–3599. https://doi.org/10.1111/gcb.13689

Hamilton, S.K., Kellndorfer, J., Lehner, B., Tobler, M., 2007. Remote sensing of floodplain geomorphology as a surrogate for biodiversity in a tropical river system (Madre de Dios, Peru). Geomorphology 89, 23–38. https://doi.org/10.1016/j.geomorph.2006.07.024

Hamilton, S.K., Sippel, S.J., Melack, J.M., 2002. Comparison of inundation patterns among major South American floodplains 107, 1–14.

Hamilton, S.K., Sippel, S.J., Melack, J.M., 2004. Seasonal inundation patterns in two large savanna floodplains of South America: the Llanos de Moxos(Bolivia) and the Llanos del Orinoco(Venezuela and Colombia). Hydrol. Process. 18, 2103–2116. https://doi.org/10.1002/hyp.5559

Hansen, M.C., Potapov, P. V., Moore, R., Hancher, M., Turubanova, S.A., Tyukavina, A., Thau, D., Stehman, S. V., Goetz, S.J., Loveland, T.R., Kommareddy, A., Egorov, A., Chini, L., Justice, C.O., Townshend, J.R.G., 2013. High-Resolution Global Maps of 21st-Century Forest Cover Change. Science (80-.). 342, 850–853. https://doi.org/10.1126/science.1244693

Harris, I., Jones, P.D., Osborn, T.J., Lister, D.H., 2014. Updated high-resolution grids of monthly climatic observations - the CRU TS3.10 Dataset. Int. J. Climatol. 34, 623–642. https://doi.org/10.1002/joc.3711

Hawes, J.E., Peres, C.A., Riley, L.B., Hess, L.L., 2012. Landscape-scale variation in structure and biomass of Amazonian seasonally flooded and unflooded

forests. For. Ecol. Manage. 281, 163–176. https://doi.org/10.1016/j.foreco.2012.06.023

Hess, L.L., Melack, J.M., Affonso, A.G., Barbosa, C., Gastil-Buhl, M., Novo, E.M.L.M., 2015. Wetlands of the Lowland Amazon Basin: Extent, Vegetative Cover, and Dual-season Inundated Area as Mapped with JERS-1 Synthetic Aperture Radar. Wetlands 35, 745–756. https://doi.org/10.1007/s13157-015-0666-y

Hess, L.L., Melack, J.M., Novo, E.M.L.M., Barbosa, C.C.F., Gastil, M., 2003. Dual-season mapping of wetland inundation and vegetation for the central Amazon basin. Remote Sens. Environ. 87, 404–428. https://doi.org/10.1016/j.rse.2003.04.001

Hoch, J.M., Haag, A. V., Van Dam, A., Winsemius, H.C., Van Beek, L.P.H., Bierkens, M.F.P., 2017. Assessing the impact of hydrodynamics on large-scale flood wave propagation: A case study for the Amazon Basin. Hydrol. Earth Syst. Sci. 21, 117–132. https://doi.org/10.5194/hess-21-117-2017

Hu, S., Niu, Z., Chen, Y., 2017. Global Wetland Datasets: a Review. Wetlands 37, 807–817. https://doi.org/10.1007/s13157-017-0927-z

Jardim, C.M., Nardoto, G.B., de Lima, A.C.B., de Jesus Silva, R., Schor, T., de Oliveira, J.A., Martinelli, L.A., 2020. The influence of seasonal river flooding in food consumption of riverine dwellers in the central Amazon region: an isotopic approach. Archaeol. Anthropol. Sci. 12. https://doi.org/10.1007/s12520-020-01172-5

Jensen, K., Mcdonald, K., 2019. Surface Water Microwave Product Series Version 3: A Near-Real Time and 25-Year Historical Global Inundated Area Fraction Time Series From Active and Passive Microwave Remote Sensing. IEEE Geosci. Remote Sens. Lett. 16, 1402–1406. https://doi.org/10.1109/lgrs.2019.2898779

Jensen, K., McDonald, K., Podest, E., Rodriguez-Alvarez, N., Horna, V., Steiner, N., 2018. Assessing L-Band GNSS-Reflectometry and Imaging Radar for Detecting Sub-Canopy Inundation Dynamics in a Tropical Wetlands Complex. Remote Sens. 10, 1431. https://doi.org/10.3390/rs10091431

Ji, X., Lesack, L.F.W., Melack, J.M., Wang, S., Riley, W.J., Shen, C., 2019. Seasonal and Interannual Patterns and Controls of Hydrological Fluxes in an Amazon Floodplain Lake With a Surface-Subsurface Process Model. Water Resour. Res. 55, 3056–3075. https://doi.org/10.1029/2018WR023897

Junk, W.J., Bayley, P.B., Sparks, R.E., 1989. The flood pulse concept in river-floodplain-systems. Can. J. Fish. Aquat. Sci. https://doi.org/10.1016/j.matchemphys.2012.10.032

Junk, W.J., Furch, K., Limnologie, M., Tropenokologie, A., Plon, W.-, 1993. A general review of tropical South American floodplains * 2, 231–238.

Junk, W.J., Piedade, M.T.F., Schöngart, J., Cohn-Haft, M., Adeney, J.M., Wittmann, F., 2011. A classification of major naturally-occurring amazonian

lowland wetlands. Wetlands 31, 623–640. https://doi.org/10.1007/s13157-011-0190-7

Lähteenoja, O., Reátegui, Y.R., Räsänen, M., Torres, D.D.C., Oinonen, M., Page, S., 2012. The large Amazonian peatland carbon sink in the subsiding Pastaza-Marañón foreland basin, Peru. Glob. Chang. Biol. 18, 164–178. https://doi.org/10.1111/j.1365-2486.2011.02504.x

Langerwisch, F., Rost, S., Gerten, D., Poulter, B., Rammig, A., Cramer, W., 2013. Potential effects of climate change on inundation patterns in the Amazon Basin. Hydrol. Earth Syst. Sci. 17, 2247–2262. https://doi.org/10.5194/hess-17-2247-2013

Langill, J.C., Abizaid, C., 2020. What is a bad flood? Local perspectives of extreme floods in the Peruvian Amazon. Ambio 49, 1423–1436. https://doi.org/10.1007/s13280-019-01278-8

Latrubesse, E.M., 2012. Amazon lakes, in: Encyclopedia of Earth Sciences Series. https://doi.org/10.1007/978-1-4020-4410-6_36

Lauerwald, R., Regnier, P., Camino-Serrano, M., Guenet, B., Guimberteau, M., Ducharne, A., Polcher, J., Ciais, P., 2017. ORCHILEAK (revision 3875): a new model branch to simulate carbon transfers along the terrestrial–aquatic continuum of the Amazon basin. Geosci. Model Dev. 10, 3821–3859. https://doi.org/10.5194/gmd-10-3821-2017

Lehner, B., Döll, P., 2004. Development and validation of a global database of lakes, reservoirs and wetlands. J. Hydrol. 296, 1–22. https://doi.org/10.1016/j.jhydrol.2004.03.028

Lehner, B., Grill, G., 2013. Global river hydrography and network routing: Baseline data and new approaches to study the world's large river systems. Hydrol. Process. https://doi.org/10.1002/hyp.9740

Lesack, L.F.W., Melack, J.M., 1995. Flooding Hydrology and Mixture Dynamics of Lake Water Derived from Multiple Sources in an Amazon Floodplain Lake. Water Resour. Res. 31, 329–345. https://doi.org/10.1029/94WR02271

Li, D., Lu, D., Moran, E., da Silva, R.F.B., 2020. Examining water area changes accompanying dam construction in the Madeira River in the Brazilian Amazon. Water (Switzerland) 12. https://doi.org/10.3390/w12071921

Lobón-Cerviá, J., Hess, L.L., Melack, J.M., Araujo-Lima, C.A.R.M., 2015. The importance of forest cover for fish richness and abundance on the Amazon floodplain. Hydrobiologia 750, 245–255. https://doi.org/10.1007/s10750-014-2040-0

Luize, B.G., Silva, T.S.F., Wittmann, F., Assis, R.L., Venticinque, E.M., Luize, B.G., Silva, T.S.F., Wittmann, F., Assis, R.L., Venticinque, E.M., 2015. Effects of the Flooding Gradient on Tree Community Diversity in Várzea Forests of the Purus River , Central Amazon , Brazil Published by : Association for Tropical Biology and Conservation Stable URL :

https://www.jstor.org/stable/10.2307/48574801 REFEREN. Biotropica 47, 137–142.

Luo, X., Li, H.-Y., Leung, L.R., Tesfa, T.K., Getirana, A., Papa, F., Hess, L.L., 2017. Modeling surface water dynamics in the Amazon Basin using MOSART-Inundation v1.0: impacts of geomorphological parameters and river flow representation. Geosci. Model Dev. 10, 1233–1259. https://doi.org/10.5194/gmd-10-1233-2017

Mansur, A. V., Brondízio, E.S., Roy, S., Hetrick, S., Vogt, N.D., Newton, A., 2016. An assessment of urban vulnerability in the Amazon Delta and Estuary: a multi-criterion index of flood exposure, socio-economic conditions and infrastructure. Sustain. Sci. 11, 625–643. https://doi.org/10.1007/s11625-016-0355-7

Martinez, J.M., Le Toan, T., 2007. Mapping of flood dynamics and spatial distribution of vegetation in the Amazon floodplain using multitemporal SAR data. Remote Sens. Environ. 108, 209–223. https://doi.org/10.1016/j.rse.2006.11.012

Martínez-Espinosa, C., Sauvage, S., Al Bitar, A., Green, P. A., Vörösmarty, C. J., & Sánchez-Pérez, J. M. (2020). Denitrification in wetlands: A review towards a quantification at global scale. Science of the total environment 754, 142398. https://doi.org/10.1016/j.scitotenv.2020.142398

Matthews, E., Fung, I., 1987. Methane emission from natural wetlands: Global distribution, area, and environmental characteristics of sources. Global Biogeochem. Cycles 1, 61–86. https://doi.org/10.1029/GB001i001p00061

Melack, J.M., 2016. Aquatic Ecosystems, in: Ecological Studies. pp. 119–148. https://doi.org/10.1007/978-3-662-49902-3_7

Melack, J.M., Coe, M.T., 2021. Amazon floodplain hydrology and implications for aquatic conservation. Aquat. Conserv. Mar. Freshw. Ecosyst. 1029–1040. https://doi.org/10.1002/aqc.3558

Melack, J.M., Forsberg, B.R., 2001. Biogeochemistry of Amazon Floodplain, in: McClain, M.E., Victoria, R., Richey, J.E. (Eds.), The Biogeochemistry of the Amazon Basin. Oxford University Press, New York, USA.

Melack, J.M., Hess, L.L., 2010. Remote Sensing of the Distribution and Extent of Wetlands in the Amazon Basin, in: Amazonian Floodplain Forests. pp. 43–59. https://doi.org/10.1007/978-90-481-8725-6_3

Melack, J.M., Hess, L.L., Gastil, M., Forsberg, B.R., Hamilton, S.K., Lima, I.B.T., Novo, E.M.L.M., 2004. Regionalization of methane emissions in the Amazon Basin with microwave remote sensing. Glob. Chang. Biol. 10, 530–544. https://doi.org/10.1111/j.1365-2486.2004.00763.x

Meyer Oliveira, A., Fleischmann, A., Paiva, R., 2020. On the contribution of remote sensing-based calibration to model multiple hydrological variables. J. Hydrol. https://doi.org/10.1016/j.jhydrol.2021.126184

Miguez-Macho, G., Fan, Y., 2012. The role of groundwater in the Amazon water cycle: 1. Influence on seasonal streamflow, flooding and wetlands. J. Geophys. Res. Atmos. 117, 1–30. https://doi.org/10.1029/2012JD017539

Nardi, F., Annis, A., Di Baldassarre, G., Vivoni, E.R., Grimaldi, S., 2019. GF-PLAIN250m, a global high-resolution dataset of Earth's floodplains. Sci. Data 6, 180309. https://doi.org/10.1038/sdata.2018.309

O'Loughlin, F.E., Paiva, R.C.D., Durand, M., Alsdorf, D.E., Bates, P.D., 2016. A multi-sensor approach towards a global vegetation corrected SRTM DEM product. Remote Sens. Environ. 182, 49–59. https://doi.org/10.1016/j.rse.2016.04.018

Ovando, A., Martinez, J.M., Tomasella, J., Rodriguez, D.A., von Randow, C., 2018. Multi-temporal flood mapping and satellite altimetry used to evaluate the flood dynamics of the Bolivian Amazon wetlands. Int. J. Appl. Earth Obs. Geoinf. 69, 27–40. https://doi.org/10.1016/j.jag.2018.02.013

Ovando, A., Tomasella, J., Rodriguez, D.A., Martinez, J.M., Siqueira-Junior, J.L., Pinto, G.L.N., Passy, P., Vauchel, P., Noriega, L., von Randow, C., 2016. Extreme flood events in the Bolivian Amazon wetlands. J. Hydrol. Reg. Stud. 5, 293–308. https://doi.org/10.1016/j.ejrh.2015.11.004

Paca, V.H. da M., Espinoza-Dávalos, G.E., Hessels, T.M., Moreira, D.M., Comair, G.F., Bastiaanssen, W.G.M., 2019. The spatial variability of actual evapotranspiration across the Amazon River Basin based on remote sensing products validated with flux towers. Ecol. Process. 8, 6. https://doi.org/10.1186/s13717-019-0158-8

Paiva, R., Buarque, D.C., Collischonn, W., Bonnet, M.P., Frappart, F., Calmant, S., Bulhões Mendes, C.A., 2013. Large-scale hydrologic and hydrodynamic modeling of the Amazon River basin. Water Resour. Res. 49, 1226–1243. https://doi.org/10.1002/wrcr.20067

Pangala, S.R., Enrich-Prast, A., Basso, L.S., Peixoto, R.B., Bastviken, D., Hornibrook, E.R.C., Gatti, L. V., Marotta, H., Calazans, L.S.B., Sakuragui, C.M., Bastos, W.R., Malm, O., Gloor, E., Miller, J.B., Gauci, V., 2017. Large emissions from floodplain trees close the Amazon methane budget. Nature 552, 230–234. https://doi.org/10.1038/nature24639

Papa, F., and F. Frappart (2021), Surface Water Storage in Rivers and Wetlands Derived from Satellite Observations: A Review of Current Advances and Future Opportunities for Hydrological Sciences, Remote Sensing, 13(20), 4162, doi:10.3390/rs13204162

Papa, F., Gu, A., Frappart, F., Prigent, C., Rossow, W.B., 2008. Variations of surface water extent and water storage in large river basins : A comparison of different global data sources 35, 1–5. https://doi.org/10.1029/2008GL033857

Papa, F., Prigent, C., Aires, F., Jimenez, C., Rossow, W.B., Matthews, E., 2010. Interannual variability of surface water extent at the global scale, 1993–2004. J.

Geophys. Res. 115, D12111. https://doi.org/10.1029/2009JD012674

Park, E., Latrubesse, E.M., 2017. The hydro-geomorphologic complexity of the lower Amazon River floodplain and hydrological connectivity assessed by remote sensing and field control. Remote Sens. Environ. 198, 321–332. https://doi.org/10.1016/j.rse.2017.06.021

Park, E., Latrubesse, E.M., 2019. A geomorphological assessment of wash-load sediment fluxes and floodplain sediment sinks along the lower Amazon River. Geology 47, 403–406. https://doi.org/10.1130/G45769.1

Parrens, M., Al Bitar, A., Frappart, F., Papa, F., Calmant, S., Crétaux, J.-F., Wigneron, J.-P., Kerr, Y., 2017. Mapping Dynamic Water Fraction under the Tropical Rain Forests of the Amazonian Basin from SMOS Brightness Temperatures. Water 9, 350. https://doi.org/10.3390/w9050350

Parrens, M., Bitar, A. Al, Frappart, F., Paiva, R., Wongchuig, S., Papa, F., Yamasaki, D., Kerr, Y., 2019. High resolution mapping of inundation area in the Amazon basin from a combination of L-band passive microwave, optical and radar datasets. Int. J. Appl. Earth Obs. Geoinf. 81, 58–71. https://doi.org/10.1016/j.jag.2019.04.011

Pekel, J., Cottam, A., Gorelick, N., Belward, A.S., 2016. High-resolution mapping of global surface water and its long-term changes. Nature 540, 418–422. https://doi.org/10.1038/nature20584

Pellet, V., Aires, F., Yamazaki, D., Papa, F., 2021. Coherent Satellite Monitoring of the Water Cycle Over the Amazon. Part 1: Methodology and Initial Evaluation. Water Resour. Res. 57, 1–21. https://doi.org/10.1029/2020wr028647

Pham-Duc, B., Prigent, C., Aires, F., Papa, F., 2017. Comparisons of global terrestrial surface water datasets over 15 years. J. Hydrometeorol. 18, 993–1007. https://doi.org/10.1175/JHM-D-16-0206.1

Pickens, A.H., Hansen, M.C., Hancher, M., Stehman, S. V., Tyukavina, A., Potapov, P., Marroquin, B., Sherani, Z., 2020. Mapping and sampling to characterize global inland water dynamics from 1999 to 2018 with full Landsat time-series. Remote Sens. Environ. 243, 111792. https://doi.org/10.1016/j.rse.2020.111792

Pinel, S., Bonnet, M., S. Da Silva, J., Sampaio, T.C., Garnier, J., Catry, T., Calmant, S., Fragoso, C.R., Moreira, D., Motta Marques, D., Seyler, F., 2019. Flooding dynamics within an Amazonian floodplain: water circulation patterns and inundation duration. Water Resour. Res. 2019WR026081. https://doi.org/10.1029/2019WR026081

Prigent, C., Jimenez, C., Bousquet, P., 2020. Satellite-Derived Global Surface Water Extent and Dynamics Over the Last 25 Years (GIEMS-2). J. Geophys. Res. Atmos. 125, 1–18. https://doi.org/10.1029/2019JD030711

Prigent, C., Matthews, E., Aires, F., Rossow, W.B., 2001. Remote sensing of

global wetland dynamics with multiple satellite data sets. Geophys. Res. Lett. 28, 4631–4634. https://doi.org/10.1029/2001GL013263

Prigent, C., Papa, F., Aires, F., Rossow, W.B., Matthews, E., 2007. Global inundation dynamics inferred from multiple satellite observations, 1993-2000. J. Geophys. Res. Atmos. 112, 1993–2000. https://doi.org/10.1029/2006JD007847

Prigent, C., Rochetin, N., Aires, F., Defer, E., Grandpeix, J.-Y., Jimenez, C., Papa, F., 2011. Impact of the inundation occurrence on the deep convection at continental scale from satellite observations and modeling experiments. J. Geophys. Res. Atmos. 116, n/a-n/a. https://doi.org/10.1029/2011JD016311

Reis, V., Hermoso, V., Hamilton, S.K., Bunn, S.E., Fluet-Chouinard, E., Venables, B., Linke, S., 2019a. Characterizing seasonal dynamics of Amazonian wetlands for conservation and decision making. Aquat. Conserv. Mar. Freshw. Ecosyst. 1–10. https://doi.org/10.1002/aqc.3051

Reis, V., Hermoso, V., Hamilton, S.K., Bunn, S.E., Linke, S., 2019b. Conservation planning for river-wetland mosaics: A flexible spatial approach to integrate floodplain and upstream catchment connectivity. Biol. Conserv. 236, 356–365. https://doi.org/10.1016/j.biocon.2019.05.042

Rennó, C.D., Nobre, A.D., Cuartas, L.A., Soares, J.V., Hodnett, M.G., Tomasella, J., Waterloo, M.J., 2008. HAND, a new terrain descriptor using SRTM-DEM: Mapping terra-firme rainforest environments in Amazonia. Remote Sens. Environ. https://doi.org/10.1016/j.rse.2008.03.018

Renó, V.F., Novo, E.M.L.M., Suemitsu, C., Rennó, C.D., Silva, T.S.F., 2011. Assessment of deforestation in the Lower Amazon floodplain using historical Landsat MSS/TM imagery. Remote Sens. Environ. 115, 3446–3456. https://doi.org/10.1016/j.rse.2011.08.008

Resende, A.F. de, Schöngart, J., Streher, A.S., Ferreira-Ferreira, J., Piedade, M.T.F., Silva, T.S.F., 2019. Massive tree mortality from flood pulse disturbances in Amazonian floodplain forests: The collateral effects of hydropower production. Sci. Total Environ. 659, 587–598. https://doi.org/10.1016/j.scitotenv.2018.12.208

Restrepo A, J.D., Kettner, A.J., Robert Brakenridge, G., 2020. Monitoring water discharge and floodplain connectivity for the northern Andes utilizing satellite data: A tool for river planning and science-based decision-making. J. Hydrol. 586, 124887. https://doi.org/10.1016/j.jhydrol.2020.124887

Richey, J.E., Hedges, J.I., Devol, A.H., Quay, P.D., Victoria, R., Martinelli, L., Forsberg, B.R., 1990. Biogeochemistry of carbon in the Amazon River. Limnol. Oceanogr. 35, 352–371. https://doi.org/10.4319/lo.1990.35.2.0352

Richey, J.E., Melack, J.M., Aufdenkampe, A.K., Ballester, V.M., Hess, L.L., 2002. Outgassing from Amazonian rivers and wetlands as a large tropical source of atmospheric CO2. Nature 416, 617–620. https://doi.org/10.1038/416617a

Ringeval, B., Decharme, B., Piao, S.L., Ciais, P., Papa, F., de Noblet-Ducoudré, N., Prigent, C., Friedlingstein, P., Gouttevin, I., Koven, C., Ducharne, A., 2012. Modelling sub-grid wetland in the ORCHIDEE global land surface model: evaluation against river discharges and remotely sensed data. Geosci. Model Dev. 5, 941–962. https://doi.org/10.5194/gmd-5-941-2012

Ringeval, B., Houweling, S., van Bodegom, P.M., Spahni, R., van Beek, R., Joos, F., Röckmann, T., 2014. Methane emissions from floodplains in the Amazon Basin: challenges in developing a process-based model for global applications. Biogeosciences 11, 1519–1558. https://doi.org/10.5194/bg-11-1519-2014

Rodriguez-Alvarez, N., Podest, E., Jensen, K., McDonald, K.C., 2019. Classifying Inundation in a Tropical Wetlands Complex with GNSS-R. Remote Sens. 11, 1053. https://doi.org/10.3390/rs11091053

Rosenqvist, A., Forsberg, B.R., Pimentel, T., Rauste, Y.A., Richey, J.E., 2002. The use of spaceborne radar data to model inundation patterns and trace gas emissions in the central Amazon floodplain. Int. J. Remote Sens. 23, 1303–1328. https://doi.org/10.1080/01431160110092911

Rosenqvist, J., Rosenqvist, A., Jensen, K., McDonald, K., 2020. Mapping of Maximum and Minimum Inundation Extents in the Amazon Basin 2014–2017 with ALOS-2 PALSAR-2 ScanSAR Time-Series Data. Remote Sens. 12, 1326. https://doi.org/10.3390/rs12081326

Rosinger, A.Y., 2018. Household water insecurity after a historic flood: Diarrhea and dehydration in the Bolivian Amazon. Soc. Sci. Med. 197, 192–202. https://doi.org/10.1016/j.socscimed.2017.12.016

Rossetti, D.F., Gribel, R., Rennó, C.D., Cohen, M.C.L., Moulatlet, G.M., Cordeiro, C.L. de O., Rodrigues, E. do S.F., 2017a. Late Holocene tectonic influence on hydrology and vegetation patterns in a northern Amazonian megafan. Catena 158, 121–130. https://doi.org/10.1016/j.catena.2017.06.022

Rossetti, D.F., Valeriano, M.M., Gribel, R., Cohen, M.C.L., Tatumi, S.H., Yee, M., 2017b. The imprint of Late Holocene tectonic reactivation on a megafan landscape in the northern Amazonian wetlands. Geomorphology 295, 406–418. https://doi.org/10.1016/j.geomorph.2017.07.026

Rudorff, C.M., Melack, J.M., Bates, P.D., 2014. Flooding dynamics on the lower Amazon floodplain: 1. Hydraulic controls on water elevation, inundation extent, and river-floodplain discharge. Water Resour. Res. 50, 619–634. https://doi.org/10.1002/2013WR014091

Ruf, C.S., Chew, C., Lang, T. et al. A New Paradigm in Earth Environmental Monitoring with the CYGNSS Small Satellite Constellation. Sci Rep 8, 8782 (2018). https://doi.org/10.1038/s41598-018-27127-4

Ruiz Agudelo, C.A., Mazzeo, N., Díaz, I., Barral, M.P., Piñeiro, G., Gadino, I., Roche, I., Acuña-Posada, R.J., 2020. Land use planning in the amazon basin:

Challenges from resilience thinking. Ecol. Soc. 25. https://doi.org/10.5751/ES-11352-250108

Santos, J.O.S., Nelson, B.W., Giovannini, C.A., 1993. Corpos de areia sob leitos abandonados de grandes rios. Ciência Hoje 16, 22–25.

Santos, L.B.L., Carvalho, T., Anderson, L.O., Rudorff, C.M., Marchezini, V., Londe, L.R., Saito, S.M., 2017. An RS-GIS-Based ComprehensiveImpact Assessment of Floods—A Case Study in Madeira River, Western Brazilian Amazon. IEEE Geosci. Remote Sens. Lett. 14, 1614–1617. https://doi.org/10.1109/LGRS.2017.2726524

Santos, M.J., Medvigy, D., Silva Dias, M.A.F., Freitas, E.D., Kim, H., 2019. Seasonal Flooding Causes Intensification of the River Breeze in the Central Amazon. J. Geophys. Res. Atmos. 124, 5178–5197. https://doi.org/10.1029/2018JD029439

Saunois, M., Stavert, A.R., Poulter, B., Bousquet, P., Canadell, J.G., Jackson, R.B., Raymond, P.A., Dlugokencky, E.J., Houweling, S., Patra, P.K., Ciais, P., Arora, V.K., Bastviken, D., Bergamaschi, P., Blake, D.R., Brailsford, G., Bruhwiler, L., Carlson, K.M., Carrol, M., Castaldi, S., Chandra, N., Crevoisier, C., Crill, P.M., Covey, K., Curry, C.L., Etiope, G., Frankenberg, C., Gedney, N., Hegglin, M.I., Höglund-Isaksson, L., Hugelius, G., Ishizawa, M., Ito, A., Janssens-Maenhout, G., Jensen, K.M., Joos, F., Kleinen, T., Krummel, P.B., Langenfelds, R.L., Laruelle, G.G., Liu, L., Machida, T., Maksyutov, S., Mc-Donald, K.C., McNorton, J., Miller, P.A., Melton, J.R., Morino, I., Müller, J., Murguia-Flores, F., Naik, V., Niwa, Y., Noce, S., O'Doherty, S., Parker, R.J., Peng, C., Peng, S., Peters, G.P., Prigent, C., Prinn, R., Ramonet, M., Regnier, P., Riley, W.J., Rosentreter, J.A., Segers, A., Simpson, I.J., Shi, H., Smith, S.J., Steele, L.P., Thornton, B.F., Tian, H., Tohjima, Y., Tubiello, F.N., Tsuruta, A., Viovy, N., Voulgarakis, A., Weber, T.S., van Weele, M., van der Werf, G.R., Weiss, R.F., Worthy, D., Wunch, D., Yin, Y., Yoshida, Y., Zhang, W., Zhang, Z., Zhao, Y., Zheng, B., Zhu, Qing, Zhu, Qiuan, Zhuang, Q., 2020. The Global Methane Budget 2000–2017. Earth Syst. Sci. Data 12, 1561–1623. https://doi.org/10.5194/essd-12-1561-2020

Schöngart, J., Wittmann, F., Faria de Resende, A., Assahira, C., Sousa Lobo, G., Rocha Duarte Neves, J., Rocha, M., Biem Mori, G., Costa Quaresma, A., Oreste Demarchi, L., Weiss Albuquerque, B., Oliveira Feitosa, Y., Silva Costa, G., Vieira Feitoza, G., Machado Durgante, F., Lopes, A., Trumbore, S.E., Sanna Freire Silva, T., Steege, H., Val, A.L., Junk, W.J., Piedade, M.T.F., 2021. The shadow of the Balbina dam: A synthesis of over 35 years of downstream impacts on floodplain forests in Central Amazonia. Aquat. Conserv. Mar. Freshw. Ecosyst. 31, 1117–1135. https://doi.org/10.1002/aqc.3526

Schroeder, R., Mcdonald, K.C., Chapman, B.D., Jensen, K., Podest, E., Tessler, Z.D., Bohn, T.J., Zimmermann, R., 2015. Development and Evaluation of a Multi-Year Fractional Surface Water Data Set Derived from Active / Passive Microwave Remote Sensing Data 16688–16732.

https://doi.org/10.3390/rs71215843

Schumann, G.J.P., Stampoulis, D., Smith, A.M., Sampson, C.C., Andreadis, K.M., Neal, J.C., Bates, P.D., 2016. Rethinking flood hazard at the global scale. Geophys. Res. Lett. 43, 10,249-10,256. https://doi.org/10.1002/2016GL070260

Silva, M.V., Paris, A., Calmant, S., Cândido, L.A., Silva, J.S. da, 2018. Relationships between pacific and atlantic ocean sea surface temperatures and water levels from satellite altimetry data in the Amazon rivers. RBRH 23. https://doi.org/10.1590/2318-0331.231820170148

Silva, T.S.F., Melack, J.M., Novo, E.M.L.M., 2013. Responses of aquatic macrophyte cover and productivity to flooding variability on the Amazon floodplain. Glob. Chang. Biol. 19, n/a-n/a. https://doi.org/10.1111/gcb.12308

Sippel, S.J., Hamilton, S.K., Melack, J.M., 1992. Inundation area and morphometry of lakes on the Amazon River floodplain, Brazil. Arch. Hydrobiol 123, 385–400.

Sippel, S.J., Hamilton, S.K., Melack, J.M., Novo, E.M.M., 1998. Passive microwave observations of inundation area and the area/stage relation in the amazon river floodplain. Int. J. Remote Sens. 19, 3055–3074. https://doi.org/10.1080/014311698214181

Siqueira, V.A., Paiva, R.C.D., Fleischmann, A.S., Fan, F.M., Ruhoff, A.L., Pontes, P.R.M., Paris, A., Calmant, S., Collischonn, W., 2018. Toward continental hydrologic–hydrodynamic modeling in South America. Hydrol. Earth Syst. Sci. 22, 4815–4842. https://doi.org/10.5194/hess-22-4815-2018

Sorribas, M.V., Paiva, R.C.D., Melack, J.M., Bravo, J.M., Jones, C., Carvalho, L., Beighley, E., Forsberg, B., Costa, M.H., 2016. Projections of climate change effects on discharge and inundation in the Amazon basin 555–570. https://doi.org/10.1007/s10584-016-1640-2

Souza, C.M., Kirchhoff, F.T., Oliveira, B.C., Ribeiro, J.G., Sales, M.H., 2019. Long-term annual surface water change in the Brazilian Amazon Biome: Potential links with deforestation, infrastructure development and climate change. Water (Switzerland) 11, 566. https://doi.org/10.3390/w11030566

Staver, A.C., Archibald, S., Levin, S.A., 2011. The global extent and determinants of savanna and forest as alternative biome states. Science (80-.). 334, 230–232. https://doi.org/10.1126/science.1210465

Taylor, C.M., Prigent, C., Dadson, S.J., 2018. Mesoscale rainfall patterns observed around wetlands in sub-Saharan Africa. Q. J. R. Meteorol. Soc. 144, 2118–2132. https://doi.org/10.1002/qj.3311

Towner, J., Cloke, H.L., Zsoter, E., Flamig, Z., Hoch, J.M., Bazo, J., De Perez, E.C., Stephens, E.M., 2019. Assessing the performance of global hydrological

models for capturing peak river flows in the Amazon basin. Hydrol. Earth Syst. Sci. https://doi.org/10.5194/hess-23-3057-2019

Trigg, M.A., Birch, C.E., Neal, J.C., Bates, P.D., Smith, A., Sampson, C.C., Yamazaki, D., Hirabayashi, Y., Pappenberger, F., Dutra, E., Ward, P.J., Winsemius, H.C., Salamon, P., Dottori, F., Rudari, R., Kappes, M.S., Simpson, A.L., Hadzilacos, G., Fewtrell, T.J., 2016. The credibility challenge for global fluvial flood risk analysis. Environ. Res. Lett. 11, 094014. https://doi.org/10.1088/1748-9326/11/9/094014

Trigg, M.A., Wilson, M.D., Bates, P.D., Horritt, M.S., Alsdorf, D.E., Forsberg, B.R., Vega, M.C., 2009. Amazon flood wave hydraulics. J. Hydrol. 374, 92–105. https://doi.org/10.1016/j.jhydrol.2009.06.004

Ward, N.D., Bianchi, T.S., Medeiros, P.M., Seidel, M., Richey, J.E., Keil, R.G., Sawakuchi, H.O., 2017. Where Carbon Goes When Water Flows: Carbon Cycling across the Aquatic Continuum. Front. Mar. Sci. 4, 1–27. https://doi.org/10.3389/fmars.2017.00007

Wilson, M.D., Bates, P., Alsdorf, D., Forsberg, B., Horritt, M., Melack, J., Frappart, F., Famiglietti, J., 2007. Modeling large-scale inundation of Amazonian seasonally flooded wetlands. Geophys. Res. Lett. 34, 4–9. https://doi.org/10.1029/2007GL030156

Wongchuig Correa, S., Paiva, R.C.D. de, Espinoza, J.C., Collischonn, W., 2017. Multi-decadal Hydrological Retrospective: Case study of Amazon floods and droughts. J. Hydrol. https://doi.org/10.1016/j.jhydrol.2017.04.019

Wongchuig, S.C., de Paiva, R.C.D., Siqueira, V., Collischonn, W., 2019. Hydrological reanalysis across the 20th century: A case study of the Amazon Basin. J. Hydrol. 570, 755–773. https://doi.org/10.1016/j.jhydrol.2019.01.025

Wongchuig-Correa, S., Cauduro Dias de Paiva, R., Biancamaria, S., Collischonn, W., 2020. Assimilation of future SWOT-based river elevations, surface extent observations and discharge estimations into uncertain global hydrological models. J. Hydrol. 590, 125473. https://doi.org/10.1016/j.jhydrol.2020.125473

Wu, J., Lakshmi, V., Wang, D., Lin, P., Pan, M., Cai, X., Wood, E.F., Zeng, Z., 2020. The Reliability of Global Remote Sensing Evapotranspiration Products over Amazon. Remote Sens. 12, 2211. https://doi.org/10.3390/rs12142211

Yamazaki, D., Ikeshima, D., Tawatari, R., Yamaguchi, T., O'Loughlin, F., Neal, J.C., Sampson, C.C., Kanae, S., Bates, P.D., 2017. A high-accuracy map of global terrain elevations. Geophys. Res. Lett. https://doi.org/10.1002/2017GL072874

Yamazaki, D., Kanae, S., Kim, H., Oki, T., 2011. A physically based description of floodplain inundation dynamics in a global river routing model. Water Resour. Res. 47, 1–21. https://doi.org/10.1029/2010WR009726

Yamazaki, D., Sato, T., Kanae, S., Hirabayashi, Y., Bates, P.D., 2014. Regional flood dynamics in a bifurcating mega delta simulated in a global river model.

Geophys. Res. Lett. 41, 3127–3135. https://doi.org/10.1002/2014GL059744

Yamazaki, D., Trigg, M.A., Ikeshima, D., 2015. Development of a global ~90m water body map using multi-temporal Landsat images. Remote Sens. Environ. https://doi.org/10.1016/j.rse.2015.10.014

Zhang, Z., Poulter, B., Fluet-Chouinard, E., Jensen, K., McDonald, K., Hugelius, G., Gumbricht, T., Carroll, M., Prigent, C., Bartsch, A., 2020. Development and evaluation of the global Wetland Area and Dynamics for Methane Modeling dataset (WAD2M). Earth Syst. Sci. Data in review, 1–50. https://doi.org/10.5194/essd-2020-262

Zhou, X., Prigent, C., Yamazaki, D., 2021. Toward improved comparisons between land-surface-water-area estimates from a global river model and satellite observations. Water Resour. Res. 57, e2020WR029256. https://doi.org/10.1029/2020WR029256

Zubieta, R., Getirana, A., Espinoza, J.C., Lavado, W., 2015. Impacts of satellite-based precipitation datasets on rainfall-runoff modeling of the Western Amazon basin of Peru and Ecuador. J. Hydrol. 528, 599–612. https://doi.org/10.1016/j.jhydrol.2015.06.064

Zubieta, R., Getirana, A., Espinoza, J.C., Lavado-Casimiro, W., Aragon, L., 2017. Hydrological modeling of the Peruvian-Ecuadorian Amazon Basin using GPM-IMERG satellite-based precipitation dataset. Hydrol. Earth Syst. Sci. 21, 3543–3555. https://doi.org/10.5194/hess-21-3543-2017

Zubieta, R., Saavedra, M., Espinoza, J.C., Ronchail, J., Sulca, J., Drapeau, G., Martin-Vide, J., 2019. Assessing precipitation concentration in the Amazon basin from different satellite-based data sets. Int. J. Climatol. 39, 3171–3187. https://doi.org/10.1002/joc.6009

Supplementary Material

Table S1. List of additional studies that mapped inundation in the Amazon, which were not included in the article analysis because of redundancy with the used datasets, or data unavailability.

	Reference	Product name / Type	Spatial. resoluti
1	Aires et al. (2013)	GIEMS + downscaling with SAR	500 m
2	Belger et al. (2011)	Radarsat-1 / C-band SAR	25 m
3	Bonnet et al. (2008)	Hydrological model	
4	Canisius et al., 2019)	Radarsat-2 / C-band SAR	2.5-2.6 m
5	Fleischmann et al. (2020)	MGB / Hydrological-hydraulic model	4 km
6	Frappart et al. (2005)	JERS-1 / L-band SAR	90 m
7	Getirana et al. (2012)	HYMAP / Hydrological model	
8	Guimberteau et al. (2012)	ORCHIDEE / Hydrological model	0.5 degrees
9	Hawes et al. (2012)	ALOS-PALSAR / L-band SAR	100 m
10	Hoch et al. (2017)	PCR-GLOBWB / Hydraulic model	30 arcmin

11	Langerwisch et al. (2013)	LPJmL / Hydrological model	0.5 degrees
12	Lauerwald et al. (2017)	ORCHIDEE-ORCHILEAK / Land surface model	0.5 degrees
13	Lesack and Melack (1995)	In situ data	-
14	Li et al. (2020)	Landsat (Mapbiomas)	30 m
15	Luo et al. (2017)	MOSART / Hydraulic model	-
16	Martinez and Le Toan (2007)	JERS-1 / SAR	25 m
17	Miguez-Macho and Fan (2012)	LEAF-Hydro-Flood / Hydrological-hydraulic model	~2 km
18	Meyer Oliveira et al. (2020)	ALOS-PALSAR / L-band SAR	100 m
19	Nardi et al. (2019)	GFPLAIN250m / geomorphic approach	250 m
20	Paiva et al. (2013)	MGB / Hydrological-hydraulic model	500 m
21	Ringeval et al. (2012)	TOPMODEL - LSM / Hydrological model	1 degree
22	Ringeval et al. (2014)	PCR-GLOBWB / Hydrological model	0.5 degrees
23	Rodriguez-Alvarez et al. (2019)	CYGNSS / GNSS-R	500 m - 7 km
24	Rosenqvist et al. (2002)	JERS-1 / L-band SAR	100 m
25	Silva et al. (2013)	Radarsat-1 / C-band SAR	25 m
26	Sippel et al. (1992)	RADAMBRASIL / Side-looking Airborne Radar	0.25 degrees
27	Souza et al. (2019)	Landsat	30 m
28	Trigg et al. (2009)	LISFLOOD-FP and HEC-RAS / Hydraulic models	180 m / irregula
29	Wilson et al. (2007)	LISFLOOD-FP / Hydraulic model	270 m
30	Fassoni-Andrade et al., 2019	MODIS	250 m

Table S2. Main characteristics of the assessed wetlands.

	Name	Location
1	Curuai floodplain	Lower Amazon R.
2	Janauacá floodplain	Middle Amazon R.
3	Uatumã floodplain	300-km reach between Balbina dam and the confluence with the Ar
4	Mamirauá Reserve	Confluence between Solimões and Japurá rivers
5	Purus floodplain	Purus River
6	Pacaya-Samiria wetlands	Upper Solimões River
7	Llanos de Moxos floodable savannas	Upper Madeira River basin
8	Negro savannas	Negro-Branco interfluvial area
9	Roraima savannas	Smaller river floodplains interspersed with areas subject to flooding

Table S3. Comparison metrics (Pearson correlation (R) and normalized root mean square error (nRMSD) for time series, and Fit metric for the spatial analysis of maximum observed inundation area) for all products against the local reference products for individual wetlands: Curuai (Arnesen et al., 2013), Uatumã (Resende et al., 2019), Janauacá (Pinel et al., 2019), Mamirauá (Ferreira-Ferreira et al., 2015), Pacaya-Samiria (Jensen et al., 2020), Llanos de Moxos (Ovando et al., 2016) and Lower Amazon (Park et al., 2019). Four additional local products were compared to the local ones mentioned above: Curuai LISFLOOD-FP model (Rudorff et al., 2014), Janauacá hydrological model

(Bonnet et al., 2017), Janauacá TELEMAC-2D model (Pinel et al., 2019), and Llanos de Moxos ALOS-PALSAR (Ovando et al., 2016). The Fit metric was applied by converting all maps to 1 km, considering a pixel with inundation fraction higher than 50% as inundated.

	Product	-	Curuai	Uatumã	Janauacá	Mamira
-	-	Period	2006-2010	2006-2011	2007-2011	2007-20
			R	nRMSD	Fit	Fit
Other local products	Curuai-Model	1994-2015	0.82	12%	0.86	-
	Janauacá-Bonnet	2006-2019	-	-	-	-
	Janauacá-Pinel	2006-2015	-	-	-	-
	Llanos de Moxos - ALOS	2006-2010	-	-	-	-
Optical sensors	G3WBM	1990-2010	-	-	0.64	0.29
	ESA-CCI	1992-2015	-	-	0.76	0.40
	GLAD	1999-2018	-	-	0.84	0.39
	GSWO	1984-2019	-	-	0.75	0.31
Multiple datasets	GLWD	1992-2004	-	-	0.88	0.45
	CIFOR	2011	-	-	0.91	0.39
	GIEMS-D15	1993-2004	-	-	0.92	0.58
	GIEMS-D3	1993-2007	-	-	0.92	0.61
	WAD2M	2000-2018	0.9	82%	-	-
SAR	Chapman	2006-2011	-	-	0.65	0.27
	Hess	1995-1996	-	-	0.96	0.47
	Rosenqvist	2014-2018	-	-	0.59	0.34
Passive micro-wave	GIEMS-2	1992-2015	0.96	21%	-	-
	SWAMPS	2000-2020	0.91	2%	-	-
	SWAF-HR	2010-2019	-	-	0.95	0.64
Hydro-logical models	CaMa-Flood	1980-2014	0.80	11%	0.97	0.73
	MGB	1980-2014	0.83	7%	0.96	0.58
	THMB	1961-2013	0.72	62%	-	-

Table S4. Long-term minimum inundation areas for the 11 local wetland areas, for the local products (up to three local products per area) and the 18 basin-scale products. The comma-separated values refer to the following local scale products, respectively: Curuai - ALOS (Arnesen et al., 2013) and LISFLOOD-FP model (Rudorff et al., 2014); Uatumã - ALOS (Resende et al., 2019); Janauacá - ALOS (Pinel et al., 2019), hydrologic model (Bonnet et al., 2017) and TELEMAC-2D model (Pinel et al., 2019); Mamirauá - ALOS (Ferreira-Ferreira et al., 2015); Pacaya-Samiria - ALOS-2 PALSAR-2 (Jensen et al., 2020); Llanos de Moxos - MODIS (Ovando et al., 2016) and ALOS (Ovando et al., 2016); and lower Amazon - MODIS (Park et al., 2019). Average, standard deviation (S.D.) and coefficient of variation (CV) are presented for each area in the last row.

	Product	Curuai	Uatumã	Janauacá	Mamirauá	Pacaya-Samiria

Optical sensors	1	Local	1690, 1278	-	108, 38, 18	715	3824
	2	G3WBM	-	-	-	-	-
	3	ESA-CCI	-	-	-	-	-
	4	GLAD	474	77	8	288	514
	5	GSWO	736	345	10	314	401
Multiple datasets	6	GLWD	-	-	-	-	-
	7	CIFOR	-	-	-	-	-
	8	GIEMS-D15	3942	1265	116	1077	3409
	9	GIEMS-D3	2712	861	151	1115	2731
	10	WAD2M	403	97	97	633	20421
SAR	11	Chapman	1894	385	68	866	6775
	12	Hess	2770	584	106	1756	32107
	13	Rosenqvist	1514	313	49	422	1077
Passive Microwave	14	GIEMS-2	995	263	183	1117	1578
	15	SWAMPS	2840	479	197	790	4433
	16	SWAF-HR	1502	544	69	469	215
Hydrological models	17	CaMa-Flood	2741	861	184	1135	8269
	18	MGB	3005	212	0	587	6101
	19	THMB	487	38	1	266	5349
		Average	1858	452	89	774	6670
		S.D.	1148	350	71	430	8978
		CV	0.62	0.77	0.80	0.56	1.35

Agreement for maximum flood extent

50%
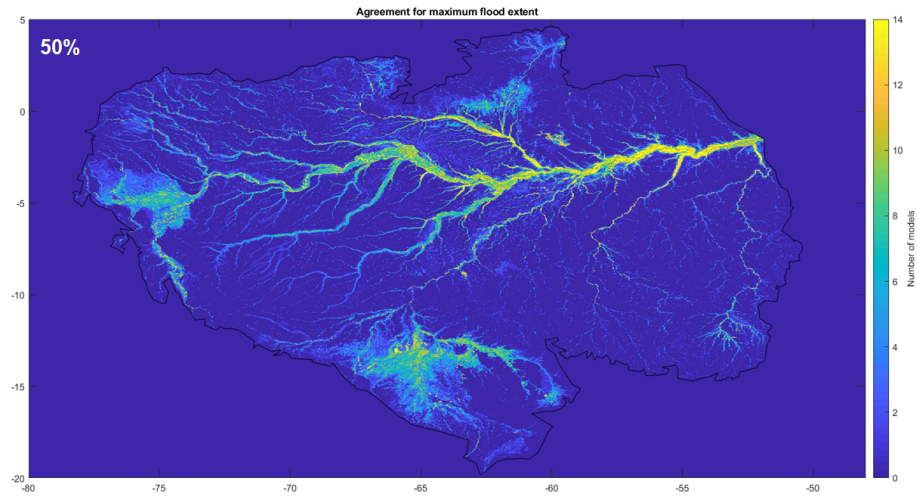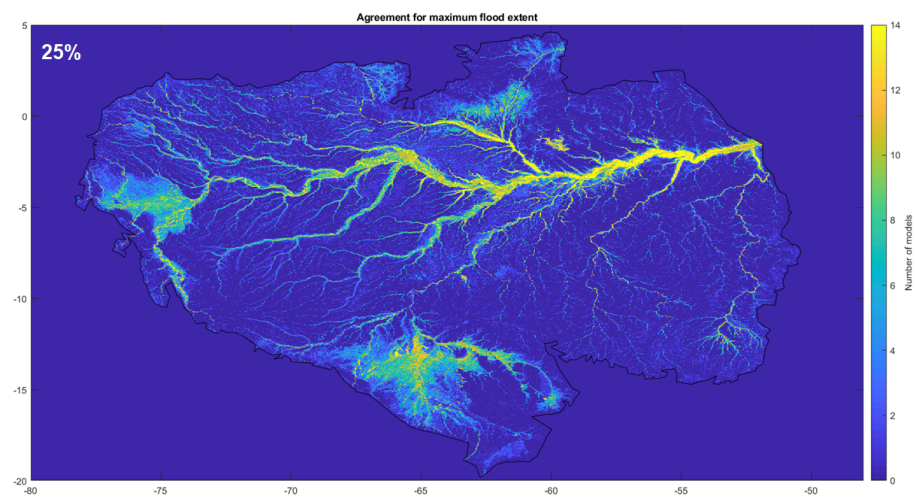
Figure S1. Sensitivity of the fraction used to define a flooded 1km pixel (25% and 50%).
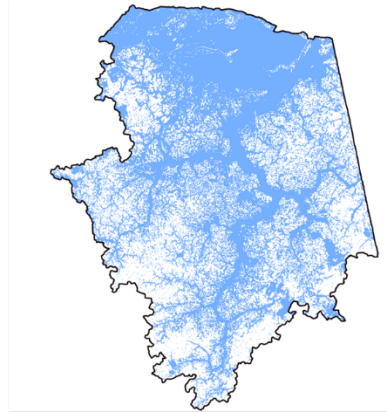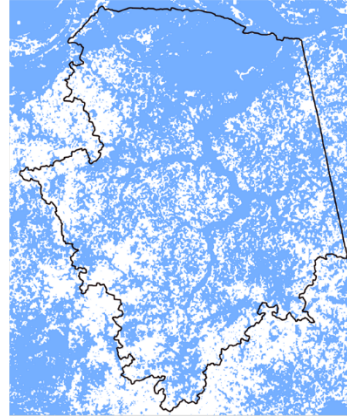
Rosenqvist – 15/16
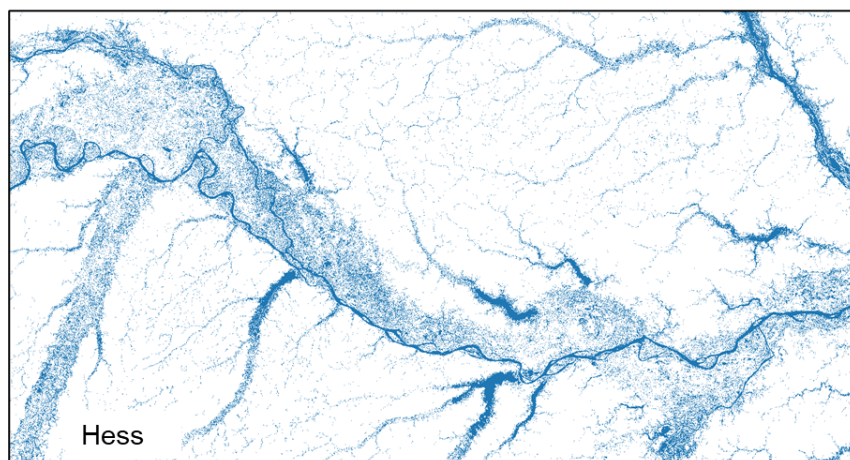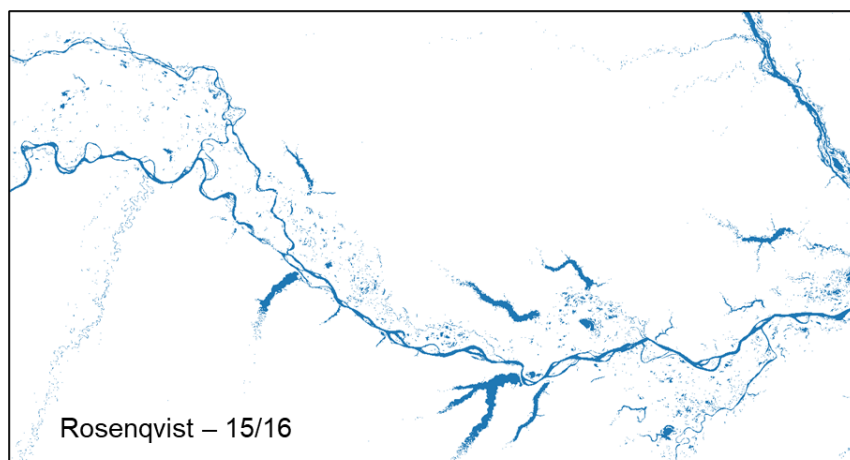
Hess

Figure S2. Minimum inundation extent for the central Amazon River, as estimated by the Rosenqvist (years 2014-2014) and Hess (1995) products.
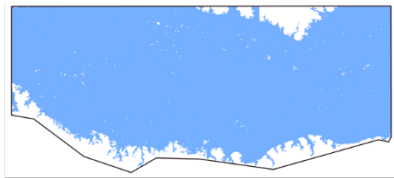
(A) Janauacá

Pinel et al. (2019) – 30 m
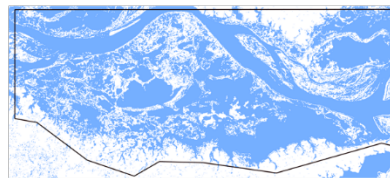
Rosenqvist et al. (2020) – 50 m
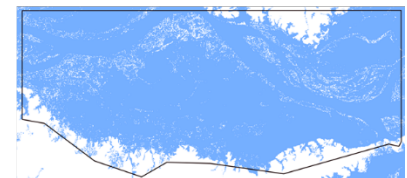
Hess et al. (2015) – 90 m

(B) Curuai

Arnesen et al. (2013) – 12.5 m

Rosenqvist et al. (2020) – 50 m

Hess et al. (2015) – 90 m

Figure S3. Comparison between the long-term maximum inundation for local reference locations (Pinel and Arnesen products) as well as the Rosenqvist and Hess datasets for the (a) Janauacá and (b) Curuai areas. The polygons refer to the area used to extract the values presented in Tables 4 and 5. The spatial resolution of each product is noted.
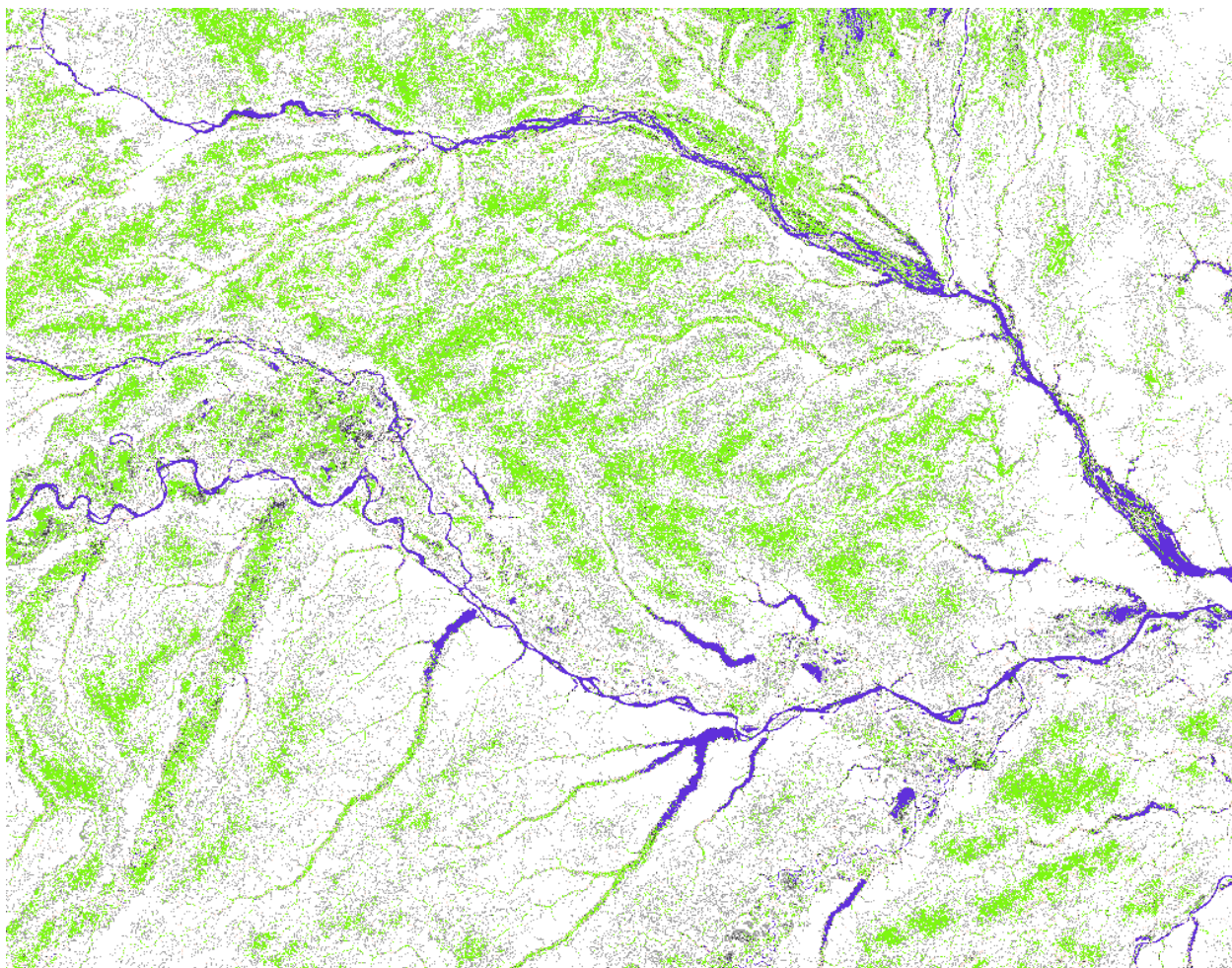
64

Figure S4. Estimation of wetland areas by Gumbricht et al. (2017) across the central Amazon River basin. Green pixels relate to the "swamps (incl. bogs)" category, which is defined as "Wet all year around, but not necessarily inundated."
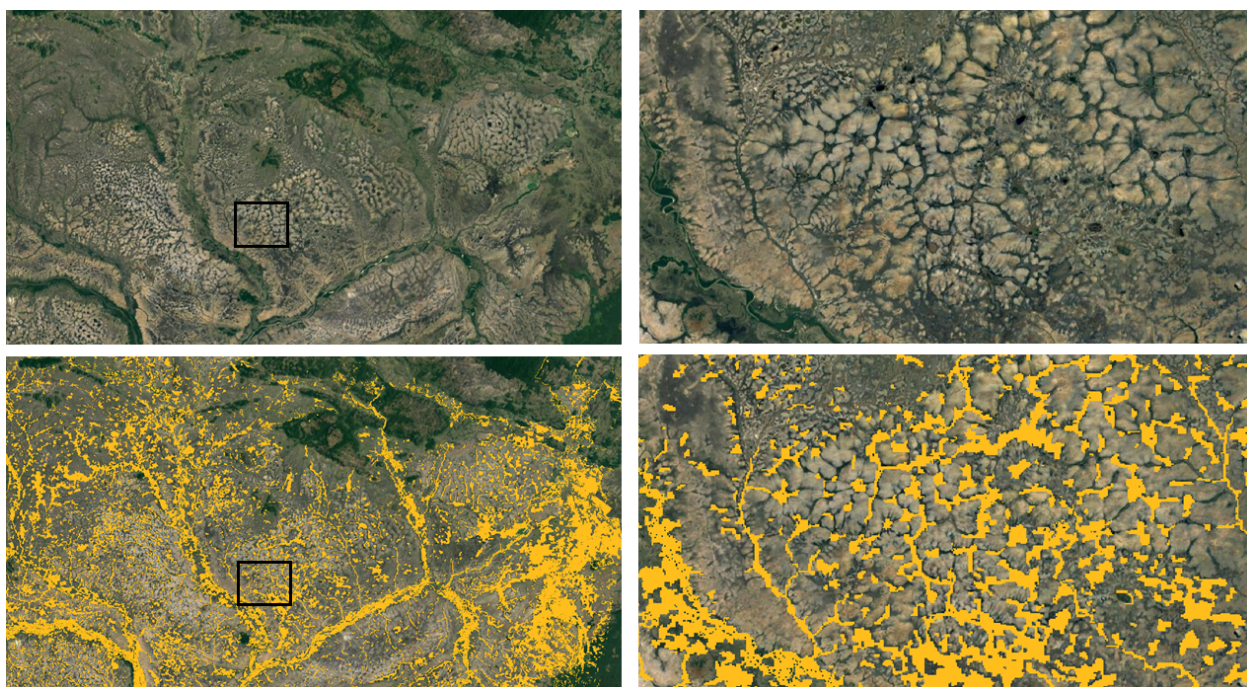
Fig S5. Roraima wetlands. Above: Google Earth imagery. Below: Hess SAR classification of floodable areas (at large scale in the left, and detailed scale in the right).
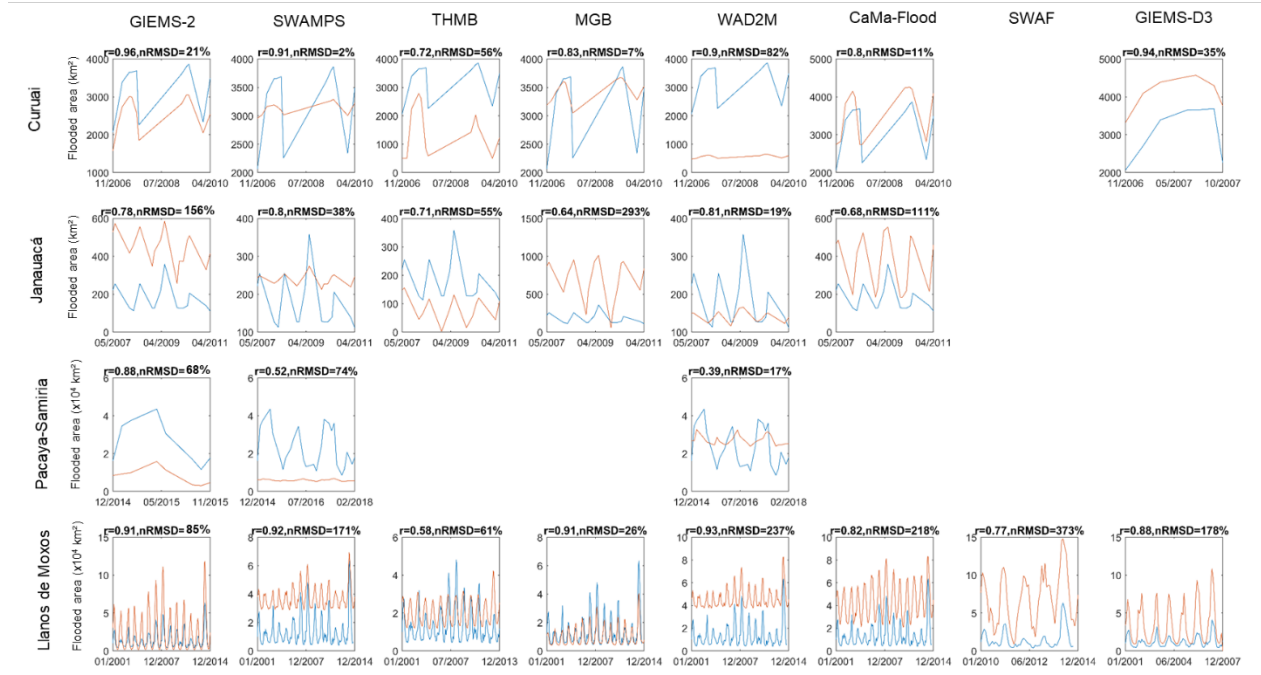
Fig S6. Inundation time series for the four wetlands with available datasets, and for the eight basin-scale dynamic products (GIEMS-2, SWAMPS, THMB, MGB, WAD2M, CaMa-Flood, SWAF-HR and GIEMS-D3). The subplots that are empty refer to areas where the basin-scale product timespans did not overlap with the local product ones. The local reference product is displayed in blue, and each of the basin-scale products in red.